8-2016

Intelligent control of a class of nonlinear systems

Phuong D. Ngo
Purdue University

Graduate School Form
30 Updated 12/26/2015

PURDUE UNIVERSITY
GRADUATE SCHOOL
Thesis/Dissertation Acceptance

This is to certify that the thesis/dissertation prepared

By PHUONG D. NGO

Entitled

INTELLIGENT CONTROL OF A CLASS OF NONLINEAR SYSTEMS

For the degree of Doctor of Philosophy

Is approved by the final examining committee:

YUNG C. SHIN
Chair

BIN YAO

PETER H. MECKL

C-S GEORGE LEE

To the best of my knowledge and as understood by the student in the Thesis/Dissertation Agreement, Publication Delay, and Certification Disclaimer (Graduate School Form 32), this thesis/dissertation adheres to the provisions of Purdue University's "Policy of Integrity in Research" and the use of copyright material.

Approved by Major Professor(s): YUNG C. SHIN

Approved by: JAY P. GORE 5/9/2016

Head of the Departmental Graduate Program Date

INTELLIGENT CONTROL OF A CLASS OF NONLINEAR SYSTEMS

A Dissertation

Submitted to the Faculty

of

Purdue University

by

Phuong D. Ngo

In Partial Fulfillment of the

Requirements for the Degree

of

Doctor of Philosophy

August 2016

Purdue University

West Lafayette, Indiana

To my family.

ACKNOWLEDGEMENTS

I would like to express my sincere gratitude to my research advisor Professor Yung C. Shin. I greatly thank him for his immense knowledge and resources, patience and motivation he has provided me during my PhD program. His comments and advices are invaluable not only for my PhD study but also for my career afterward.

I also thank my lab mates for all of their chats and discussions, especially Kyung-Min Hong for the support and insight knowledge to conduct the laser-welding project.

I am also very grateful to my wife Tran Ngoc Nha Vi, who is always on my side, providing emotional support and encouragement during both good and difficult times. Last but not least, I want to thank my parents for their continuous assistance, understanding and encouragement.

TABLE OF CONTENTS

Page

Page

Page

LIST OF TABLES

Table Page

Appendix Table

LIST OF FIGURES

Figure Page

Figure Page

Appendix Figure

Appendix Figure Page

ABSTRACT

Ngo, Phuong D. Ph.D., Purdue University, August 2016. Intelligent Control of a Class of Nonlinear Systems. Major Professor: Dr. Yung C. Shin.

The objective of this study is to improve and propose new fuzzy control algorithms for a class of nonlinear systems. In order to achieve the objectives, novel stability theorems as well as modeling techniques are also investigated. Fuzzy controllers in this work are designed based on the fuzzy basis function neural networks and the type-2 Takagi-Sugeno fuzzy models.

For a class of single-input single-output nonlinear systems, a new stability condition is derived to facilitate the design process of proportional-integral Mamdani fuzzy controllers. The stability conditions require a new technique to calculate the dynamic gains of nonlinear systems represented by fuzzy basis function network models. The dynamic gain of a fuzzy basis function network can be approximated by finding the maximum of norm values of the locally linearized systems or by solving a non-smooth optimal control problem. Based on the new stability theorem, a multilevel fuzzy controller with self-tuning algorithm is proposed and simulated in a tower crane control system.

For a class of multi-input multi-output nonlinear systems with measurable state variables, a new method for modeling unstructured uncertainties and robust control of unknown nonlinear dynamic systems is proposed by using a novel robust Takagi-Sugeno

fuzzy controller. First, a new training algorithm for an interval type-2 fuzzy basis function network is presented. Next, a novel technique is derived to convert the interval type-2 fuzzy basis function network to an interval type-2 Takagi-Sugeno fuzzy model. Based on the interval type-2 Takagi-Sugeno and type-2 fuzzy basis function network models, a robust controller is presented with an adjustable convergence rate. Simulation results on an electrohydraulic actuator show that the robust Takagi-Sugeno fuzzy controller can reduce steady-state error under different conditions while maintaining better responses than the other robust sliding mode controllers can.

Next, the study presents an implementation of type-2 fuzzy basis function networks and robust Takagi-Sugeno fuzzy controllers to data-driven modeling and robust control of a laser keyhole welding process. In this work, the variation of the keyhole diameter during the welding process is approximated by a type-2 fuzzy-basis-function network, while the keyhole penetration depth is modelled by a type-1 fuzzy basis function network. During the laser welding process, a CMOS camera integrated with the welding system was used to provide a feedback signal of the keyhole diameter. An observer was implemented to estimate the penetration depth in real time based on the adaptive divided difference filter and the feedback signal from the camera. A robust Takagi-Sugeno fuzzy controller was designed based on the fuzzy basis function networks representing the welding process with uncertainties to adjust the laser power to ensure that the penetration depth of the keyhole is maintained at a desired value. Experimental results demonstrated that the fuzzy models provided an accurate estimation of both the welding geometry and its variations due to uncertainties, and the robust Takagi-Sugeno fuzzy controller successfully reduced the penetration depth variation and improved the quality of the welding process.

CHAPTER 1. INTRODUCTION

1.1 Motivation

Fuzzy controllers have been developed with the advantages of being able to deal with uncertainties and nonlinearities in complex nonlinear systems. Two major types of fuzzy controllers are Mamdani fuzzy controller and Takagi-Sugeno (T-S) fuzzy controller. This study aims at providing novel fuzzy control algorithms for a class of nonlinear systems and expanding the applications of fuzzy controllers for nonlinear systems.

The design process of a fuzzy Mamdani controller incorporates the expert knowledge and human operator experiences [1], which is suitable for ill-defined systems where an exact mathematical model is not easy to obtain. Such a controller is also attractive because of its insensitivity to noise and parameter changes. Mamdani fuzzy controllers use the difference between the output signal and the reference signal to control the plant, hence they have advantages in cases when the state variables of the nonlinear systems are not available during implementation. However, Mamdani fuzzy controllers generally suffer from the lack of a systematic analysis of performance; among them is the stability analysis. In order to improve the performance of a Mamdani fuzzy controller, a new stability condition that does not need an accurate model is required to provide a systematic method for selecting the parameters of the controller. In other words, a stable range of the

controller's parameters such as input or output gains can be established. Based on that, novel Mamdani fuzzy control mechanisms can be developed.

In the case that full states of the nonlinear system are available for measurement, T-S fuzzy controllers can be used to improve the performance of the fuzzy control systems. Most of the T-S fuzzy control methods in the current body of literature are designed based on the T-S fuzzy model, which represents a nonlinear system by its local linear models. Linear control design process can be applied for each rule of the Takagi-Sugeno fuzzy model. The design process is normally done by solving linear matrix inequalities to guarantee system stability in the sense of Lyapunov. Hence, the stabilization and performance of the T-S controller depends on the accuracy of the system model. Many real-world systems, however, are highly nonlinear and complex in behavior. Like other nonlinear controllers, a T-S fuzzy controller can produce good responses when an accurate mathematical model is available; however, when the uncertainties and model inaccuracies exist, the same controller may not be able to stabilize the actual system. For that reason, robust T-S fuzzy control algorithms have been developed based on T-S fuzzy models with norm-bounded uncertainties. However, the stability conditions based on the norm-bounded T-S fuzzy models are very conservative since norm-bounded coefficient matrices cannot tightly capture uncertainties, especially unstructured uncertainties.

Hence, new methods to model and control unknown nonlinear systems are necessary to guarantee the stability, which is the most important performance factor to ensure safety in the operation of a plant. A data-driven model can be used to represent the unknown plant dynamics when a mathematical model is unavailable. Furthermore, a data-driven model that can capture unstructured uncertainties also helps in designing robust

fuzzy controllers for many systems in which high performance and reliability are required. Fuzzy basis function networks are suitable candidates to be used for modeling nonlinear systems since it has been proven that any nonlinear function can be approximated by an FBFN model [2]. However, a new training mechanism is required so that the FBFN not only can predict the output of the nonlinear system accurately but also can capture unstructured uncertainties. In addition, a controller design strategy is needed to use such FBFN models to build a robust T-S fuzzy controller.

1.2 Literature Review

1.2.1 Stability Analysis of Fuzzy Control Systems

Many studies have been conducted to create a framework for identifying the stability condition of a fuzzy controller. These studies can be categorized into the following methods: energetic method [3], fuzzy transfer function [4], classical system method [5]–[7], Lyapunov theorem [8], passivity theorem [9] and small gain theorem [10], [11]. The applications of the small gain theorem [10], [11] and the passivity theory [9] in fuzzy control systems show greater advantages compared to other stability methods. These stability theories do not require an exact mathematical representation of the plant and, therefore, they can be applied to nonlinear systems with unknown mathematical models.

Since a Mamdani fuzzy controller is designed based on expert knowledge and experiences of human operator, the stability analysis of the control systems is very limited. Calcev et al. [12] provided a framework to analyze the stability of a fuzzy control system by using the passivity theory. Xu and Shin [9] used the passivity theory to prove the stability of sectorial multilevel fuzzy control systems. However, stability analysis of fuzzy

control systems using passivity theory requires the plant in the control system to be passive to guarantee system stability.

With the small gain theorem, Chen and Ying [13] demonstrated how the parameters of a proportional-integral (PI) fuzzy controller could be chosen to ensure the input-output stability of a nonlinear system. However, the stability criteria developed are only limited to a certain type of fuzzy controllers with two input and three output membership functions. Since Chen and Ying [13] divided the stability problem according to the locations of the error and the time rate of change of the error with respect to zero, the complexity of the problem would exponentially increase if the number of input and output membership functions increases.

The most popular method for deriving the stability conditions for T-S fuzzy controllers is using the Lyapunov function. Xiu and Ren [14] proposed a stability analysis for T-S fuzzy control systems in a form of linear matrix inequalities (LMIs). Chang et al. used the passivity theory to derive a stability condition on a discrete affine T-S fuzzy system [15] and continuous-time affine T-S fuzzy models with relaxed stability conditions [16]. Many studies in the literature also investigated the stability of T-S fuzzy control systems with structured uncertainties [17]–[20]. Unstructured uncertainties, however, represent a much more general class of nonlinear systems and can incorporate both the model inaccuracies and measurement noise. Gao et al. [21] presented an approach to analyzing the stability of controlling general nonlinear systems based on Takagi-Sugeno (T-S) fuzzy dynamic models. The method uses LMI approach to design the TS fuzzy controller to stabilize systems with norm-bounded unstructured uncertainties. However, the LMI conditions for norm-bounded uncertainties are generally conservative.

1.2.2 Fuzzy Controller with Self-Tuning Mechanism

With the introduction of fuzzy logic, fuzzy controllers have been developed and implemented in many applications [22]–[25], where there are many possible controller structures with different numbers of input, output fuzzy sets and membership functions. The fuzzy inference mechanism such as Mamdani or Sugeno can be chosen by a control designer based on the performance requirement of the control system. Therefore, selecting a correct fuzzy structure requires in-depth knowledge or heuristic information of the plant dynamics to be controlled. Various studies have been conducted to improve the performance of fuzzy controllers. Haj-Ali and Ying [26] and Arya [27] analyzed the structures of PI fuzzy controllers and found the effects of nonlinear and asymmetrical input sets on the performance of the controllers. Chen and Ying [13] and Haj-Ali and Ying [26] demonstrated that fuzzy PI and PID controllers could be treated as nonlinear PI and PID controllers. Mudi and Pal [28] presented a method to tune the output-scaling factors of fuzzy controllers by using the error and the time rate of change of the error signals. However, this method is based only on an intuitive analysis of the desired performance to keep the system stable; no mathematical stability analysis was provided in their work.

In many applications when the heuristic information is not sufficient, the parameter values of a fuzzy controller can be computed off-line by using data-driven methods such as training with input and output data [29]–[31]. However, under the presence of disturbance or time-varying parameters, online adaptation of control parameters based on the data gathered during the controlling process would be more effective. Adaptive controller schemes have been developed to make various systems function properly under such conditions [9], [32]–[38]. These schemes can be divided into two types [33]: direct

[9], [34], [35] and indirect fuzzy control [36]–[38]. In indirect fuzzy control, the plant model is estimated online by some identification algorithm, and then the fuzzy controller's parameters are updated accordingly from the model. In direct fuzzy controllers, the controller's parameters are tuned directly using the measurement data.

Among the parameters to be tuned in fuzzy controllers, fuzzy rule base and input-output gains (or scaling factors) are most popularly used. Wong et al. [39] introduced a switching-type fuzzy controller with switching scaling factors in each operating region. In [40], a PID-type fuzzy controller was proposed with self-tuning scaling factors. Ying [41] introduced a method for obtaining the parameters of a PI fuzzy controller by tuning a linear PI controller. However, the global stability of the control system could not be guaranteed, since Ying's method only showed local stability around the equilibrium points, nor could it determine the size of the region of local stability. Li and Tong [42] proposed a hybrid control system that consists of a state observer, an adaptive fuzzy mechanism, an H^{∞} control and a sliding mode control. Boubakir et al. [43] used a different approach to tune the parameters of a proportional-integral-derivative (PID) controller for multi-input multi-output (MIMO) dynamic systems by minimizing the error between an ideal controller and the PID controller. However, the controllers developed by both Li and Tong [42] and Boubakir et al. [43] can only be applied to a certain class of nonlinear dynamic systems where the input is represented by a linear term in the system's mathematical model. However, Pellegrinetti and Bentsman [44] offer an example of nonlinear systems that cannot be represented in this form. Furthermore, stability conditions for the controllers presented in these studies must be calculated based on the upper bounds of the model

functions. These values are difficult to obtain in many cases where the system models are unknown.

In Woo et al. [40], a PID fuzzy controller was proposed with self-tuning algorithms for both input and output scaling factors, but lacked a systematic stability analysis. The multilevel fuzzy controller (MLFC) system was proposed by Xu and Shin [9], wherein the controller has an adaptive mechanism designed to tune the output membership functions based on the system outputs. Although the MLFC has been successfully utilized in different applications [45], [46], the controller still has some limits when dealing with time-variant systems such as sectorial restrictions on membership functions.

1.2.3 Modeling of Nonlinear Systems by Using FBFNs

Since an analytical mathematical model for many nonlinear systems cannot be easily obtained, fuzzy basis function networks (FBFN) that have a similar structure to radial basis function neural networks (RBFN) can be used to capture the plant's dynamics. The FBFN was adopted in different applications [47]–[49] since it can be used to accurately represent the relationship between the inputs and the outputs of a nonlinear dynamic system. With a set of input and output data, it has been proven that any nonlinear system can be approximated by an FBFN model [2]. With these advantages, an FBFN-based fuzzy controller should provide an effective way of controlling any nonlinear system. However, Mamdani fuzzy control by using FBFN is still very limited because there has not been a systematic approach to the design of control systems with guaranteed stability.

To capture the uncertainties in systems, type-2 fuzzy systems [50] have been introduced, wherein the type-2 fuzzy set is utilized. However, due to the complexity of the

rule uncertainties and computational requirements to calculate the output, modeling nonlinear systems by using type-2 fuzzy systems is a computationally intensive process. This leads to the concept of an interval type-2 fuzzy-logic system, in which the secondary membership functions of either the antecedents or the consequents are simplified to an interval set. Similar to type-1 fuzzy systems, the combination of type-2 fuzzy systems and neural networks brings different intelligent modeling and optimization techniques to obtain rule bases and membership functions without the need for an expert knowledge. Méndez and de los Angeles Hernandez [51] presented a technique to obtain an interval type-2 fuzzy neural network by the orthogonal least square and back propagation methods. Rubio-Solis and Panoutsos [52] proposed a modeling framework for an interval type-2 radial basis function neural network via a granular computing and adaptive back propagation approaches. However, the uncertainties represented in type-2 fuzzy neural systems are normally not in a form that can be easily used to design a robust controller. Furthermore, there is a lack of a theoretical stability analysis for control systems based on type-2 fuzzy neural networks.

1.2.4 Robust Fuzzy Control of Nonlinear System with Unstructured Uncertainties

For unknown dynamic systems, many robust adaptive control techniques have been proposed based on the parameters of a universal approximator [53], [54]. Goyal et al. [55] introduced a robust sliding mode control based on Chebyshev neural networks. Chadli and Guerra [56] proposed a robust static output feedback for a discrete Takagi-Sugeno (T-S) fuzzy system. The stability conditions in their studies are represented in terms of a set of linear matrix inequalities (LMI). An observer-based output feedback nonlinear robust

control of nonlinear systems with parametric uncertainties was introduced by Yao et al. [57] to provide a sufficient condition for robust stabilization of the systems when all state variables are not available for measurement. By using a Lyapunov-Krasovskii function (LKF), Hu et al. [58] introduced a stability condition to stabilize discrete stochastic systems with mixed time delays, randomly-occurring uncertainties, and randomly-occurring nonlinearities. However, since these methods represented uncertainties as functions of system parameters, they are not applicable to cases where the causes of uncertainties are not known (unstructured uncertainties).

One method to represent unstructured uncertainties is to model a nonlinear system by a set of linear systems with norm-bounded uncertain matrices. Wang et al. [59] proposed a set of LMIs that need to be solved at each time step to obtain a control solution that satisfies some performance criteria. However, since finding the LMI solution requires special computing tools, real-time computation is a challenge in this case, especially when the sampling time is relatively small. Furthermore, the solution of the LMIs might not be found because representing a highly nonlinear system by a linear system will lead to large values of uncertainty norms due to linearization error. Another approach that deals with nonlinear systems with unstructured uncertainties is a combination of backstepping and small gain theorem [60]–[62]. However, these methods can only be applied to a certain class of nonlinear dynamic systems where the input is represented by a linear term in the system's mathematical model. Gao et al. [21] presents an approach to controlling general nonlinear systems with norm-bounded unstructured uncertainties. However, obtaining the bounded norms of uncertain nonlinear systems was not addressed in their study.

1.3 Research Objectives

The objective of this research study is to develop effective and robust fuzzy controllers for nonlinear systems. The following tasks were carried out in this research:

- Develop a stability theorem for the multilevel Mamdani fuzzy control systems based on the FBFN representation of nonlinear systems.
- Propose a multilevel Mamdani fuzzy controller with a self-organizing output scaling-factor for a class of nonlinear systems with unknown state variables.
- Derive a novel training algorithm for type-2 FBFNs to capture unstructured uncertainties in nonlinear systems.
- Design a method to control nonlinear systems with measurable state variables by using a robust Takagi-Sugeno fuzzy controller.

1.4 Outline of Dissertation

The first chapter presents the motivation, literature review and objectives of the work. For a class of nonlinear system with unknown state variables, chapter 2 presents a stability analysis of the fuzzy control system and methods to estimate the dynamic gain of a nonlinear system. The chapter also discusses the design process for a new MLFC with a self-tuning output scaling-factor. Chapter 3 describes a new method to train an interval type-2 fuzzy basis function network (FBFN). A new technique is also proposed to convert an interval type-2 FBFN to an interval type-2 T-S fuzzy model. Based on the interval type-2 T-S model and the interval type-2 FBFN, a robust controller that is not only robust but also produces good transient performance when implemented on nonlinear systems with unstructured uncertainties is presented. Chapter 4 presents a new laser keyhole-welding

model and an observer to estimate the penetration depth. Based on the welding model proposed, an implementation of the robust Takagi-Sugeno fuzzy controller (RTSFC) is described, which can increase the accuracy and quality of the laser welding process in the presence of uncertainties. Experiments conducted on titanium samples to evaluate the accuracy and effectiveness of the model and the RTSFC are presented.

CHAPTER 2. STABILITY CONDITION FOR A CLASS OF MAMDANI FUZZY CONTROL SYSTEM AND THE MULTILEVEL FUZZY CONTROLLER WITH SELF TUNING OUTPUT SCALING-FACTOR

This chapter aims to improve the performances and applications of Mamdani fuzzy controllers. Proportional-integral (PI) Mamdani fuzzy controllers are useful in cases when the state variables of the nonlinear systems are not available during implementation since only the reference and system outputs are required. Expert knowledge can also be applied during the design process of a Mamdani fuzzy controller.

First a new stability condition for a class of nonlinear systems controlled by proportional-integral Mamdani fuzzy controllers is proposed in this chapter. The stability analysis of a Mamdani fuzzy control system can now be determined based on the scaling-factor of the fuzzy controller. This chapter also presents methods to estimate the dynamic gain of a class of nonlinear systems and proposes a new Mamdani fuzzy controller with self-tuning output scaling-factor.

2.1 Problem Formulation

Consider a class of single input – single output (SISO) nonlinear systems. Assume that the output of the system only depends on the current input value, the past values of the input, and the histories of the output itself. This type of nonlinear system can be represented in an input and output form as follows:

$$y(k) = \mathcal{N}\left(u(k-1), u(k-2), ..., u(k-m), y(k-1), y(k-2), ..., y(k-n)\right) \quad (2.1)$$

where *u(k)* is the input and *y(k)* denotes the output of the nonlinear system at time instance *k*, the indices *m* and *n* are the system orders of the input and the output, respectively. The notation $\mathcal{N}$ represents an unknown nonlinear function, which is assumed to be locally Lipschitz.

It has been proven by Wang and Mendel [2] that an FBFN can uniformly approximate any real and continuous nonlinear function on a compact set to a prescribed accuracy with a finite number of basis functions. Hence, a fuzzy basis function can be constructed from the input and output data to represent this system through a set of *l* fuzzy rules, where the i^{th} rule R^i is described as follows:

$$\begin{aligned} \mathrm{R}^i: \quad & \text{If } u(k-1) = A_1^i \text{ AND } u(k-2) = A_2^i \text{ AND } \ldots \text{AND } u(k-m) = A_m^i \text{ AND} \\ & y(k-1) = B_1^i \text{ AND } y(k-2) = B_2^i \cdots \text{AND } y(k-n) = B_n^i \\ & \text{then } y(k) = b^i \end{aligned} \quad (2.2)$$

where *u(k)* is the input and *y(k)* denotes the output of the nonlinear system at time instant *k.* The notations *m* and *n* represent the system orders of the input and the output. $A_1 \ldots A_m$ and $B_1 \ldots B_n$ are fuzzy membership sets. *b* represents a singleton function of the output.

2.2 Dynamic Gain Estimation of Nonlinear Dynamic Systems

The stability analysis of nonlinear fuzzy control systems based on the small gain theorem requires the dynamic-gain estimation of the plant model. Two methods are proposed in this section to calculate the gain of a class of nonlinear systems represented by FBFN models. In the first method, the dynamic gain can be approximated by finding the

maximum norm of locally-linearized systems. The second method provides an analytical computation technique of the dynamic gain based on a non-smooth optimal control problem.

2.2.1 Local Linear Model of a Class of Nonlinear Systems Represented by FBFN Models

Consider a class of nonlinear dynamic systems as described in Eq. (2.1) that can be represented by the FBFN model as in Eq. (2.2). Further assume that the considered nonlinear system has a finite dynamic gain. By using singleton fuzzification, product inference and centroid defuzzification methods, the FBFN model that represent the dynamic system can be written in the following state space equations:

$$\begin{aligned} \mathbf{x}(k) &= \mathbf{f}(\mathbf{x}(k-1), \mathbf{u}(k-1)) \\ y(k) &= \mathbf{c}^{\mathrm{T}} \mathbf{x}(k) \end{aligned} \tag{2.3}$$

where $$\mathbf{x}(k) = \left[y(k), \ldots y(k-n+1) \right]^{\mathrm{T}}, \ \mathbf{u}(k-1) = [u(k-1), \ldots, u(k-m)]^{\mathrm{T}}, \tag{2.4}$$

$$\mathbf{f}(\mathbf{x}(k-1), \mathbf{u}(k-1)) = \begin{bmatrix} f(\mathbf{x}(k-1), \mathbf{u}(k-1)) \\ y(k-1) \\ \vdots \\ y(k-n+1) \end{bmatrix}, \quad \mathbf{c} = [1, 0, \ldots 0]^{\mathrm{T}} \tag{2.5}$$

The nonlinear mapping $f : \mathbf{u} \subset \Re^m, \mathbf{x} \subset \Re^n \rightarrow y \subset \Re$ in Eq. (2.5) is described through the fuzzification process as follows:

$$f\left(\mathbf{x}(k-1), \mathbf{u}(k-1)\right) = \frac{\sum_{i=1}^{l} \left(b^i \cdot \left\{ \prod_{t_u=1}^{m} \mu_{A_{t_u}^i} [u(k-t_u)] \right\} \cdot \left\{ \prod_{t_y=1}^{n} \mu_{B_{t_y}^i} [y(k-t_y)] \right\} \right)}{\sum_{i=1}^{l} \left(\left\{ \prod_{t_u=1}^{m} \mu_{A_{t_u}^i} [u(k-t_u)] \right\} \cdot \left\{ \prod_{t_y=1}^{n} \mu_{B_{t_y}^i} [y(k-t_y)] \right\} \right)}, \tag{2.6}$$

where $\mu_{A_{t_u}^i}[u(k-t_u)]$ and $\mu_{B_{t_y}^i}[y(k-t_y)]$ are Gaussian input and output membership functions:

$$\mu_{A_{t_u}^i}[u(k-t_u)] = \exp\left\{-\frac{1}{2}\left[\frac{u(k-t_u)-m_{t_u}^i}{\sigma_{t_u}^i}\right]^2\right\},\ \mu_{B_{t_y}^i}[y(k-t_y)] = \exp\left\{-\frac{1}{2}\left[\frac{y(k-t_y)-m_{t_y}^i}{\sigma_{t_y}^i}\right]^2\right\} \tag{2.7}$$

m_t^i and σ_t^i are parameters that represent the center and width of each Gaussian MF; $t_u = 1...m$ and $t_y = 1...n$ are the numbers of delay terms of the system input and output, respectively; and l is the number of the FBFN's rules.

When the states of the system are around a certain operating condition described by $\mathbf{x}_0$ and $\mathbf{u}_0$:

$$\begin{gathered}\mathbf{x}_0(k-1) = \left[y_0(k-1),\ldots,y_0(k-n)\right]^{\mathrm{T}},\quad \mathbf{u}_0(k-1) = \left[u_0(k-1),\ldots,u_0(k-m)\right]^{\mathrm{T}} \\ \mathbf{x}_0(k) = \mathbf{f}(\mathbf{x}_0(k-1),\mathbf{u}_0(k-1))\end{gathered} \tag{2.8}$$

the local linear model of the nonlinear system represented by Eq. (2.3) can be obtained as follows:

$$\begin{aligned}\mathbf{x}(k) = {} & \mathbf{f}\left(\mathbf{x}_0(k-1),\mathbf{u}_0(k-1)\right) + \mathbf{A}\left(\mathbf{x}_0(k-1),\mathbf{u}_0(k-1)\right)\left[\mathbf{x}(k-1)-\mathbf{x}_0(k-1)\right] \\ & + \mathbf{B}\left(\mathbf{x}_0(k-1),\mathbf{u}_0(k-1)\right)\left[\mathbf{u}(k-1)-\mathbf{u}_0(k-1)\right] \\ y(k) = {} & \mathbf{c}^{\mathrm{T}}\mathbf{x}(k)\end{aligned} \tag{2.9}$$

where $\mathbf{A}\left(\mathbf{x}_0,\mathbf{u}_0\right) = \begin{bmatrix} a_1 & a_2 & \ldots & a_n \\ 0 & 1 & \ldots & 0 \\ \vdots & & & \\ 0 & 0 & \ldots & 1 \end{bmatrix}$, $\mathbf{B}\left(\mathbf{x}_0,\mathbf{u}_0\right) = \begin{bmatrix} b_1 & b_2 & \ldots & b_m \\ 0 & 1 & \ldots & 0 \\ \vdots & & & \\ 0 & 0 & \ldots & 1 \end{bmatrix}$, $\mathbf{x}(0) = [0,0,...,0]^{\mathrm{T}}$

(2.10)

The matrices **A** and **B** includes the linearizing coefficients a_{t_y} and b_{t_u} ($t_y = 1...n$ and $t_u = 1...m$), which can be calculated by the following formulas [63]:

$$a_{t_y} = \left.\frac{\partial f}{\partial y(k-t_y)}\right|_{\substack{\mathbf{x}=\mathbf{x}_0,\\ \mathbf{u}=\mathbf{u}_0}} = -\frac{\sum_{i=1}^{l}\left\{b^i \cdot \left[\prod_{t_u=1}^{m}\mu_{A_{t_u}^i}[u(k-t_u)]\right]\cdot\left[\prod_{t_y=1}^{n}\mu_{B_{t_y}^i}[y(k-t_y)]\right]\left[\frac{y(k-t_y)-c_{t_y}^i}{\sigma_{t_y}^{i\,2}}\right]\right\}}{\sum_{i=1}^{l}\left[\left\{\prod_{t_u=1}^{m}\mu_{A_{t_u}^i}[u(k-t_u)]\right\}\cdot\left\{\prod_{t_y=1}^{n}\mu_{B_{t_y}^i}[y(k-t_y)]\right\}\right]}$$

$$+\frac{\left(\left(\sum_{i=1}^{l}\left\{b^i \cdot \left[\prod_{t_u=1}^{m}\mu_{A_{t_u}^i}[u(k-t_u)]\right]\cdot\left[\prod_{t_y=1}^{n}\mu_{B_{t_y}^i}[y(k-t_y)]\right]\right\}\right)\times \left(\sum_{i=1}^{l}\left\{\left\{\prod_{t_u=1}^{m}\mu_{A_{t_u}^i}[u(k-t_u)]\right\}\cdot\left\{\prod_{t_y=1}^{n}\mu_{B_{t_y}^i}[y(k-t_y)]\right\}\left[\frac{y(k-t_y)-c_{t_y}^i}{\sigma_{t_y}^{i\,2}}\right]\right\}\right)\right)}{\left\{\sum_{i=1}^{l}\left[\left\{\prod_{t_u=1}^{m}\mu_{A_{t_u}^i}[u(k-t_u)]\right\}\cdot\left\{\prod_{t_y=1}^{n}\mu_{B_{t_y}^i}[y(k-t_y)]\right\}\right]\right\}^2} \quad (2.11)$$

and

$$b_{t_u} = \left.\frac{\partial f}{\partial u(k-t_u)}\right|_{\substack{\mathbf{x}=\mathbf{x}_0,\\ \mathbf{u}=\mathbf{u}_0}} = -\frac{\sum_{i=1}^{l}\left\{b^i \cdot \left[\prod_{t_u=1}^{m}\mu_{A_{t_u}^i}[u(k-t_u)]\right]\cdot\left[\prod_{t_y=1}^{n}\mu_{B_{t_y}^i}[y(k-t_y)]\right]\left[\frac{u(k-t_u)-c_{t_u}^i}{\sigma_{t_u}^{i\,2}}\right]\right\}}{\sum_{i=1}^{l}\left[\left\{\prod_{t_u=1}^{m}\mu_{A_{t_u}^i}[u(k-t_u)]\right\}\cdot\left\{\prod_{t_y=1}^{n}\mu_{B_{t_y}^i}[y(k-t_y)]\right\}\right]}$$

$$+\frac{\left(\left(\sum_{i=1}^{l}\left\{b^i \cdot \left[\prod_{t_u=1}^{m}\mu_{A_{t_u}^i}[u(k-t_u)]\right]\cdot\left[\prod_{t_y=1}^{n}\mu_{B_{t_y}^i}[y(k-t_y)]\right]\right\}\right)\cdot \left(\sum_{i=1}^{l}\left\{\left\{\prod_{t_u=1}^{m}\mu_{A_{t_u}^i}[u(k-t_u)]\right\}\cdot\left\{\prod_{t_y=1}^{n}\mu_{B_{t_y}^i}[y(k-t_y)]\right\}\left[\frac{u(k-t_u)-c_{t_u}^i}{\sigma_{t_u}^{i\,2}}\right]\right\}\right)\right)}{\left\{\sum_{i=1}^{l}\left[\left\{\prod_{t_u=1}^{m}\mu_{A_{t_u}^i}[u(k-t_u)]\right\}\cdot\left\{\prod_{t_y=1}^{n}\mu_{B_{t_y}^i}[y(k-t_y)]\right\}\right]\right\}^2} \quad (2.12)$$

By changing the variables, Eq. (2.9) becomes

$$\begin{aligned}\tilde{\mathbf{x}}(k) &= \mathbf{A}\left(\mathbf{x}_0, \mathbf{u}_0\right)\tilde{\mathbf{x}}(k-1) + \mathbf{B}\left(\mathbf{x}_0, \mathbf{u}_0\right)\tilde{\mathbf{u}}(k-1) \\ \tilde{y}(k) &= \mathbf{c}^{\mathrm{T}}\tilde{\mathbf{x}}(k)\end{aligned} \tag{2.13}$$

where $\tilde{\mathbf{x}}(k) = \mathbf{x}(k) - \mathbf{x}_0(k)$, $\tilde{\mathbf{u}}(k) = \mathbf{u}(k) - \mathbf{u}_0(k)$, $\tilde{y}(k) = y(k) - \mathbf{c}^{\mathrm{T}}\mathbf{x}_0(k)$.

For a nonlinear dynamic system as described in Eq. (2.1), it has been proven by Nikolaou and Manousiouthakis [64] that its dynamic gain can be calculated from the maximum value of the gains of its local linear systems.

$$\| \mathcal{N} \|_p = \sup_{\substack{\mathbf{u}_1, \mathbf{u}_2 \in L_{pe}^m \\ \mathbf{u}_1 \neq \mathbf{u}_2}} \frac{\| \mathcal{N}(\mathbf{x}(k), \mathbf{u}_1(k)) - \mathcal{N}(\mathbf{x}(k), \mathbf{u}_2(k)) \|_p}{\| \mathbf{u}_1(k) - \mathbf{u}_2(k) \|_p} = \sup_{\mathbf{x}_0 \in L_{pe}^n, \mathbf{u}_0 \in L_{pe}^m} \| \mathcal{L}_{\mathbf{x}_0, \mathbf{u}_0} \|_p, \quad p \in [1, \infty] \tag{2.14}$$

where $\mathcal{L}$ is the linear model of the nonlinear system at the operating condition $\mathbf{x}_0$ and $\mathbf{u}_0$, the notations $\mathbf{u}_1$ and $\mathbf{u}_2$ are any two input values that belong to the extended space L_{pe}^m. The notations L_p^m and L_{pe}^m are defined as the finite p-norm (Banach) space and the extended Banach space, given by:

$$\begin{aligned} L_p^m &= \left\{ \mathbf{u} : [0, \infty) \to R^m : \| \mathbf{u} \|_p < \infty \right\} \\ L_{pe}^m &= \left\{ \mathbf{u} : [0, \infty) \to R^m : \mathbf{u}_T \in L_p^n \text{ for all } T \geq 0 \right\} \end{aligned} \tag{2.15}$$

Based on the obtained models, the methods to estimate the L_2 gain and L_∞ gain of FBFN systems are provided in the next subsections.

2.2.2 L_2 Gain Estimation of Nonlinear Systems Represented by FBFN Models

In addition to the Nikolaou and Manousiouthakis' theorem described above, it has been proven by Schaft [65] that if the local linear model of a nonlinear system has its L_2 gains less than a constant γ then the local L_2 gain of the nonlinear system will also be less than γ. Since the L_2 gain of a linear system is also its $H\infty$ norm, the L_2 gain of the FBFN can be approximated by finding the maximum of the $H\infty$ norm values of all locally linearized systems:

$$\| \mathcal{N} \|_2 = \sup_{\mathbf{x}_0 \in L_{pe}^n, \mathbf{u}_0 \in L_{pe}^m} \| \mathcal{L}_{\mathbf{x}_0, \mathbf{u}_0} \|_{H\infty} \tag{2.16}$$

The local linear systems $\mathcal{L}_{\mathbf{x}_0, \mathbf{u}_0}$ are provided in the form of state space equations as given in Eq. (2.13). Fast computing techniques such as Bruinsma and Steinbuch [66] can be used to calculate the values of their H_∞ norm.

2.2.3 L_∞ Gain Estimation of Nonlinear Systems Represented by FBFN Models

This subsection provides an analytical computation of the L_∞ gain for discrete nonlinear systems and FBFN models. This work is an expansion of Nikolaou and Manousiouthakis' [67] techniques, which have only been applied to continuous nonlinear systems. In Theorem 1, the L_∞ gain of an FBFN is proven to be the solution of a non-smooth optimal control problem, which can be solved numerically by using the non-smooth Newton's method [68].

Theorem 1 (Dynamic infinity gain of FBFN systems)**:**

The dynamic infinity gain of a nonlinear system represented by an FBFN model, which is described by Eq. (2.3), over a convex set $W \triangleq \{\mathbf{u} \in L_\infty : \| \mathbf{u}(k) \| \leq \delta\}$ can be found by solving the following non-smooth optimal control problem:

$$\| \mathcal{N} \|_\infty = \sup_{k \in (0,\infty)} \left[- \inf_{\mathbf{x}_0 \in L^n_{\infty e}, \mathbf{u}_0 \in L^m_{\infty e}} \sum_{l=0}^{k-1} - \left\| \mathbf{c}^T \mathbf{\Phi}(k, l+1) \mathbf{B} \right\|_i \right] \tag{2.17}$$

under the dynamic constraints:

$$\begin{aligned} &\mathbf{\Phi}(k+1, l) = \mathbf{A} \mathbf{\Phi}(k, l) \\ &\mathbf{\Phi} : (0,\infty) \times [0,\infty) \to \mathbb{R}^{n \times n},\ \mathbf{\Phi}(k,k) = \mathbf{I} \end{aligned} \tag{2.18}$$

where **A** and **B** are the coefficient matrices given in Eq. (2.10). $\| \cdot \|_i$ represents any induced norm.

Proof: For a system represented by Eq. (2.13), the unique solution can be found as follows [69]:

$$\begin{aligned} \tilde{\mathbf{x}}(k) &= \mathbf{\Phi}(k,0) \tilde{\mathbf{x}}(0) + \sum_{l=0}^{k-1} \mathbf{\Phi}(k, l+1) \mathbf{B}(l) \tilde{\mathbf{u}}(l) \\ \tilde{y}(k) &= \mathbf{c}^T \tilde{\mathbf{x}}(k) \end{aligned}, \tag{2.19}$$

where the state transition matrix $\mathbf{\Phi}(k,l)$ relates the state at time *k* to the state at an earlier time *l*:

$$\tilde{\mathbf{x}}(k) = \mathbf{\Phi}(k,l) \tilde{\mathbf{x}}(l) \tag{2.20}$$

and has the following properties:

$$\begin{aligned} \mathbf{\Phi}(k,k) &= \mathbf{I} \\ \tilde{\mathbf{x}}(k) &= \mathbf{\Phi}(k,0) \tilde{\mathbf{x}}(0) \\ \mathbf{\Phi}(k+1,l) &= \mathbf{A}(k) \mathbf{\Phi}(k,l) \end{aligned} \tag{2.21}$$

From Eq. (2.3) and Eq. (2.19), the output of the system can be calculated from its solution:

$$\tilde{y}(k) = \sum_{l=0}^{k-1} \mathbf{c}^T \mathbf{\Phi}(k, l+1)\mathbf{B}(l)\tilde{\mathbf{u}}(l) \tag{2.22}$$

Eq. (2.22) can be rewritten as follows:

$$\tilde{y}(k) = \sum_{l=0}^{k-1} \mathbf{G}_l(k)\tilde{\mathbf{u}}(l) \tag{2.23}$$

where $\mathbf{G}_l(k) = \mathbf{c}^T \mathbf{\Phi}(k, l+1)\mathbf{B}(l)$. It has been proven by Desoer and Vidyasagar [70] that if a linear system has the responses as provided in Eq. (2.23) then its L_∞ gain is given as follows:

$$\left\| \mathcal{L} \right\|_\infty = \sup_{k \in (0,\infty)} \sum_{l=0}^{k-1} \left\| \mathbf{G}_l(k) \right\|_i \tag{2.24}$$

where $\left\| \mathbf{G}_l(k) \right\|_i$ is any induced norm of $\mathbf{G}_l(k)$.

By using Eq. (2.14) and Eq. (2.24), the infinity gain of the nonlinear system represented by an FBFN model becomes the solution of the following non-smooth optimal control problem:

$$\begin{aligned} \| \mathcal{N} \|_\infty &= \sup_{\mathbf{x}_0 \in L^n_{\infty e}, \mathbf{u}_0 \in L^m_{\infty e}} \| \mathcal{L}_{\mathbf{x}_0, \mathbf{u}_0} \|_\infty \\ &= \sup_{\mathbf{x}_0 \in L^n_{\infty e}, \mathbf{u}_0 \in L^m_{\infty e}} \left[\sup_{k \in (0,\infty)} \sum_{l=0}^{k-1} \left\| \mathbf{c}^T \mathbf{\Phi}(k, l+1)\mathbf{B}(l) \right\|_i \right] \\ &= \sup_{k \in (0,\infty)} \left[- \inf_{\mathbf{x}_0 \in L^n_{\infty e}, \mathbf{u}_0 \in L^m_{\infty e}} \sum_{l=0}^{k-1} - \left\| \mathbf{c}^T \mathbf{\Phi}(k, l+1)\mathbf{B}(l) \right\|_i \right] \end{aligned} \tag{2.25}$$

where $L_{\infty e}^{n}$ and $L_{\infty e}^{m}$ are the extended-infinity-norm space as defined in Eq. (2.15) with $p = \infty$. The notations n and m indicate the dimensions of the state variables and input vector, respectively.

■

2.3 Stability Condition for a Class of PI Fuzzy Control System

Consider a class of nonlinear system that can be represented in an input and output form as shown in Eq. (2.1) and a proportional-integral fuzzy controller in a feedback closed loop system as shown in Figure 2-1. The summation symbol represents the integration operation. The controller uses two input signals: error (e) and change in error (r), which are defined by the following formulas:

$$e(k) = y_{ref}(k) - y(k) \tag{2.26}$$

$$r(k) = \frac{e(k) - e(k-1)}{T} \tag{2.27}$$

where $y_{ref}(k)$ is the referenced signal, T is the sampling time and k is the sampling instant.

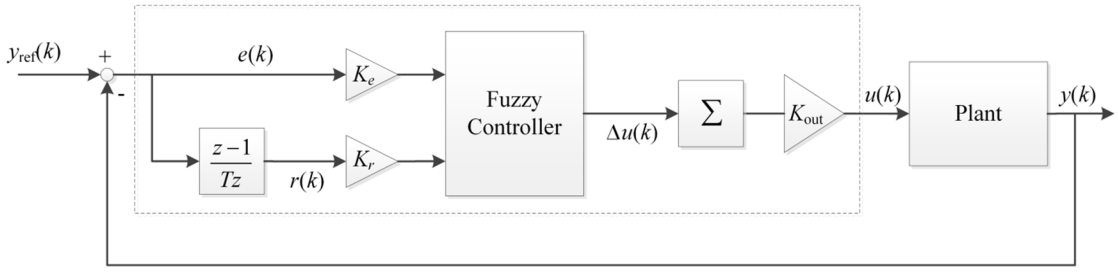

Figure 2-1: The closed loop fuzzy control system

The scaling-factors K_e and K_r of the input signals are adopted to normalize the values of e and r into the range $[-1,1]$:

$$\begin{aligned} \overline{e}(k) &= K_e e(k) \\ \overline{r}(k) &= K_r r(k) \end{aligned} \tag{2.28}$$

The actual control effort $u(k)$ can be computed from the integration of the output of the fuzzy controller $\Delta u(k)$ and the output scaling-factor K_{out}, this makes the controller become a PI type fuzzy controller:

$$\begin{aligned} \overline{u}(k) &= \overline{u}(k-1) + T\Delta u(k) \\ u(k) &= K_{out}\overline{u}(k) \end{aligned} \tag{2.29}$$

For each input, $2n+1$ membership functions are assigned such that the membership functions are distributed evenly with *n* membership functions on the left half plane, *n* membership functions on the right half plane and one membership function at the center. The membership functions of the error and change in error are denoted by E_i and R_j respectively with $i, j = -n, -n+1, \ldots, n-1, n$ (Figure 2-2). Since the input range is scaled into $[-1,1]$, the distance *L* between two adjacent membership functions is equal to $1/n$. The output of the controller $\Delta u(k)$ is computed by using the Mamdani inference method with the fuzzy rules represented in linguistic form as following:

Rule (i, j): *IF* $\overline{e}$ is E_i AND $\overline{r}$ is R_j THEN Δu is $U_{i,j}$

where $U_{i,j}$ is the membership function of the output. Assume that *m* number of output membership functions are used, the distribution of the output membership functions can be found in Figure 2-3.

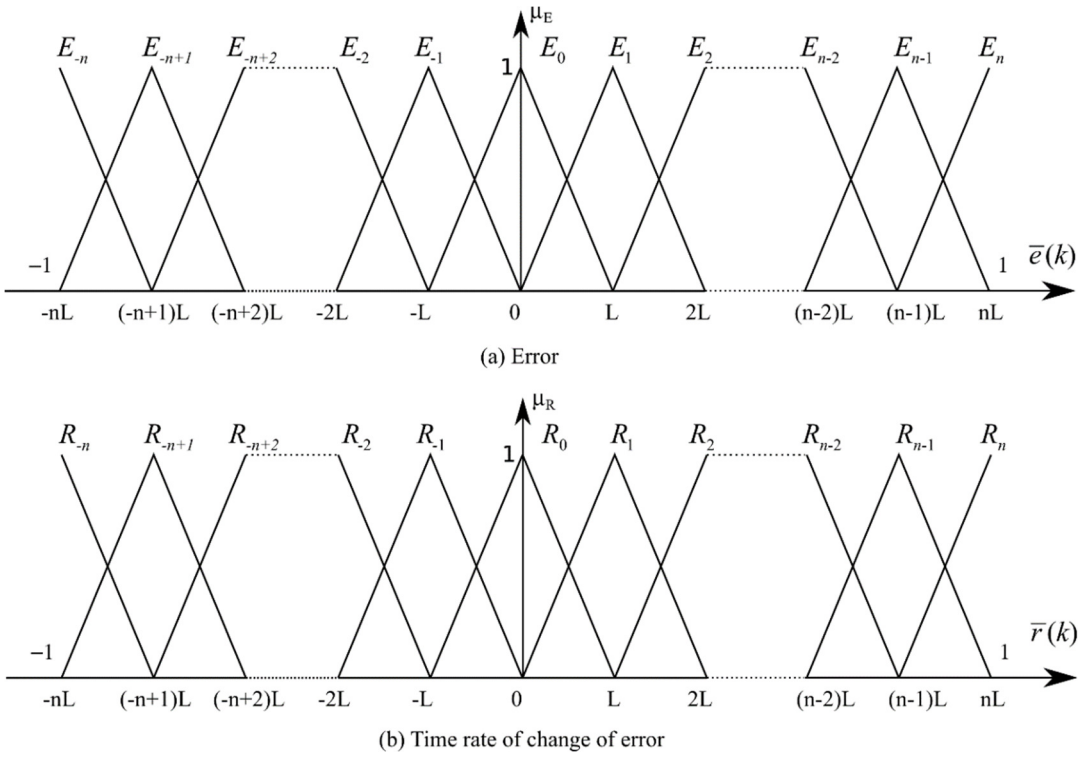

Figure 2-2: Input membership functions.

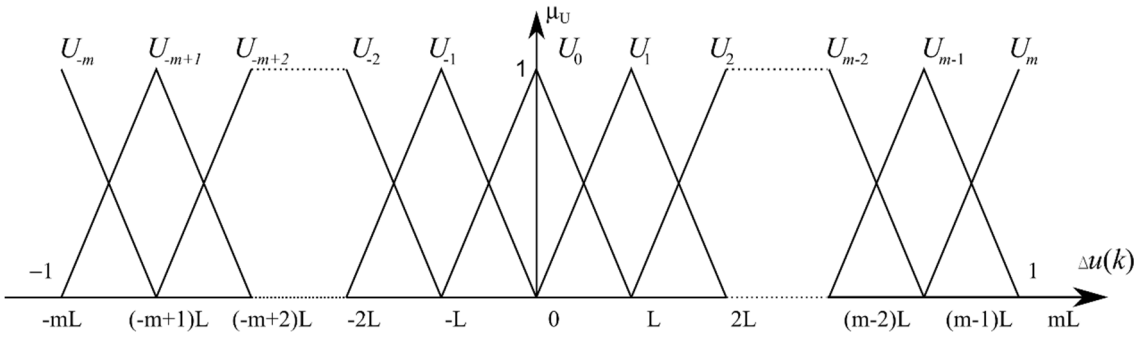

Figure 2-3: Output membership functions.

With the distribution of the input membership functions as shown in Figure 2-2, a maximum of two membership functions for each input will have non-zero values at each instant. Assume that E_p, E_{p+1}, R_q and R_{q+1} ($p, q = -n, -n+1, \ldots, n-1, n$) are the four non-

zero input membership functions of the error and change in error signal, then four fuzzy rules are activated accordingly:

$$\begin{aligned}
&\text{Rule } (p,q): && IF\ \bar{e} \text{ is } \mathrm{E}_p \text{ AND } \bar{r} \text{ is } \mathrm{R}_q \text{ THEN } \Delta u \text{ is } U_{p,q} \\
&\text{Rule } (p+1,q): && IF\ \bar{e} \text{ is } \mathrm{E}_{p+1} \text{ AND } \bar{r} \text{ is } \mathrm{R}_q \text{ THEN } \Delta u \text{ is } U_{p+1,q} \\
&\text{Rule } (p,q+1): && IF\ \bar{e} \text{ is } \mathrm{E}_p \text{ AND } \bar{r} \text{ is } \mathrm{R}_{q+1} \text{ THEN } \Delta u \text{ is } U_{p,q+1} \\
&\text{Rule } (p+1,q+1): && IF\ \bar{e} \text{ is } \mathrm{E}_{p+1} \text{ AND } \bar{r} \text{ is } \mathrm{R}_{q+1} \text{ THEN } \Delta u \text{ is } U_{p+1,q+1}
\end{aligned}$$

Depending on the location of error and change in error with respect to the centers of the non-zero membership functions, the stability problem can be by investigated dividing it into eight different cases as shown in Figure 2-4 and Table 2-1.

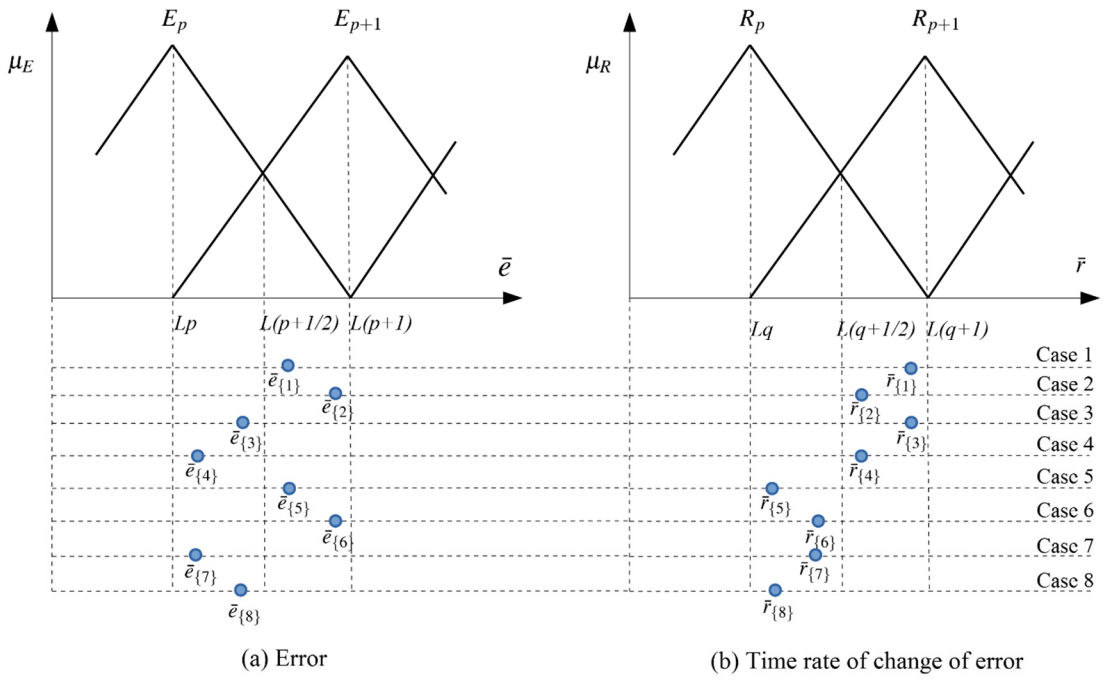

Figure 2-4: Locations of the error and the time rate of change of the error in relation to the activated membership functions.

Table 2-1: Conditions of error and rate of change in error.

Case	Conditions of the error and the time rate of change of the error
1	$L\left(p+\frac{1}{2}\right)<\bar{e}<L(p+1)$ AND $L\left(q+\frac{1}{2}\right)<\bar{r}<L(q+1)$ AND $\bar{e}-L\left(p+\frac{1}{2}\right)<\bar{r}-L\left(q+\frac{1}{2}\right)$
2	$L\left(p+\frac{1}{2}\right)<\bar{e}<L(p+1)$ AND $L\left(q+\frac{1}{2}\right)<\bar{r}<L(p+1)$ AND $\bar{e}-L\left(p+\frac{1}{2}\right)>\bar{r}-L\left(q+\frac{1}{2}\right)$
3	$Lp<\bar{e}<L\left(p+\frac{1}{2}\right)$ AND $L\left(q+\frac{1}{2}\right)<\bar{r}<L(q+1)$ AND $L\left(p+\frac{1}{2}\right)-\bar{e}<\bar{r}-L\left(q+\frac{1}{2}\right)$
4	$Lp<\bar{e}<L\left(p+\frac{1}{2}\right)$ AND $L\left(q+\frac{1}{2}\right)<\bar{r}<L(q+1)$ AND $L\left(p+\frac{1}{2}\right)-\bar{e}>\bar{r}-L\left(q+\frac{1}{2}\right)$
5	$L\left(p+\frac{1}{2}\right)<\bar{e}<L(p+1)$ AND $Lq<\bar{r}<L\left(q+\frac{1}{2}\right)$ AND $\bar{e}-L\left(p+\frac{1}{2}\right)<L\left(q+\frac{1}{2}\right)-\bar{r}$
6	$L\left(p+\frac{1}{2}\right)<\bar{e}<L(p+1)$ AND $Lq<\bar{r}<L\left(q+\frac{1}{2}\right)$ AND $\bar{e}-L\left(p+\frac{1}{2}\right)>L\left(q+\frac{1}{2}\right)-\bar{r}$
7	$Lp<\bar{e}<L\left(p+\frac{1}{2}\right)$ AND $Lq<\bar{r}<L\left(q+\frac{1}{2}\right)$ AND $\bar{e}-Lp<\bar{r}-Lq$
8	$Lp<\bar{e}<L\left(p+\frac{1}{2}\right)$ AND $Lq<\bar{r}<L\left(q+\frac{1}{2}\right)$ AND $\bar{e}-Lp>\bar{r}-Lq$

By utilizing the small gain theorem, an approach similar to that proposed by [13] is used in the current work to obtain the stability condition for a class of fuzzy control systems. However, to investigate the stability of the fuzzy control system, Chen and Ying [13] analyzed the structure of the fuzzy controller based on the locations of the error and the change of the error with respect to zero. Hence, the upper bounds of the fuzzy controller have different values whenever the error or the time rate of change of the error moves from one membership function to the other. The stability analysis cannot be easily extended since the complexity of the problem will grow significantly when the numbers of input and output membership functions are increased. Therefore, only fuzzy controllers with two input and three output membership functions were analyzed by Chen and Ying [13]. In this work, the stability theorem is developed based on the locations of the error and the time rate of change of the error with respect to the activated membership functions, as shown in Figure 2-4 and Table 2-1. Since the upper bounds of the fuzzy controller have been found to have similar values in each location, the results can be generalized for fuzzy controllers with large numbers of input and output membership functions.

By calculating the control effort based on the error and change in error signals for all the cases (APPENDIX A to APPENDIX H), the change in control output $\Delta u(k)$ can be formulated into the following form:

$$\Delta u(k) = \frac{G_e K_e e + G_r K_r r + C}{D} \tag{2.30}$$

where the parameters G_e, G_r, C and D are given in Table 2-2 and Table 2-3.

Table 2-2: Values of G_e, G_r, and D.

Case	G_e	G_r	D
1	$-U_{p,q+1}+U_{p+1,q+1}$	$-U_{p,q}-U_{p+1,q}$	$2qL+3L-2K_r r$
2	$-U_{p,q}-U_{p,q+1}$	$-U_{p+1,q}+U_{p+1,q+1}$	$2Lp+3L-2K_e e$
3	$-U_{p,q+1}+U_{p+1,q+1}$	$-U_{p,q}-U_{p+1,q}$	$2qL+3L-2K_r r$
4	$U_{p+1,q}+U_{p+1,q+1}$	$-U_{p,q}+U_{p,q+1}$	$2K_e e+L-2Lp$
5	$-U_{p,q}+U_{p+1,q}$	$U_{p,q+1}+U_{p+1,q+1}$	$2K_r r-2qL+L$
6	$-U_{p,q}-U_{p,q+1}$	$-U_{p+1,q}+U_{p+1,q+1}$	$2Lp+3L-2K_e e$
7	$U_{p+1,q}+U_{p+1,q+1}$	$-U_{p,q}+U_{p,q+1}$	$2K_e e+L-2Lp$
8	$-U_{p,q}+U_{p+1,q}$	$U_{p,q+1}+U_{p+1,q+1}$	$2K_r r-2qL+L$

Table 2-3: Value of C.

Case	C
1	$qL\left(U_{p,q}+U_{p+1,q}\right)+pL\left(U_{p,q+1}-U_{p+1,q+1}\right)+L\left(U_{p,q}+U_{p+1,q}+U_{p,q+1}\right)$
2	$qL\left(U_{p+1,q}-U_{p+1,q+1}\right)+pL\left(U_{p,q}+U_{p,q+1}\right)+L\left(U_{p,q}+U_{p+1,q}+U_{p,q+1}\right)$
3	$qL\left(U_{p,q}+U_{p+1,q}\right)+pL\left(U_{p,q+1}-U_{p+1,q+1}\right)+L\left(U_{p,q}+U_{p+1,q}+U_{p,q+1}\right)$
4	$qL\left(U_{p,q}-U_{p,q+1}\right)+pL\left(-U_{p+1,q}-U_{p+1,q+1}\right)+LU_{p,q}$
5	$qL\left(-U_{p,q+1}-U_{p+1,q+1}\right)+pL\left(U_{p,q}-U_{p+1,q}\right)+LU_{p,q}$
6	$qL\left(U_{p+1,q}-U_{p+1,q+1}\right)+pL\left(U_{p,q}-U_{p,q+1}\right)+L\left(U_{p,q}+U_{p+1,q}+U_{p,q+1}\right)$
7	$qL\left(U_{p,q}-U_{p,q+1}\right)+pL\left(U_{p+1,q}-U_{p+1,q+1}\right)+LU_{p,q}$
8	$qL\left(-U_{p,q+1}-U_{p+1,q+1}\right)+pL\left(U_{p,q}-U_{p+1,q}\right)+LU_{p,q}$

From here, the stability condition for nonlinear PI fuzzy control systems can be stated as follows:

Theorem 2: Consider a class of nonlinear systems that is described in the form given by Eq. (2.1) and the PI fuzzy control algorithm given in Eq. (2.29). The conditions for the fuzzy control system to be input-and-output stable are as follows:

1. The nonlinear process has a finite p-gain: $\| \mathcal{N} \|_p < \infty$

2. The maximum output scaling factor of the PI fuzzy controller satisfies the following condition:

$$K_{out} \le K_{\max} = \frac{L}{2\left(K_e T + K_r\right) \| \mathcal{N} \|_p} \tag{2.31}$$

Proof: First, an equivalent closed-loop system to the original fuzzy control system shown in Figure 2-1 is constructed. The equivalent system includes two nonlinear processes connected in a feedback loop (Figure 2-5): S_1 and S_2, which are defined as follows:

$$\begin{aligned} S_1(e_1(k)) &= T\Delta u(k) = T\frac{\left(G_e K_e + \frac{G_r K_r}{T}\right)e(k) - \frac{G_r K_r}{T}e(k-1) + C}{D} \\ S_2(e_2(k)) &= \mathcal{N}(u(k)) = \mathcal{N}(K_{out} e_2(k)) \end{aligned} \tag{2.32}$$

where G_e, G_r, C and D are given in Table 2-2 and Table 2-3, $\mathcal{N}(u(k))$ is the nonlinear operator that represents the plant. The inputs of the equivalent closed-loop system are u_1 and u_2:

$$u_1(k) = y_{ref}(k), u_2(k) = \frac{\overline{u}(k-1)}{K_{out}} \tag{2.33}$$

From the schematic diagram in Figure 2-5, the values of $e_1(k)$ and $e_2(k)$ can be found as follows:

$$e_1(k) = u_1(k) - S_2(e_2(k)) = y_d(k) - \mathcal{N}(u(k)) = e(k) \tag{2.34}$$

$$e_2(k) = S_1(e_1(k)) + u_2(k) = T\Delta u(k) + \frac{\bar{u}(k-1)}{K_{out}} = \frac{u(k)}{K_{out}} = \bar{u}(k) \tag{2.35}$$

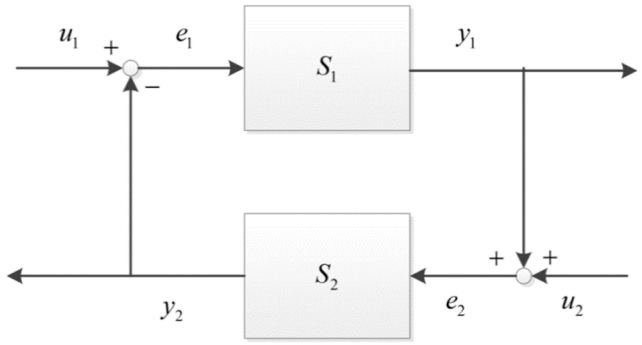

Figure 2-5: An equivalent closed-loop control system.

APPENDIX A to APPENDIX H show that the gain of the operator S_1 can be calculated by:

$$\|S_1\|_p = \gamma_1 = \frac{2(K_e T + K_r)}{L}, \tag{2.36}$$

which is a finite number. By applying the small gain theorem to the feedback system in Figure 2-5, the requirements for the fuzzy closed-loop system to be input-output stable are as follows:

$$\gamma_2 = K_{out} \|\mathcal{N}\|_p < \infty \text{ and } \gamma_1\gamma_2 < 1 \tag{2.37}$$

Because $K_{out} < \infty$, by substituting γ_1 and γ_2 found above into Eq. (2.37), the stability requirements become:

$$\|\mathcal{N}\|_p < \infty \text{ and } \frac{2\left(K_e T + K_r\right)}{L} K_{out} \|\mathcal{N}\|_p < 1 \tag{2.38}$$

Therefore, the maximum output scaling factor of the fuzzy controller is as follows:

$$K_{\max} = \frac{L}{2\left(K_e T + K_r\right) \| \mathcal{N} \|_p} \tag{2.39}$$

■

Theorem 2 provides a systematic stability condition for controlling nonlinear systems by using PI fuzzy controllers. The proposed stability condition is a simple design practice since it only requires the output scaling-factor of a PI fuzzy controller to be bounded.

2.4 Fuzzy Controller with Self-Tuning Output Scaling-Factor

Consider a class of single-input single-output nonlinear dynamic systems that can be represented in an input and output form as described in Eq. (2.1). Further assume that the nonlinear system has a finite p-gain. Based on the stability theorem developed in section 2.3, a novel multilevel fuzzy controller (MLFC) with self-tuning output scaling-factor is proposed in this section. The first layer of the proposed controller acts as a conventional fuzzy controller while the second and third layers are used to tune the output scaling factor of the first layer.

Figure 2-6 describes the implementation of the proposed fuzzy controller in the closed loop control system. The control effort $u(k)$ that drives the plant can be computed as follows:

$$\begin{aligned} \overline{u}(k) &= \overline{u}(k-1) + T\Delta u(k) \\ u(k) &= K_{out}\overline{u}(k) \end{aligned} \tag{2.40}$$

where $\Delta u(k)$ is the output of the first layer and K_{out} is the output scaling factor, which can be adjusted by the second and third layers.

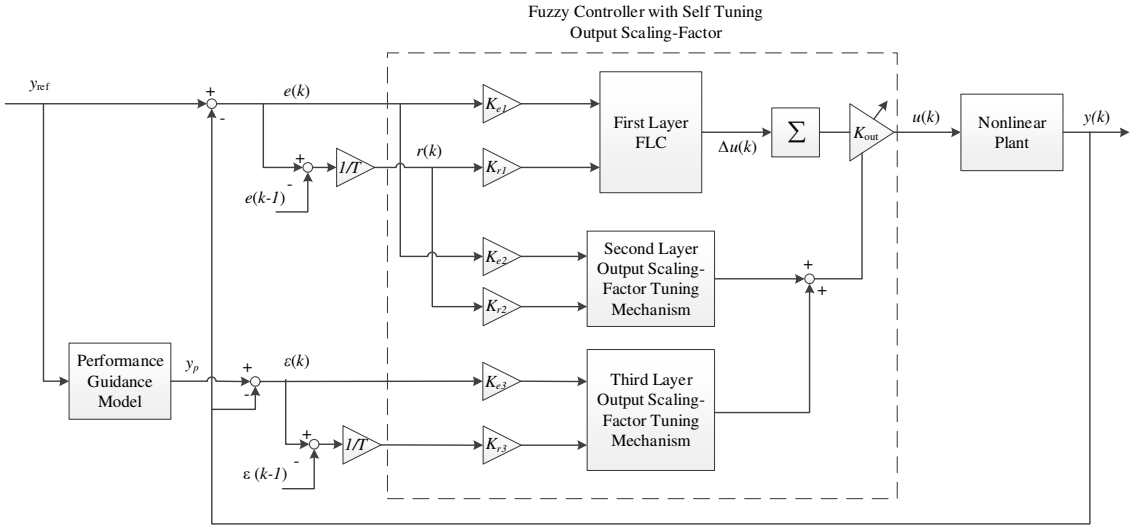

Figure 2-6: Multilevel fuzzy control system with self-tuning output scaling factor.

As shown in Figure 2-6, the first layer fuzzy mechanism uses two input signals, which are the error $e(k)$ and the time rate of change of error $r(k)$:

$$e(k) = y_{ref}(k) - y(k), \qquad r(k) = \frac{e(k) - e(k-1)}{T} \tag{2.41}$$

where $y_{ref}(k)$ is the reference signal, T is the sampling time, and k is the sampling instant. The input gains K_{e1} and K_{r1} of the first layer are adopted to normalize the values of $e(k)$ and $r(k)$:

$$\overline{e}(k) = K_{e1} e(k), \qquad \overline{r}(k) = K_{r1} r(k) \tag{2.42}$$

Each input of the first layer has $2n+1$ membership-functions. The membership functions of the error and change in error are denoted by E_i and R_j respectively with

$i, j = -n, -n+1, \ldots, n-1, n$ (Figure 2-2). The membership functions of the output are denoted by $U_{i,j}$.

The fuzzy rules to calculate the controller output $\Delta u(k)$ are presented in linguistic form as follows:

$$\text{Rule } (i, j)\text{: } IF\ \overline{e} \text{ is } \mathrm{E}_i \text{ AND } \overline{r} \text{ is } \mathrm{R}_j \text{ THEN } \Delta u \text{ is } U_{i,j} \tag{2.43}$$

where $U_{i,j}$ is the output membership function corresponding to the input membership functions E_i and R_j. The rule base of the first layer (Table 2-4) is similar to the conventional PI fuzzy controller and can be regarded as a human expert who makes the decision for control effort based on the input signals. In Table 2-4 [9], the entries near the center position, where the output signal is near the set point, always have smaller values. A small control effort provides a fast convergence rate and reduces the overshoot when the signal is near the set points. As the signal moves away from the set point, the control effort increases in order to reduce the transient time. It should also be noted that the rule-base table is symmetric about the set point.

The second layer (Figure 2-6) uses the error and the time rate of change of the error signals to adjust the output scaling factor of the first layer to reduce the rise time and suppress the oscillation of the system output. In this layer, the change in the output scaling-factor $\Delta K_\alpha(k)$ is computed by using the following fuzzy rules:

$$\text{Rule } (i,j)\text{: If } K_{e2} \cdot e \text{ is } E_i \text{ and } K_{r2} \cdot r \text{ is } R_j \text{ then } \Delta K_\alpha(k) \text{ is } D_\alpha \tag{2.44}$$

where K_{e2} and K_{r2} are the input gains of the second layer, the notation D_α is the linguistic value of $\Delta K_\alpha(k)$. The rule base for the second layer (Table 2-5) was developed based on

the fuzzy rule base designed by Mudi and Pal [28]. However, while Mudi and Pal's objective was to determine the value of the scaling factor based on the error and the time rate of change of the error signal, the rule base in this paper is designed for the calculation of the necessary change in the output scaling factor. As shown in Table 2-5, if there is a large error in the output signal while the output is moving away from the reference signal, the scaling factor is increased ($D_\alpha \to 0.5$) so that the rise and settling times can be reduced. When the system output is moving into the reference signal or the error and the time rate of change of the error are very small, the scaling factor is reduced $(D_\alpha \to -0.5)$ to suppress the amount of overshoot. This rule base is not unique and modifications may be made in accordance with desired system responses.

Table 2-4: Rule base of the first and third layer of the proposed MLFC.

		Time rate of change of the error										
Error		-1.0	-0.8	-0.6	-0.4	-0.2	0.0	0.2	0.4	0.6	0.8	1.0
	-1.0	1.00	1.00	1.00	1.00	1.00	1.00	0.80	0.60	0.30	0.10	0.00
	-0.8	1.00	1.00	1.00	1.00	1.00	0.80	0.60	0.30	0.10	0.00	-0.10
	-0.6	1.00	1.00	1.00	1.00	0.80	0.60	0.30	0.10	0.00	-0.10	-0.30
	-0.4	1.00	1.00	1.00	0.80	0.60	0.30	0.10	0.00	-0.10	-0.30	-0.60
	-0.2	1.00	1.00	0.80	0.60	0.30	0.11	0.00	-0.10	-0.30	-0.60	-0.80
	0.0	1.00	0.80	0.60	0.30	0.10	0.00	-0.10	-0.30	-0.60	-0.80	-1.00
	0.2	0.80	0.60	0.30	0.10	0.00	-0.10	-0.31	-0.60	-0.80	-1.00	-1.00
	0.4	0.60	0.30	0.10	0.00	-0.10	-0.30	-0.60	-0.80	-1.00	-1.00	-1.00
	0.6	0.30	0.10	0.00	-0.10	-0.30	-0.60	-0.80	-1.00	-1.00	-1.00	-1.00
	0.8	0.10	0.00	-0.10	-0.30	-0.60	-0.80	-1.00	-1.00	-1.00	-1.00	-1.00
	1.0	0.00	-0.10	-0.30	-0.60	-0.80	-1.00	-1.00	-1.00	-1.00	-1.00	-1.00

Table 2-5: Fuzzy rule base of the second layer of the proposed MLFC.

		Time rate of change of the error						
Error		-1	-0.7	-0.3	0	0.3	0.7	1
	-1	0.5	0.5	0.5	0.3	0.1	-0.1	-0.3
	-0.8	0.5	0.5	0.3	0.1	-0.1	-0.3	-0.5
	-0.6	0.5	0.3	0.1	-0.1	-0.3	-0.5	-0.5
	-0.4	0.3	0.1	-0.1	-0.3	-0.5	-0.5	-0.5
	-0.2	0.1	-0.1	-0.3	-0.4	-0.5	-0.5	-0.5
	0	-0.5	-0.5	-0.5	-0.5	-0.5	-0.5	-0.5
	0.2	-0.5	-0.5	-0.5	-0.4	-0.3	-0.1	0.1
	0.4	-0.5	-0.5	-0.5	-0.3	-0.1	0.1	0.3
	0.6	-0.5	-0.5	-0.3	-0.1	0.1	0.3	0.5
	0.8	-0.5	-0.5	-0.1	0.1	0.3	0.5	0.5
	1	-0.3	-0.1	0.1	0.3	0.5	0.5	0.5

In order to achieve the desired system performances such as rise time, settling time, and percent overshoot, the designer can specify a performance guidance model for the tuning process. The objective of the third layer is to make the output of the closed-loop system approach that of the performance guidance model. This layer uses the performance error ϵ and the time rate of change of the performance error $\dot{\epsilon}$ between the output of the control system and the reference model to tune the output scaling factor:

$$\epsilon(k) = y_p(k) - y(k), \quad \dot{\epsilon}(k) = \frac{\epsilon(k) - \epsilon(k-1)}{T} \tag{2.45}$$

where $y_p(k)$ is the output of the performance guidance model. The performance error and the time rate of change of performance error signals have membership functions similar to those of the output error and the time rate of change of the error (Figure 2-2).

Since the output error $e(k)$ and the time rate of change of the error signal $r(k)$ always exist whenever there is a change in command signals, the performance errors $\epsilon(k)$ and $\dot{\epsilon}(k)$ are used for the third layer instead of the output error signals. This way, the tuning of the third layer can be minimized when the system output has approached the performance guidance model output. The rule base of the first layer (Table 2-4) is applied in the third layer since they have similar functional objectives. Similar to the first layer, the Mamdani fuzzy inference mechanism is also applied in the third layer to compute the output scaling factor updating value $\Delta K_\beta(k)$ by the following fuzzy rules:

$$\text{Rule } (i,j): \text{If } K_{e3} \cdot e \text{ is } E_i \text{ and } K_{r3} \cdot r \text{ is } R_j \text{ then } \Delta K_\beta(k) \text{ is } D_\beta \tag{2.46}$$

where K_{e3} and K_{r3} are the input gains of the second layer, the notation D_β is the linguistic value of $\Delta K_\beta(k)$.

With the addition of the second and third layers, the output scaling-factor of the first layer can be calculated by using the following formula:

$$K_{out}(k) = \min\left(K_{out}(k-1) + \alpha \Delta K_\alpha(k) + \beta \Delta K_\beta(k), K_{\max}\right) \tag{2.47}$$

where α and β are the adaptation rates of the second layer and the third layer, respectively. Based on Theorem 2, the minimum function in Eq. (2.47) ensures that the output scaling factor K_{out} does not exceed the maximum value $K_{\max}$ at which the control system remains stable:

$$K_{\max} = \frac{L}{2\left(K_e T + K_r\right)\left\|\mathcal{N}\right\|_p} \tag{2.48}$$

where $\left\|\mathcal{N}\right\|_p$ is the p-gain of the nonlinear plant.

2.5 Simulation Results on a Three-Dimensional Tower Crane System

Performance comparisons between the MLFC with self-tuning algorithm and the robust adaptive fuzzy controller (RAFC) proposed by Wu et al. [72] are presented in this section. MATLAB/SIMULINK simulations were conducted on a three-dimensional tower crane system [72].

The control variables of the tower crane system are the tower motor voltage M_θ (V) and the trolley motor voltage M_F (V):

$$u_1 = M_\theta,\ u_2 = M_F \tag{2.49}$$

The distance between the trolley and the tower is denoted as x_p, the slew angle of the tower is θ_r. The variables x_p and θ_r are also the outputs of the system:

$$y_1 = x_p,\ y_2 = \theta_r \tag{2.50}$$

The notations α and β are the deflection angles of the payload in the Y-Z, and the X-Z plane. By using $x_{11} = x_p$, $x_{12} = \dot{x}_p$, $x_{21} = \beta$, $x_{22} = \dot{\beta}$, $x_{31} = \theta_r$, $x_{32} = \dot{\theta}_r$, $x_{41} = \alpha$, $x_{42} = \dot{\alpha}$ as the state variables, the equations of motion of the tower crane system are [72]:

$$\begin{aligned}
\dot{x}_{12} &= K_{mx}u_1 - m_t g x_{21} + h_1(t)x_{11}(t-\tau_1) + d_1 \\
\dot{x}_{22} &= \frac{K_{mx}}{L}u_1 - \frac{m_t g}{L}x_{21} - \frac{g}{L}x_{21} - \frac{K_{mr}x_{41}u_2}{1+M_r x_{11}^2} - \frac{m_r g x_{11}x_{41}^2}{1+M_r x_{11}^2} + h_2(t)x_{21}(t-\tau_2) + d_2 \\
\dot{x}_{32} &= \frac{K_{mr}u_2 + m_r g x_{11}x_{41}}{1+M_r x_{11}^2} + h_3(t)x_{31}(t-\tau_3) + d_3 \\
\dot{x}_{42} &= \frac{(K_{mr}u_2 + m_r g x_{11}x_{41})x_{21}}{1+M_r x_{11}^2} - \frac{g x_{41}}{L} - \frac{(K_{mr}u_2 + m_r g x_{11}x_{41})x_{11}}{1+M_r x_{11}^2} + h_4(t)x_{41}(t-\tau_4) + d_4
\end{aligned} \tag{2.51}$$

where $\tau_1 = 0.2s$, $\tau_2 = 0.1s$, $\tau_3 = 0.15s$, $\tau_4 = 0.1s$ are time-delay constants, $m_t = m/M$, $m_r = m/J_0$, $M_r = M/J_0$, $h_q(t), q = 1...4$ are time-varying functions:

$$h_1 = h_3 = 0.01\sin(t), \quad h_2 = h_4 = 0.01\cos(t) \tag{2.52}$$

The disturbances d_1, d_2, d_3, and d_4 are functions of time:

$$d_1 = d_3 = 0.1\sin(t)\exp(-0.2t), \quad d_2 = d_4 = 0.1\cos(t)\exp(-0.2t) \tag{2.53}$$

Other system parameters can be found in Table 2-6.

Simple feedback gains can be used to stabilize the plant:

$$u_1 = \gamma_1 - k_{11}x_{11} - k_{12}x_{12}, \quad u_2 = \gamma_2 - k_{31}x_{31} - k_{32}x_{32} - k_{41}x_{41} - k_{42}x_{42} \tag{2.54}$$

where $k_{11} = k_{12} = k_{31} = k_{32} = 1$, $k_{41} = k_{42} = -10$, γ_1 and γ_2 are new system inputs. By substituting u_1 and u_2 in Eq. (2.54) to Eq. (2.51), the equations of the system then become:

$$\begin{aligned}
\dot{x}_{12} &= K_{mx}(\gamma_1 - k_{11}x_{11} - k_{12}x_{12}) - m_t g x_{21} + h_1(t)x_{11}(t-\tau_1) + d_1 \\
\dot{x}_{22} &= \frac{K_{mx}}{L}(\gamma_1 - k_{11}x_{11} - k_{12}x_{12}) - \frac{m_t g}{L}x_{21} - \frac{g}{L}x_{21} - \frac{K_{mr}x_{41}(\gamma_2 - k_{31}x_{31} - k_{32}x_{32} - k_{41}x_{41} - k_{42}x_{42})}{1 + M_r x_{11}^2} \\
&\quad - \frac{m_r g x_{11}x_{41}^2}{1 + M_r x_{11}^2} + h_2(t)x_{21}(t-\tau_2) + d_2 \\
\dot{x}_{32} &= \frac{K_{mr}(\gamma_2 - k_{31}x_{31} - k_{32}x_{32} - k_{41}x_{41} - k_{42}x_{42}) + m_r g x_{11}x_{41}}{1 + M_r x_{11}^2} + h_3(t)x_{31}(t-\tau_3) + d_3 \\
\dot{x}_{42} &= \frac{[K_{mr}(\gamma_2 - k_{31}x_{31} - k_{32}x_{32} - k_{41}x_{41} - k_{42}x_{42}) + m_r g x_{11}x_{41}]x_{21}}{1 + M_r x_{11}^2} - \frac{g x_{41}}{L} \\
&\quad - \frac{\left[K_{mr}(\gamma_2 - k_{31}x_{31} - k_{32}x_{32} - k_{41}x_{41} - k_{42}x_{42}) + m_r g x_{11}x_{41}\right]x_{11}}{1 + M_r x_{11}^2} + h_4(t)x_{41}(t-\tau_4) + d_4
\end{aligned} \tag{2.55}$$

Two FBFNs were then used to model the outputs $y_1 = x_{11} = \mathcal{N}_1(\gamma_1)$ and $y_2 = x_{31} = \mathcal{N}_2(\gamma_2)$.

Table 2-6: Parameters of the tower crane system [72].

Parameter	Notation	Value
Payload length	L	0.1 m
Mass of trolley	M	0.465 kg
Mass of payload	m	0.125 kg
Motor equivalent moment of inertia	J_0	0.877 $kg.m^2$
Acceleration gain for trolley servo	K_{mx}	0.9 m/s^2
Acceleration gain for tower servo	K_{mr}	3.33 rad/s^2V

By using least square methods and genetic algorithms [73], the training of the FBFNs was conducted on MATLAB. Figure 2-7 shows the non-dimensional error indices (NDEI) during the training process. Two FBFN models with 61 and 26 hidden nodes were obtained to approximate the first and the second process, respectively:

Rule i ($\gamma_1 - y_1$): If $\gamma_1(k-1) = A_{11}^i, \ldots, \gamma_1(k-6) = A_{16}^i, y_1(k-1) = B_{11}^i, \ldots, y_1(k-6) = B_{16}^i,$

then $y_1(k) = b_1^i$

Rule i ($\gamma_2 - y_2$): If $\gamma_2(k-1) = A_{21}^i, \ldots, \gamma_2(k-3) = A_{23}^i, y_2(k-1) = B_{21}^i, \ldots, y_2(k-3) = B_{23}^i,$

then $y_2(k) = b_2^i$

From the obtained FBFNs, linearized models of the systems at different operating conditions were calculated by Eq. (2.10). Their H∞ norms can then be found by using the non-smooth Newton's method [68] and are given in Figure 2-8 for all the training data sets. The L_2-gains of the FBFNs were estimated by taking the maximum values of the linearized models' H∞ norms:

$$\| \mathcal{N}_1 \|_2 = 0.1, \quad \| \mathcal{N}_2 \|_2 = 0.04 \tag{2.56}$$

where $\| \mathcal{N}_1 \|_2$ and $\| \mathcal{N}_2 \|_2$ denote the L_2-gains of the first process ($\gamma_1 - y_1$), and the second process $(\gamma_2 - y_2)$, respectively.

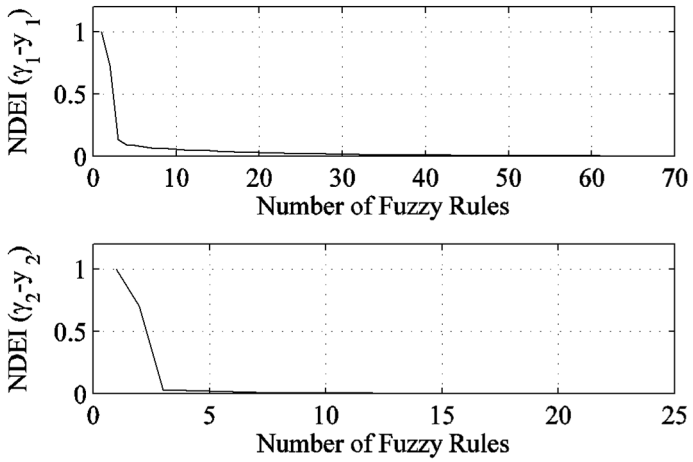

Figure 2-7: NDEI during FBFN training of the tower crane system.

The reference signals for the trolley translational position and the jib angular position are 0.06 m and 0.6 rad, respectively. Two MLFCs with self-tuning output scaling-factors were used to control the two subsystems. The scaling factors for three layers of each fuzzy controller were selected as follows:

First process ($\gamma_1 - y_1$):

$$K_{e1} = 6,\ K_{r1} = 0.1,\ K_{e2} = 10,\ K_{r2} = 15,\ K_{e3} = 30,\ K_{r3} = 30,$$
$$K_{out1(\text{initial})} = 3,\ \alpha = 0.01,\ \beta = 2 \tag{2.57}$$

Second process ($\gamma_2 - y_2$):

$$K_{e1} = 1,\ K_{r1} = 0.1,\ K_{e2} = 0.1,\ K_{r2} = 5,\ K_{e3} = 0.05,\ K_{r3} = 30,$$
$$K_{out1(\text{initial})} = 1,\ \alpha = 0.001,\ \beta = 0.01 \tag{2.58}$$

Discrete linear models with the following transfer functions were chosen as the performance guidance models:

$$Y_1(z) = \frac{0.005}{z - 0.995}\Gamma_1(z), \qquad Y_2(z) = \frac{0.005}{z - 0.995}\Gamma_2(z) \tag{2.59}$$

here $\Gamma_1(z)$ and $\Gamma_2(z)$ are the input functions in frequency domain, $Y_1(z)$ and $Y_2(z)$ are the output functions in frequency domain.

By using the stability criteria given in Eq. (2.39), the maximum output scaling-factor of the MLFCs can be calculated as follows:

$$K_{\max 1} = \frac{L}{2\left(K_e T + K_r\right) \| \mathcal{N}_1 \|_2} = \frac{0.2}{2(6 \cdot 0.01 + 0.1) \cdot 0.1} = 6.25 \tag{2.60}$$

$$K_{\max 2} = \frac{L}{2\left(K_e T + K_r\right) \| \mathcal{N}_2 \|_2} = \frac{0.2}{2(1 \cdot 0.01 + 0.1) \cdot 0.04} = 22.7 \tag{2.61}$$

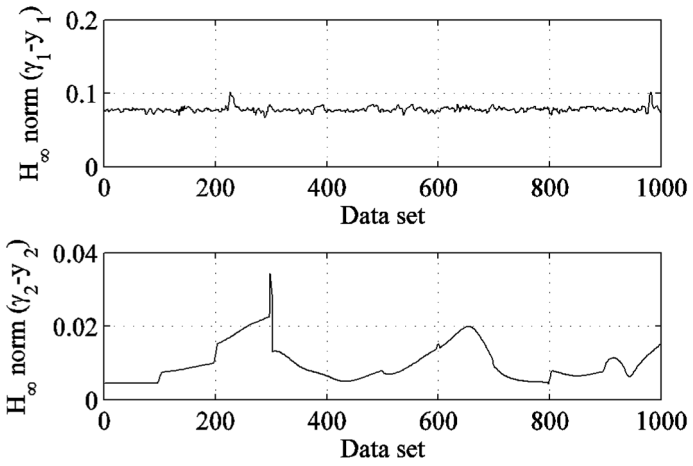

Figure 2-8: H∞ norm of the tower crane's local systems.

Figure 2-9 shows the responses of the tower crane system controlled by the MLFC with self-tuning output scaling-factor versus the RAFC. It shows that both outputs of the tower crane controlled by the MLFC with self-tuning output scaling-factor achieve steady-state values in approximately five seconds, which is much faster compared with those controlled by the RAFC. There is also significantly less oscillation with the MLFC with

self-tuning output scaling-factor due to the adaptation of the output scaling factors as shown in Figure 2-10, even though the control efforts of the MLFC with self-tuning output scaling-factor are smoother than the control efforts of the RAFC. The self-tuning capability also makes the overshoots of both outputs of the MLFC control system less than ten percent.

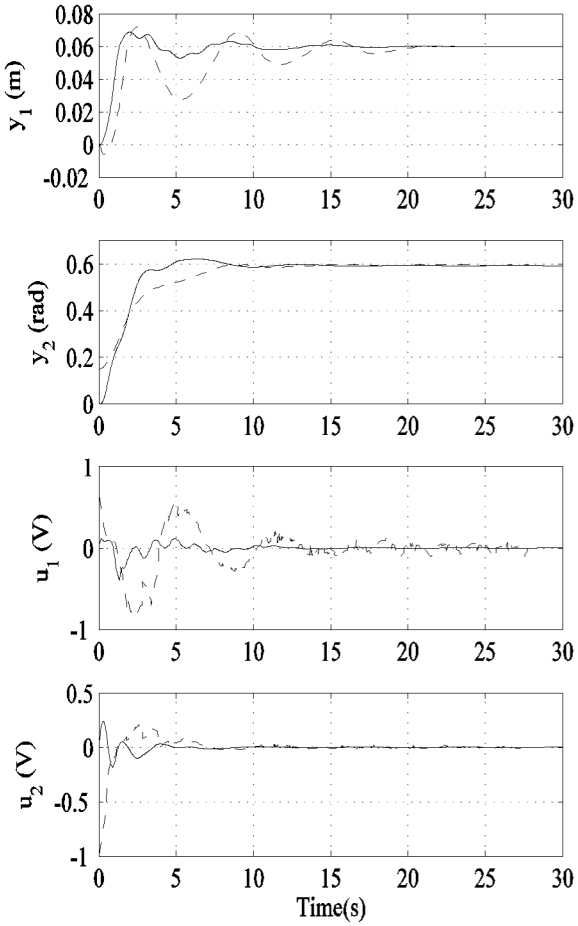

Figure 2-9: System response comparison between the MLFC with self-tuning output scaling-factor (solid) and RAFC (dash) ($y_{ref1} = 0.06$ m, $y_{ref2} = 0.6$ rad).

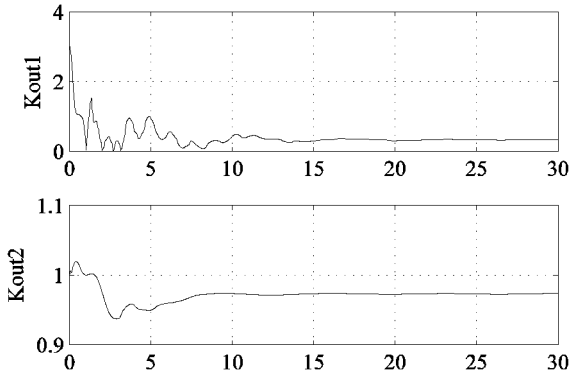

Figure 2-10: Output scaling factor of the MLFC with self-tuning output scaling-factor during control of the tower crane system.

CHAPTER 3. MODELING OF UNSTRUCTURED UNCERTAINTIES AND ROBUST CONTROL OF NONLINEAR DYNAMIC SYSTEMS BASED ON TYPE-2 FUZZY BASIS FUNCTION NETWORKS

As described, Chapter 2 provides a framework for designing Mamdani fuzzy controllers based on the dynamic gains of nonlinear systems. Proportional-integral (PI) Mamdani fuzzy controllers are useful in cases when the state variables of the nonlinear systems are not available during implementation. However, the method can only be applied to a class of single-input single-output nonlinear systems that have finite dynamic gains. For multi-input multi-output nonlinear systems with measurable state variables, Takagi-Sugeno fuzzy controllers can be used to improve the performance of the fuzzy control systems since a linear control design process can be applied to each rule of the Takagi-Sugeno fuzzy model.

However, the performance of Takagi-Sugeno (T-S) fuzzy controllers depends on the accuracy of the Takagi-Sugeno model that is used to approximate the nonlinear system. If there exist uncertainties in the system or the T-S model cannot approximate the nonlinear system well, the stability analysis of the control system is no longer valid. Chapter 3 tackles this problem by proposing a new method to train an interval type-2 fuzzy basis function networks (FBFN) that can capture unstructured uncertainties and model inaccuracy in a class of nonlinear systems. The training algorithm not only further improves the performance of the fuzzy neural network system but also provides a framework to design

a robust T-S fuzzy controller. FBFNs have been used as models for many nonlinear systems in the literature [74]–[76] since a FBFN was proven to be a universal approximator [2]. The antecedent of the interval type-2 FBFN in this study is obtained by using the adaptive least square with genetic algorithm while the interval values of the consequent are obtained by the active set method. A new technique is also proposed to convert the interval type-2 FBFN to an interval type-2 T-S fuzzy model. Based on the interval type-2 T-S model and the interval type-2 FBFN, a robust controller that is not only robust but also produces good transient performance when implemented on nonlinear systems with unstructured uncertainties is presented.

3.1 Training Interval Type-2 FBFN Models by Using Genetic Algorithm and Active Set Method

Consider a class of nonlinear dynamical system with *m* inputs and *n* state variables (*m* and *n* are positive integers), which can be represented by the following state space equation:

$$\mathbf{x}(k+1) = \mathbf{f}(\mathbf{x}(k), \mathbf{u}(k)), \;\; \mathbf{x}(0) = \mathbf{x}_0 \tag{3.1}$$

where $\mathbf{x}(k) = [x_1(k), \ldots, x_n(k)]^{\mathrm{T}}$ is the vector of measurable state variables, $\mathbf{u}(k) = [u_1(k), \ldots, u_m(k)]^{\mathrm{T}}$ is the input vector, k is the time instance, $\mathbf{f}$ is the vector of unknown functions that are assumed to be locally Lipschitz nonlinear:

$$\mathbf{f} = [f_1(k), \ldots, f_n(k)]^{\mathrm{T}} \tag{3.2}$$

The locally Lipschitz property of $\mathbf{f}$ ensures that the solution of the state space equations exists and is unique [77].

It has been proven by Wang and Mendel [2] that a linear combination of fuzzy basis functions are capable of uniformly approximating any real continuous function on a compact set to arbitrary accuracy. In this paper, to approximate a future state of the state variable x_p $(p = 1,\ldots,n)$ of the nonlinear system, an interval type-2 FBFN model can be constructed from the input and measurable state variable data through a set of *J* fuzzy rules, in which rule R^j has the following form:

$$\begin{aligned}\text{Rule } R^j : \text{IF } & x_1(k) \text{ is } X_1^j \text{ AND } \ldots\ x_n(k) \text{ is } X_n^j \text{ AND } u_1(k) \text{ is } U_1^j \text{ AND } \ldots\ u_m(k) \text{ is } U_m^j \\ & \text{THEN } \tilde{x}_p(k+1) = \tilde{Y}^j, \qquad j = 1,\ldots,J\end{aligned} \tag{3.3}$$

where $u_1(k)\ldots u_m(k)$ are the inputs at time instance *k*.

$x_1(k)\ldots x_n(k)$ are the measured state variables.

$\tilde{x}_p(k+1)$ is the future interval value of the state variable x_p.

$X_1^j \ldots X_n^j$ and $U_1^j \ldots U_m^j$ are type-1 fuzzy sets of rule R^j characterized by Gaussian membership functions $\mu_{X_p^j}(x_p)$ and $\mu_{U_q^j}(u_q)$ $(p = 1,\ldots,n;\ q = 1,\ldots,m)$ with the centers c_{Xp}^j, c_{Uq}^j and standard deviations σ_{Xp}^j, σ_{Uq}^j:

$$X_p^j = \left(x_p, \mu_{X_p^j}(x_p)\right), \quad \mu_{X_p^j}(x_p) = \exp\left[-\frac{1}{2}\left(\frac{x_p - c_{Xp}^j}{\sigma_{Xp}^j}\right)^2\right] \tag{3.4}$$

$$U_q^j = \left(u_q, \mu_{U_q^j}(u_q)\right), \quad \mu_{U_q^j}(u_q) = \exp\left[-\frac{1}{2}\left(\frac{u_q - c_{Uq}^j}{\sigma_{Uq}^j}\right)^2\right] \tag{3.5}$$

$\tilde{Y}^j$ is a type-2 interval fuzzy set. $\tilde{Y}^j$ is determined by w_l^j and w_r^j, which are the two end points of its centroid interval set: $\tilde{Y}^j = \left(x, \mu_{\tilde{Y}^j}(x)\right)$, $\mu_{\tilde{Y}^j}(x) = 1$ when x $\in \left[w_l^j \;\; w_r^j \right]$.

By assuming that singleton fuzzification, product inference and centroid defuzzification methods are used in the inferencing process, for a crisp input vector:

$$\mathbf{z} = (z_1, \ldots, z_{m+n}) = (x_1, \ldots, x_n, u_1, \ldots, u_m)^{\mathrm{T}}, \tag{3.6}$$

the output of the type-2 FBFN described in (3.3) is an interval number and can be calculated by [73], [78]:

$$\begin{aligned} \tilde{x}_p(k+1) = [y_l, y_r] &= \left[\frac{\sum_{j=1}^{J} w_l^j \left(\prod_{i=1}^{m+n} \mu_i^j(z_i) \right)}{\sum_{j=1}^{J} \left(\prod_{i=1}^{m+n} \mu_i^j(z_i) \right)}, \frac{\sum_{j=1}^{J} w_r^j \left(\prod_{i=1}^{m+n} \mu_i^j(z_i) \right)}{\sum_{j=1}^{J} \left(\prod_{i=1}^{m+n} \mu_i^j(z_i) \right)} \right] \\ &= \left[\sum_{j=1}^{J} w_l^j p_j(\mathbf{z}), \sum_{j=1}^{J} w_r^j p_j(\mathbf{z}) \right] \end{aligned} \tag{3.7}$$

where $p_j(\mathbf{z}) = \dfrac{\prod_{i=1}^{n} \mu_i^j(z_i)}{\sum_{j=1}^{J} \left(\prod_{i=1}^{n} \mu_i^j(z_i) \right)}$ is the pseudo fuzzy basis function of rule R^j, z_i is the i^{th} element of the crisp input vector $\mathbf{z}$, J is the number of fuzzy rules.

Assume that N input-output training pairs $\{\mathbf{z}_{pt\{i\}}(k), x_{pt\{i\}}(k+1)\}$ (with $i = 1, \ldots, N$) are available, the task of training a type-2 FBFN is to determine the pseudo fuzzy basis functions $p_j(\mathbf{z})$ with $j = 1, \ldots, J$ and the output interval fuzzy set characterized by w_l^j and w_r^j in order to minimize the errors $e_l(i)$, $e_r(i)$, $\delta y_l(i)$ and $\delta y_r(i)$ defined by the following equations:

$$x_{pt\{i\}}(k+1) = \sum_{j=1}^{J} p_j(\mathbf{z}_{pt\{i\}}(k)) w_l^j + e_l(i) + \delta y_l(i) = \sum_{j=1}^{J} p_j(\mathbf{z}_{pt\{i\}}(k)) w_r^j - e_r(i) - \delta y_r(i) \tag{3.8}$$

where $e_l(i)$ and $e_r(i)$ are the training errors, and $\delta y_l(i)$ and $\delta y_r(i)$ are the errors due to system uncertainties. $e_l(i)$, $e_r(i)$, $\delta y_l(i)$ and $\delta y_r(i)$ must be kept positive during the training process to obtain the lower and upper bounds of the output interval fuzzy set. By defining the problem as in Eq. (3.8), the type-2 FBFN accounts for both the uncertainties existing within the nonlinear system as well as the training errors.

The above equations can be rearranged into matrix forms as follows:

$$\mathbf{x}_{pt} = \mathbf{P}\mathbf{w}_l + \boldsymbol{\varepsilon}_l = \mathbf{P}\mathbf{w}_r - \boldsymbol{\varepsilon}_r \tag{3.9}$$

where $\mathbf{x}_{pt} = [x_{pt\{1\}}, \ldots, x_{pt\{2\}}]^{\mathrm{T}}$, $\mathbf{w}_l = [w_{l1}, \ldots, w_{lJ}]^{\mathrm{T}}$, $\mathbf{w}_r = [w_{r1}, \ldots, w_{rJ}]^{\mathrm{T}}$,

$\boldsymbol{\varepsilon}_l = [e_l(1) + \delta y_l(1), \ldots, e_l(N) + \delta y_l(1)]^{\mathrm{T}}$, $\boldsymbol{\varepsilon}_r = [e_r(1) + \delta y_r(1), \ldots, e_r(N) + \delta y_r(1)]^{\mathrm{T}}$ and

$$\mathbf{P} = \begin{bmatrix} p_1(\mathbf{z}_t(1)) & \cdots & p_J(\mathbf{z}_t(1)) \\ \vdots & \ddots & \vdots \\ p_1(\mathbf{z}_t(N)) & \cdots & p_J(\mathbf{z}_t(N)) \end{bmatrix} \tag{3.10}$$

The pseudo fuzzy basis functions $p_j(\mathbf{z})$ with $j = 1, \ldots, J$ can be found in a similar way as in the type-1 FBFN [73]. By using the genetic algorithm, the method starts with a preset pseudo fuzzy basis function and sequentially selects basis functions that will decrease the error the most. In other words, each added pseudo fuzzy basis function will maximize the following error reduction measure:

$$[err] = \| \mathbf{P}\mathbf{P}^{+}\mathbf{y}_t \|^2 \tag{3.11}$$

where $\mathbf{P}^{+}$ is the pseudo inverse of the pseudo fuzzy basis function matrix $\mathbf{P}$. The pseudo-fuzzy basis function $p_j(\mathbf{z})$ is characterized by a nonlinear parameter set $\lambda_j = \{\mathbf{c}_j, \boldsymbol{\sigma}_j\}$, where $\mathbf{c}_j = (c_1^j, \ldots, c_{m+n}^j)$ and $\boldsymbol{\sigma}_j = (\sigma_1^j, \ldots, \sigma_{m+n}^j)$ are the vectors of the means and standard deviations of input membership functions. In order to obtain the optimal values of these

parameters, the parameters are encoded into binary strings and the evolution of the population is conducted through reproduction, cross over and mutation. The fitness of each individual in the population is chosen to be a linear function of the error:

$$g(\lambda) = a[err] + b \tag{3.12}$$

where *a* and *b* are scalar parameters. The use of genetic algorithms for fuzzy basis function networks has been proven to be effective for obtaining the pseudo fuzzy basis functions [49]. The training can be done offline based on the input and output data of the nonlinear system. The parameters of the model will be used to design the controller. Hence real-time computation with generic algorithms is not required during the implementation of the controller.

Once the response vector matrix $\mathbf{P}$ is determined, finding $\mathbf{w}_l$ and $\mathbf{w}_r$ becomes two constrained linear least-squares problems:

$$\begin{cases} \min\limits_{\mathbf{w}_l} \left\| \mathbf{P}\mathbf{w}_l - \mathbf{y}_t \right\|_2, \mathbf{P}\mathbf{w}_l \le \mathbf{y}_t \\ \min\limits_{\mathbf{w}_r} \left\| \mathbf{P}\mathbf{w}_r - \mathbf{y}_t \right\|_2, \mathbf{P}\mathbf{w}_r \ge \mathbf{y}_t \end{cases} \tag{3.13}$$

In this work, only the first case is considered since the second case can be transformed to the first case by replacing the condition $\mathbf{P}\mathbf{w}_r \ge \mathbf{y}_t$ with an equivalent condition $-\mathbf{P}\mathbf{w}_r \le -\mathbf{y}_t$.

With $\mathbf{H} = \mathbf{P}^{\mathrm{T}}\mathbf{P}$ and $\mathbf{c} = -\mathbf{P}^{\mathrm{T}}\mathbf{y}_t$, the following can be obtained:

$$\begin{aligned} \frac{1}{2}\left\| \mathbf{P}\mathbf{w}_l - \mathbf{y}_t \right\|_2 &= \frac{1}{2}\left(\mathbf{P}\mathbf{w}_l - \mathbf{y}_t \right)^{\mathrm{T}} \left(\mathbf{P}\mathbf{w}_l - \mathbf{y}_t \right) \\ &= \frac{1}{2}\mathbf{w}_l^{\mathrm{T}}\mathbf{P}^{\mathrm{T}}\mathbf{P}\mathbf{w}_l - \mathbf{y}_t^{\mathrm{T}}\mathbf{P}\mathbf{w}_l + \frac{1}{2}\mathbf{y}_t^{\mathrm{T}}\mathbf{y}_t \\ &= \frac{1}{2}\mathbf{w}_l^{\mathrm{T}}\mathbf{H}\mathbf{w}_l + \mathbf{c}^{\mathrm{T}}\mathbf{w}_l + \frac{1}{2}\mathbf{y}_t^{\mathrm{T}}\mathbf{y}_t \end{aligned} \tag{3.14}$$

Since $\mathbf{y}_t^{\mathrm{T}}\mathbf{y}_t$ is constant, the first constrained linear least square problem given in Eq. (3.13) becomes a constrained quadratic programing problem:

$$\min_{\mathbf{w}_l}\left\|\mathbf{P}\mathbf{w}_l-\mathbf{y}_t\right\|_2, \mathbf{P}\mathbf{w}_l \le \mathbf{y}_t \Leftrightarrow \min_{\mathbf{w}_l}\left\{\mathbf{c}^{\mathrm{T}}\mathbf{w}_l+\frac{1}{2}\mathbf{w}_l^{\mathrm{T}}\mathbf{H}\mathbf{w}_l\right\} \text{ subject to } \mathbf{P}\mathbf{w}_l \le \mathbf{y}_t \quad (3.15)$$

The solution of (3.15) can be solved by using the active-set method. The active set method is described in [79]–[81] and is available as a commercial package by using the MATLAB optimization toolbox. The steps to obtain $\mathbf{w}_l$ by using the active set method is described as follows:

Step 1: Construct the active constraint matrix $\mathbf{S}_k$ whose rows are taken from the constraints given in matrix $\mathbf{P}$ that are active at the solution point (equality constraint is satisfied). k is the iteration number.

Step 2: Assume that $\mathbf{Q}_k$ and $\mathbf{R}_k$ are the QR decomposition matrices of $\mathbf{S}_k$ ($\mathbf{Q}_k$ is an orthogonal matrix and $\mathbf{R}_k$ is an upper triangular matrix). From the last $N-l$ columns of $\mathbf{Q}_k$, where N is the number of training data and l is the number of active constraints, form matrix $\mathbf{Z}_k$:

$$\mathbf{Z}_k = \mathbf{Q}_k[:, l+1:N] \text{ where } \mathbf{Q}_k^{\mathrm{T}}\mathbf{S}_k^{\mathrm{T}} = \mathbf{R}_k \quad (3.16)$$

Step 3: Calculate the search direction $\mathbf{d}_k$ as a linear combination of the columns of $\mathbf{Z}_k$: $\mathbf{d}_k = \mathbf{Z}_k\mathbf{r}$ for some vector $\mathbf{r}$.

Step 4: Update the value of vector $\mathbf{w}_l$ by the search direction $\mathbf{d}_k$:

$$\mathbf{w}_{l\{k+1\}} = \mathbf{w}_{l\{k\}} + \alpha\mathbf{d}_k \quad (3.17)$$

where $\alpha = \min_{i=\{1,\ldots,N\}} \dfrac{-\left(\mathbf{p}_i \mathbf{w}_{l\{k\}} - y_t(i)\right)}{\mathbf{p}_i \mathbf{d}_k}$ and $\mathbf{p}_i$ is the i^{th} row vector of matrix $\mathbf{P}$.

Step 5: Calculate the Lagrange multiplier vector $\boldsymbol{\lambda}_k$, which satisfies:

$$\mathbf{S}_k^{\mathrm{T}} \boldsymbol{\lambda}_k = \mathbf{c} \tag{3.18}$$

Step 6: If all the elements of $\boldsymbol{\lambda}_k$ are positive, $\mathbf{w}_{l\{k+1\}}$ is the optimal solution. Otherwise, go to step 1.

3.2 Obtaining the Interval Type-2 T-S Fuzzy Model from the Interval Type-2 A1-C2 FBFN Model

Since type-2 T-S fuzzy models have been used extensively to design robust controllers, this section introduces a method to convert an interval type-2 FBFN to an interval type-2 A1-C2 T-S fuzzy model. In the interval type-2 A1-C2 T-S fuzzy model, the antecedents are type-1 fuzzy set (A1) while the consequents are type 2 interval numbers (C2). This method will expand the applications of the type-2 FBFN in many areas since existing robust controllers can be easily implemented on nonlinear systems with unstructured uncertainties.

Consider a class of nonlinear systems with p state variables as described in Eq. (3.1). Each state variable of the nonlinear system can be approximated by an interval type-2 FBFN model as described in the previous section. The structure of rule R_p^j of the type-2 FBFN that calculates the state variable x_p, $(p = 1 \ldots n)$ has the following form:

$$\begin{aligned} R_p^j: \quad & \text{IF } x_1(k) \text{ is } X_{p,1}^j \text{ and } \ldots\ x_n(k) \text{ is } X_{p,n}^j \text{ and } u_1(k) \text{ is } U_{q,1}^j \text{ and } \ldots\ u_m(k) \text{ is } U_{q,m}^j \\ & \text{THEN } \tilde{x}_p(k+1) = \tilde{G}_p^j, \quad j = 1, \ldots, J \end{aligned} \tag{3.19}$$

where X^j and U^j are type-1 fuzzy sets with Gaussian membership functions. $\tilde{G}_p^j$ is an interval type-2 fuzzy set with its centroid $\tilde{w}_p^j$ as an interval set: $\tilde{w}_p^j = [w_{pl}^j, w_{pr}^j]$. $\tilde{x}_p(k+1)$ is the predicted interval value of the state variable x_p.

Consider $\mathbf{x}(k) = [x_1(k),\ x_2(k),\ \ldots x_n(k)]^{\mathrm{T}}$ as the vector of the measured state variables and $\mathbf{u}(k) = [u_1(k),\ u_2(k),\ \ldots u_m(k)]^{\mathrm{T}}$ as the input vector. From Eq. (3.7), $\tilde{x}_p(k+1)$ can be computed by an uncertain nonlinear mapping $\tilde{f}_p : \mathbf{u}(k) \subset \Re^m, \mathbf{x}(k) \subset \Re^n \to \tilde{x}_p(k+1) \subset \Re$. The mapping includes $\tilde{w}_p^j$ in the function as the uncertain parameter:

$$\begin{aligned}
\tilde{x}_p(k+1) = \tilde{f}_p(\mathbf{x}(k), \mathbf{u}(k)) &= \frac{\sum_{j=1}^{J} \tilde{w}_p^j \prod_{i=1}^{n} \mu_{X_{p,i}^j}(x_i(k)) \prod_{i=1}^{m} \mu_{U_{q,i}^j}(u_i(k))}{\sum_{j=1}^{J} \prod_{i=1}^{n} \mu_{X_{p,i}^j}(x_i(k)) \prod_{i=1}^{m} \mu_{U_{q,i}^j}(u_i(k))} \\
&= \left[f_{pl}(\mathbf{x}(k), \mathbf{u}(k)),\ f_{pr}(\mathbf{x}(k), \mathbf{u}(k)) \right] \\
&= \left[\frac{\sum_{j=1}^{J} w_{pl}^j \prod_{i=1}^{n} \mu_{X_{p,i}^j}(x_i(k)) \prod_{i=1}^{m} \mu_{U_{q,i}^j}(u_i(k))}{\sum_{j=1}^{J} \prod_{i=1}^{n} \mu_{X_{p,i}^j}(x_i(k)) \prod_{i=1}^{m} \mu_{B_{q,i}^j}(u_i(k))}, \right. \\
&\qquad \left. \frac{\sum_{j=1}^{J} w_{pr}^j \prod_{i=1}^{n} \mu_{X_{p,i}^j}(x_i(k)) \prod_{i=1}^{m} \mu_{U_{q,i}^j}(u_i(k))}{\sum_{j=1}^{J} \prod_{i=1}^{n} \mu_{X_{p,i}^j}(x_i(k)) \prod_{i=1}^{m} \mu_{U_{q,i}^j}(u_i(k))} \right]
\end{aligned} \tag{3.20}$$

When the states of the system are around a certain operating condition:

$$\mathbf{x} \approx \boldsymbol{\chi}_i = [\chi_i^{(1)}, \ldots, \chi_i^{(n)}]^{\mathrm{T}},\ \mathbf{u} \approx \boldsymbol{\upsilon}_i = \left[\upsilon_i^{(1)}, \ldots, \upsilon_i^{(m)} \right]^{\mathrm{T}} \tag{3.21}$$

the local linear models of the nonlinear system represented by Eq. (3.19) can be used to construct fuzzy rules in the interval type-2 T-S fuzzy model. By choosing enough operating points, the interval type-2 T-S fuzzy model will become a good approximation of the

nonlinear dynamic system. At each operating point, the interval type-2 T-S fuzzy rule can be obtained as follows:

$$\begin{aligned} R^i: \quad & \text{IF } x_1(k) \text{ is } X_1^i \text{ and } \ldots\ x_n(k) \text{ is } X_n^i \text{ and } u_1(k) \text{ is } U_1^i \text{ and } \ldots\ u_m(k) \text{ is } U_m^i \\ & \text{THEN } \tilde{\mathbf{x}}(k+1) = \boldsymbol{\chi}_i + \tilde{\mathbf{A}}_i(\boldsymbol{\chi}_i, \boldsymbol{\upsilon}_i)\left[\mathbf{x}(k) - \boldsymbol{\chi}_i\right] + \tilde{\mathbf{B}}_i(\boldsymbol{\chi}_i, \boldsymbol{\upsilon}_i)\left[\mathbf{u}(k) - \boldsymbol{\upsilon}_i\right] \end{aligned} \tag{3.22}$$

where $X_1, \ldots, X_n$ and $U_1 \ldots U_m$ are type-1 fuzzy sets with triangular membership functions that describe the operating condition. Each element in the coefficient matrices $\tilde{\mathbf{A}}_i(\boldsymbol{\chi}_i, \boldsymbol{\upsilon}_i)$ and $\tilde{\mathbf{B}}_i(\boldsymbol{\chi}_i, \boldsymbol{\upsilon}_i)$ in Eq. (3.22) is an interval number. $\tilde{\mathbf{A}}_i(\boldsymbol{\chi}_i, \boldsymbol{\upsilon}_i)$ and $\tilde{\mathbf{B}}_i(\boldsymbol{\chi}_i, \boldsymbol{\upsilon}_i)$ are computed as follows:

$$\tilde{\mathbf{A}}_i(\boldsymbol{\chi}_i, \boldsymbol{\upsilon}_i) = \left[\begin{matrix} \dfrac{\partial \tilde{f}_1(\mathbf{x},\mathbf{u})}{\partial x_1} & \cdots & \dfrac{\partial \tilde{f}_1(\mathbf{x},\mathbf{u})}{\partial x_n} \\ \vdots & \ddots & \vdots \\ \dfrac{\partial \tilde{f}_n(\mathbf{x},\mathbf{u})}{\partial x_1} & \cdots & \dfrac{\partial \tilde{f}_n(\mathbf{x},\mathbf{u})}{\partial x_n} \end{matrix}\right]\Bigg|_{\substack{\mathbf{x}=\boldsymbol{\chi}_i, \\ \mathbf{u}=\boldsymbol{\upsilon}_i}} \quad \tilde{\mathbf{B}}_i(\boldsymbol{\chi}_i, \boldsymbol{\upsilon}_i) = \left[\begin{matrix} \dfrac{\partial \tilde{f}_1(\mathbf{x},\mathbf{u})}{\partial u_1} & \cdots & \dfrac{\partial \tilde{f}_1(\mathbf{x},\mathbf{u})}{\partial u_m} \\ \vdots & \ddots & \vdots \\ \dfrac{\partial \tilde{f}_n(\mathbf{x},\mathbf{u})}{\partial u_1} & \cdots & \dfrac{\partial \tilde{f}_n(\mathbf{x},\mathbf{u})}{\partial u_m} \end{matrix}\right]\Bigg|_{\substack{\mathbf{x}=\boldsymbol{\chi}_i, \\ \mathbf{u}=\boldsymbol{\upsilon}_i}} \tag{3.23}$$

The partial derivative of the nonlinear mapping f_p, $(p = 1 \ldots n)$ with respect to the state variable x_q, $(p = 1 \ldots n)$ can be calculated by the following formula:

$$\frac{\partial \tilde{f}_p(\mathbf{x},\mathbf{u})}{\partial x_q} = \mathbf{a}_{p,q}^{\mathrm{T}}(\mathbf{x},\mathbf{u}) \cdot \tilde{\mathbf{w}}_p \tag{3.24}$$

where $\tilde{\mathbf{w}}_p = \left[\tilde{w}_p^{(1)}, \tilde{w}_p^{(2)}, \ldots \tilde{w}_p^{(J)}\right]^{\mathrm{T}}$ and $\mathbf{a}_{p,q} = \left[a_{p,q}^{(1)} \quad a_{p,q}^{(2)} \quad \ldots \quad a_{p,q}^{(J)}\right]^{\mathrm{T}}$. The j^{th} element of vector $\mathbf{a}_{p,q}$ can be calculated as:

$$a_{p,q}^{(j)}(\mathbf{x},\mathbf{u}) = \frac{\left(-\frac{x_q - c_{X_{p,q}^j}}{\sigma^2_{X_{p,q}^j}}\right)\prod_{r=1}^{n}\mu_{X_{p,r}^j}(x_r)\prod_{r=1}^{m}\mu_{U_{q,r}^j}(u_r)}{\sum_{j=1}^{J}\prod_{r=1}^{n}\mu_{X_{p,r}^j}(x_r)\prod_{r=1}^{m}\mu_{U_{q,r}^j}(u_r)} - \frac{\left[\prod_{r=1}^{n}\mu_{X_{p,r}^j}(x_r)\prod_{r=1}^{m}\mu_{U_{q,r}^j}(u_r)\right]\left[\sum_{j=1}^{J}\left(-\frac{x_q - c_{X_{p,q}^j}}{\sigma^2_{X_{p,q}^j}}\right)\prod_{i=1}^{n}\mu_{X_{p,r}^j}(x_r)\prod_{j=1}^{m}\mu_{U_{q,r}^j}(u_r)\right]}{\left[\sum_{j=1}^{J}\prod_{r=1}^{n}\mu_{X_{p,r}^j}(x_r)\prod_{r=1}^{m}\mu_{U_{q,r}^j}(u_r)\right]^2} \tag{3.25}$$

Within rule *j* of the FBFN model (for the output x_p), $c_{X_{p,q}^j}$ and $\sigma_{X_{p,q}^j}$ are, respectively, the mean and standard deviation of the Gaussian membership function of x_q.

Similarly, the partial derivative of the nonlinear mapping f_p with respect to the state variable u_q can be computed by:

$$\frac{\partial \tilde{f}_p(\mathbf{x},\mathbf{u})}{\partial u_q} = \mathbf{b}_{p,q}^{\mathrm{T}}(\mathbf{x},\mathbf{u})\cdot\tilde{\mathbf{w}}_p \tag{3.26}$$

where $\tilde{\mathbf{w}}_p = \left[\tilde{w}_p^{(1)}, \tilde{w}_p^{(2)}, \ldots \tilde{w}_p^{(M)}\right]^{\mathrm{T}}$ and $\mathbf{b}_{p,q} = \left[b_{p,q}^{(1)} \quad b_{p,q}^{(2)} \quad \ldots \quad b_{p,q}^{(M)}\right]^{\mathrm{T}}$. The j^{th} element of vector $\mathbf{b}_{p,q}$ can be calculated as:

$$b_{q,p}^{(j)}(\mathbf{x},\mathbf{u}) = \frac{\left(-\frac{u_q - c_{U_{p,q}^j}}{\sigma^2_{U_{p,q}^j}}\right)\prod_{r=1}^{n}\mu_{X_{p,r}^j}(x_r)\prod_{r=1}^{m}\mu_{U_{q,r}^j}(u_r)}{\sum_{j=1}^{J}\prod_{r=1}^{n}\mu_{X_{p,r}^j}(x_r)\prod_{r=1}^{m}\mu_{U_{q,r}^j}(u_r)} - \frac{\left[\prod_{r=1}^{n}\mu_{X_{p,r}^j}(x_r)\prod_{r=1}^{m}\mu_{U_{q,r}^j}(u_r)\right]\left[\sum_{j=1}^{J}\left(-\frac{u_q - c_{U_{p,q}^j}}{\sigma^2_{U_{p,q}^j}}\right)\prod_{r=1}^{n}\mu_{X_{p,r}^j}(x_r)\prod_{r=1}^{m}\mu_{U_{q,r}^j}(u_r)\right]}{\left[\sum_{j=1}^{J}\prod_{r=1}^{n}\mu_{X_{p,r}^j}(x_r)\prod_{r=1}^{m}\mu_{U_{q,r}^j}(u_r)\right]^2} \tag{3.27}$$

Assume that $\mathbf{A}_{i\min}$, $\mathbf{A}_{i\max}$, $\mathbf{B}_{i\min}$ and $\mathbf{B}_{i\max}$ are matrices that contain the lower and upper values of each element of matrices $\tilde{\mathbf{A}}_i$ and $\tilde{\mathbf{B}}_i$, respectively. Finding $\mathbf{A}_{i\min}$, $\mathbf{A}_{i\max}$, $\mathbf{B}_{i\min}$ and $\mathbf{B}_{i\max}$ becomes the problem of obtaining the maximum and minimum values of $\mathbf{a}_{p,q}^{\mathrm{T}}(\mathbf{x},\mathbf{u})\big|_{\mathbf{x}=\boldsymbol{\chi}_i,\mathbf{u}=\boldsymbol{\upsilon}_i}\cdot\tilde{\mathbf{w}}_p$ and $\mathbf{b}_{p,q}^{\mathrm{T}}(\mathbf{x},\mathbf{u})\big|_{\mathbf{x}=\boldsymbol{\chi}_i,\mathbf{u}=\boldsymbol{\upsilon}_i}\cdot\tilde{\mathbf{w}}_p$, respectively. Since the elements of matrices $\mathbf{a}_{p,q}$ and $\mathbf{b}_{p,q}$ are crisp numbers while the elements of vector $\tilde{\mathbf{w}}_p$ are interval numbers, the solution can be obtained easily by using existing linear programming methods such as the simplex method [82] or interior-point methods [83], [84].

In addition to $\mathbf{A}_{i\min}$, $\mathbf{A}_{i\max}$, $\mathbf{B}_{i\min}$ and $\mathbf{B}_{i\max}$, finding the coefficient matrices of the type-2 T-S fuzzy model that produce the upper and lower bounds of the output is important for the controller design purpose. With $f_{pl}(\mathbf{x}(k),\mathbf{u}(k))$ and $f_{pr}(\mathbf{x}(k),\mathbf{u}(k))$ defined in Eq. (3.20), the matrices $\mathbf{A}_{il}$, $\mathbf{B}_{il}$ are introduced as the linearized coefficient matrices of $f_{pl}(\mathbf{x}(k),\mathbf{u}(k))$ through the linearization process as given in Eq. (3.23). Similarly, $\mathbf{A}_{ir}$, $\mathbf{B}_{ir}$ are introduced as the linearized coefficient matrices of $f_{pr}(\mathbf{x}(k),\mathbf{u}(k))$. Then, when $\mathbf{x}(k)\approx\boldsymbol{\chi}_i$, $\mathbf{u}(k)\approx\boldsymbol{\upsilon}_i$ the following approximations can be obtained:

$$\boldsymbol{\chi}_i+\mathbf{A}_{il}(\boldsymbol{\chi}_i,\boldsymbol{\upsilon}_i)[\mathbf{x}(k)-\boldsymbol{\chi}_i]+\mathbf{B}_{il}(\boldsymbol{\chi}_i,\boldsymbol{\upsilon}_i)[\mathbf{u}(k)-\boldsymbol{\upsilon}_i]\approx f_{pl}(\mathbf{x}(k),\mathbf{u}(k)) \quad (3.28)$$

and

$$\boldsymbol{\chi}_i+\mathbf{A}_{ir}(\boldsymbol{\chi}_i,\boldsymbol{\upsilon}_i)[\mathbf{x}(k)-\mathbf{x}_0]+\mathbf{B}_{ir}(\boldsymbol{\chi}_i,\boldsymbol{\upsilon}_i)[\mathbf{u}(k)-\boldsymbol{\upsilon}_i]\approx f_{pr}(\mathbf{x}(k),\mathbf{u}(k)) \quad (3.29)$$

In other words, $\mathbf{A}_{il}$ and $\mathbf{B}_{il}$ are the coefficient matrices of the local linear model that approximate the lower bound of the nonlinear system output, $\mathbf{A}_{ir}$ and $\mathbf{B}_{ir}$ are the coefficient matrices that are used to approximate the upper bound of the output. It is noted

that the values of $\mathbf{A}_{il}$, $\mathbf{B}_{il}$, $\mathbf{A}_{ir}$ and $\mathbf{B}_{ir}$ are different from the values of $\mathbf{A}_{i\min}$, $\mathbf{A}_{i\max}$, $\mathbf{B}_{i\min}$ and $\mathbf{B}_{i\max}$.

With $\mathbf{w}_{pl}$ and $\mathbf{w}_{pr}$ as the lower and upper bounds of $\tilde{\mathbf{w}}_p$, respectively, the element $A_{il\{p,q\}}$ (on the p^{th} row and q^{th} column) of matrix $\mathbf{A}_{il}$ can be calculated by using Eq. (3.24) as follows:

$$A_{il\{p,q\}} = \mathbf{a}_{p,q}^{\mathrm{T}}(\mathbf{x},\mathbf{u})\Big|_{\mathbf{x}=\boldsymbol{\chi}_i,\mathbf{u}=\boldsymbol{\upsilon}_i} \cdot \mathbf{w}_{pl} \tag{3.30}$$

Similarly:

$$A_{ir\{p,q\}} = \mathbf{a}_{p,q}^{\mathrm{T}}(\mathbf{x},\mathbf{u})\Big|_{\mathbf{x}=\boldsymbol{\chi}_i,\mathbf{u}=\boldsymbol{\upsilon}_i} \cdot \mathbf{w}_{pr} \tag{3.31}$$

$$B_{il\{p,q\}} = \mathbf{b}_{p,q}^{\mathrm{T}}(\mathbf{x},\mathbf{u})\Big|_{\mathbf{x}=\boldsymbol{\chi}_i,\mathbf{u}=\boldsymbol{\upsilon}_i} \cdot \mathbf{w}_{pl} \tag{3.32}$$

$$B_{ir\{p,q\}} = \mathbf{b}_{p,q}^{\mathrm{T}}(\mathbf{x},\mathbf{u})\Big|_{\mathbf{x}=\boldsymbol{\chi}_i,\mathbf{u}=\boldsymbol{\upsilon}_i} \cdot \mathbf{w}_{pr} \tag{3.33}$$

By defining the following matrices:

$$\mathbf{A}_i = \frac{\mathbf{A}_{i\max} + \mathbf{A}_{i\min}}{2},\ \mathbf{B}_i = \frac{\mathbf{B}_{i\min} + \mathbf{B}_{i\max}}{2},\ \Delta\tilde{\mathbf{A}}_i = \tilde{\mathbf{A}}_i - \mathbf{A}_i,\ \Delta\tilde{\mathbf{B}}_i = \tilde{\mathbf{B}}_i - \mathbf{B}_i, \tag{3.34}$$

in order to derive the upper bound of the Lyapunov equation proposed in the next section, the matrices $\Delta\mathbf{A}_{im}$ and $\Delta\mathbf{B}_{im}$ are introduced such that

$$\left(\Delta\mathbf{A}_{im}\mathbf{x} + \Delta\mathbf{B}_{im}\mathbf{u}\right)^T\left(\Delta\mathbf{A}_{im}\mathbf{x} + \Delta\mathbf{B}_{im}\mathbf{u}\right) = \max_{\Delta\mathbf{A}\in\Delta\tilde{\mathbf{A}}_i,\,\Delta\mathbf{B}\in\Delta\tilde{\mathbf{B}}_i}\left[\left(\Delta\mathbf{A}\mathbf{x} + \Delta\mathbf{B}\mathbf{u}\right)^T\left(\Delta\mathbf{A}\mathbf{x} + \Delta\mathbf{B}\mathbf{u}\right)\right] \tag{3.35}$$

Further introductions of $\boldsymbol{\delta}\mathbf{a}_{im}^p$, $\boldsymbol{\delta}\mathbf{a}_{il}^p$, $\boldsymbol{\delta}\mathbf{a}_{ir}^p$, $\boldsymbol{\delta}\tilde{\mathbf{a}}_i^p$, $\boldsymbol{\delta}\mathbf{b}_{im}^p$, $\boldsymbol{\delta}\mathbf{b}_{il}^p$, $\boldsymbol{\delta}\mathbf{b}_{ir}^p$, $\boldsymbol{\delta}\tilde{\mathbf{b}}_i^p$, $\mathbf{a}_{il}^p$. $\mathbf{a}_{ir}^p$, $\mathbf{b}_{il}^p$, $\mathbf{b}_{ir}^p$, $\mathbf{a}_i^p$, $\mathbf{b}_i^p$ as the p^{th} rows of matrices $\Delta\mathbf{A}_{im}$, $\Delta\mathbf{A}_{il}$, $\Delta\mathbf{A}_{ir}$, $\Delta\tilde{\mathbf{A}}_i$, $\Delta\mathbf{B}_{im}$, $\Delta\mathbf{B}_{il}$, $\Delta\mathbf{B}_{ir}$, $\Delta\tilde{\mathbf{B}}_i$, $\mathbf{A}_{il}$, $\mathbf{A}_{ir}$, $\mathbf{B}_{il}$, $\mathbf{B}_{ir}$, $\mathbf{A}_i$ and $\mathbf{B}_i$, respectively, and $\boldsymbol{\chi}_{i\{p\}}$ as the p^{th} row of the operating condition vector $\boldsymbol{\chi}_i$ are needed to construct the matrices $\Delta\mathbf{A}_{im}$ and $\Delta\mathbf{B}_{im}$.

If the operating condition $\boldsymbol{\chi}_{i\{p\}}$ is positive, from the definitions of $\mathbf{A}_{ir}$ and $\mathbf{B}_{ir}$, the following can be obtained when $x_p(k)$ is near $\boldsymbol{\chi}_{i\{p\}}$:

$$\max_{\boldsymbol{\delta a}\in\boldsymbol{\delta}\tilde{\mathbf{a}}_i^p,\boldsymbol{\delta b}\in\boldsymbol{\delta}\tilde{\mathbf{b}}_i^p}\left[\left(\boldsymbol{\delta a}\mathbf{x}+\boldsymbol{\delta b}\mathbf{u}\right)^{\mathrm{T}}\left(\boldsymbol{\delta a}\mathbf{x}+\boldsymbol{\delta b}\mathbf{u}\right)\right]=\left(\boldsymbol{\delta a}_{ir}^p\mathbf{x}+\boldsymbol{\delta b}_{ir}^p\mathbf{u}\right)^{\mathrm{T}}\left(\boldsymbol{\delta a}_{ir}^p\mathbf{x}+\boldsymbol{\delta b}_{ir}^p\mathbf{u}\right) \tag{3.36}$$

Similarly, if the operating condition $\boldsymbol{\chi}_{i\{p\}}$ is negative, the following can be obtained when $x_p(k)$ is near $\boldsymbol{\chi}_{i\{p\}}$:

$$\max_{\boldsymbol{\delta a}\in\boldsymbol{\delta}\tilde{\mathbf{a}}_i^p,\boldsymbol{\delta b}\in\boldsymbol{\delta}\tilde{\mathbf{b}}_i^p}\left[\left(\boldsymbol{\delta a}\mathbf{x}+\boldsymbol{\delta b}\mathbf{u}\right)^{\mathrm{T}}\left(\boldsymbol{\delta a}\mathbf{x}+\boldsymbol{\delta b}\mathbf{u}\right)\right]=\left(\boldsymbol{\delta a}_{il}^p\mathbf{x}+\boldsymbol{\delta b}_{il}^p\mathbf{u}\right)^{\mathrm{T}}\left(\boldsymbol{\delta a}_{il}^p\mathbf{x}+\boldsymbol{\delta b}_{il}^p\mathbf{u}\right) \tag{3.37}$$

Hence, the rows of $\Delta\mathbf{A}_{im}$ and $\Delta\mathbf{B}_{im}$ can be computed by:

$$\begin{aligned}&\text{if } \boldsymbol{\chi}_{i\{p\}}<0:\ \boldsymbol{\delta a}_{im}^p=\mathbf{a}_{il}^p-\mathbf{a}_i^p,\ \boldsymbol{\delta b}_{im}^p=\mathbf{b}_{il}^p-\mathbf{b}_i^p\\&\text{if } \boldsymbol{\chi}_{i\{p\}}\geq 0:\ \boldsymbol{\delta a}_{im}^p=\mathbf{a}_{ir}^p-\mathbf{a}_i^p,\ \boldsymbol{\delta b}_{im}^p=\mathbf{b}_{ir}^p-\mathbf{b}_i^p\end{aligned} \tag{3.38}$$

3.3 Robust T-S Fuzzy Controller with Integral Term

In this section, by using the parameters of the interval type-2 T-S model and the interval type-2 FBFN, a robust controller that is based on a relaxed stability condition is presented. Consider a class of nonlinear systems with *p* state variables as described in Eq. (3.1). Assume that the nonlinear system can be approximated by an interval type-2 T-S model with *M* rules. The structure of rule R^i of the model is described as follows:

$$\begin{aligned}R^i:\quad &\text{IF } x_1(k) \text{ is } X_1^i \text{ and } \ldots\ x_n(k) \text{ is } X_n^i \text{ and } u_1(k) \text{ is } U_1^i \text{ and } \ldots\ u_m(k) \text{ is } U_m^i\\&\text{THEN } \tilde{\mathbf{x}}(k+1)=\tilde{\mathbf{A}}_i\mathbf{x}(k)+\tilde{\mathbf{B}}_i\mathbf{u}(k)\end{aligned} \tag{3.39}$$

where $\tilde{\mathbf{x}}(k+1)$ is the predicted interval value of the state variable vector $\mathbf{x}$. $X_1^i,\ldots,X_n^i$ and $U_1^i,\ldots,U_n^i$ are type-1 fuzzy sets with triangular membership functions. Each element in the

coefficient matrices $\tilde{\mathbf{A}}_i$ and $\tilde{\mathbf{B}}_i$ is an interval number. By using the T-S fuzzy inference mechanism, the predicted interval output of the fuzzy model can be derived as follows:

$$\begin{aligned}\tilde{\mathbf{x}}(k+1) &= \sum_{i=1}^{M} \bar{\mu}_i(\mathbf{x}(k),\mathbf{u}(k)) \cdot \left\{ \tilde{\mathbf{A}}_i \mathbf{x}(k) + \tilde{\mathbf{B}}_i \mathbf{u}(k) \right\} \\ &= \sum_{i=1}^{M} \bar{\mu}_i(\mathbf{x}(k),\mathbf{u}(k)) \cdot \left\{ (\mathbf{A}_i + \Delta\tilde{\mathbf{A}}_i)\mathbf{x}(k) + (\mathbf{B}_i + \Delta\tilde{\mathbf{B}}_i)\mathbf{u}(k) \right\} \\ \tilde{\mathbf{y}}(k) &= \mathbf{C}\tilde{\mathbf{x}}(k)\end{aligned} \tag{3.40}$$

where $\mathbf{A}_i$, $\mathbf{B}_i$, $\Delta\tilde{\mathbf{A}}_i$, $\Delta\tilde{\mathbf{B}}_i$ are defined in Eq. (3.34). $\bar{\mu}_i$ is the normalized weighting function:

$$\bar{\mu}_i(\mathbf{x}(k),\mathbf{u}(k)) = \frac{\prod_{t=1}^{n} \mu_{X_t^i}(x_t) \prod_{t=1}^{m} \mu_{U_t^i}(u_t)}{\sum_{i=1}^{M} \prod_{t=1}^{n} \mu_{X_t^i}(x_t) \prod_{t=1}^{m} \mu_{U_t^i}(u_t)} \tag{3.41}$$

$\mu_{X_t^i}(x_t)$ and $\mu_{U_t^i}(u_t)$ are the membership functions of x_t and u_t, respectively. $\mathbf{x}(k) = [x_1(k), \ldots x_n(k)]^T \in \mathbb{R}^n$ is the state variable matrix, $\mathbf{u}(k) \in \mathbb{R}^m$ is the control input vector and $\tilde{\mathbf{y}}(k)$ is the output of the system.

A dynamic state feedback robust T-S fuzzy controller (RTSFC) (Figure 3-1) with *N* rules is proposed. The structure of rule R^j of the controller is described as follows:

$$\begin{aligned}&R^j : \text{IF } x_1(k) \text{ is } X_1^j \text{ and } \ldots\ x_n(k) \text{ is } X_n^j \\ &\text{THEN } \mathbf{u}(k) = \mathbf{K}_j \mathbf{x}(k) + \mathbf{k}_j \boldsymbol{\zeta}(k), \\ &\qquad \boldsymbol{\zeta}(k) = \boldsymbol{\zeta}(k-1) + \mathbf{e}(k), \quad \mathbf{e}(k) = \mathbf{r}(k) - \mathbf{C}\mathbf{x}(k)\end{aligned} \tag{3.42}$$

where $\boldsymbol{\zeta}$ is the integral of the error vector **e**. $\mathbf{K}_j$ is the proportional feedback gain and $\mathbf{k}_j$ is the integral gain of rule *j*. **r**(*k*) is the reference signal. By using the TS inference

mechanism, the output of the controller $\mathbf{u}(k)$ described by Eq. (3.42) at time instance k can be calculated as:

$$\mathbf{u}(k) = \sum_{j=1}^{N} \overline{v}_j \left(\mathbf{x}(k)\right) \cdot \left\{ \mathbf{K}_j \mathbf{x}(k) + \mathbf{k}_j \boldsymbol{\zeta}(k) \right\} \tag{3.43}$$

where $\mathbf{x}(k) = [x_1(k), \ldots x_n(k)]^T \in \mathbb{R}^n$ is the state variable matrix, $\overline{v}_j$ is the normalized firing strength of the j^{th} rule:

$$\overline{v}_j \left(\mathbf{x}(k)\right) = \frac{\prod_{t=1}^{n} \nu_{X_t^j}(x_t)}{\sum_{j=1}^{N} \prod_{t=1}^{n} \nu_{X_t^j}(x_t)} \tag{3.44}$$

and $\nu_{X_t^i}(x_t)$ is the membership function of x_t.

By substituting Eq. (3.43) into Eq. (3.40), the closed-loop system dynamic equations can be obtained:

$$\begin{aligned} \tilde{\mathbf{x}}(k+1) &= \sum_{i=1}^{M} \sum_{j=1}^{N} \overline{\mu}_i(\mathbf{x}(k), \mathbf{u}(k)) \overline{v}_j \left(\mathbf{x}(k)\right) \cdot \left\{ \left(\mathbf{A}_i + \Delta\tilde{\mathbf{A}}_i + \mathbf{B}_i \mathbf{K}_j \right) \mathbf{x}(k) + \mathbf{B}_i \mathbf{k}_j \boldsymbol{\zeta}(k) + \Delta\tilde{\mathbf{B}}_i \mathbf{u}(k) \right\} \\ &= \left(\mathbf{A}_0 + \Delta\tilde{\mathbf{A}}_0 + \mathbf{B}_0 \mathbf{K}_0 \right) \mathbf{x}(k) + \mathbf{B}_0 \mathbf{k}_0 \boldsymbol{\zeta}(k) + \Delta\tilde{\mathbf{B}}_0 \mathbf{u}(k) \\ \boldsymbol{\zeta}(k) &= \boldsymbol{\zeta}(k-1) + \mathbf{r}(k-1) - \mathbf{C}\mathbf{x}(k-1) \end{aligned} \tag{3.45}$$

where $\mathbf{A}_0 = \sum_{i=1}^{M} \overline{\mu}_i \mathbf{A}_i$, $\Delta\mathbf{A}_0 = \sum_{i=1}^{M} \overline{\mu}_i \Delta\mathbf{A}_i$, $\mathbf{B}_0 = \sum_{i=1}^{M} \overline{\mu}_i \mathbf{B}_i$, $\Delta\mathbf{B}_0 = \sum_{i=1}^{M} \overline{\mu}_i \Delta\mathbf{B}_i$, $\mathbf{K}_0 = \sum_{j=1}^{N} \overline{v}_j \mathbf{K}_j$ and $\mathbf{k}_0 = \sum_{j=1}^{N} \overline{v}_j \mathbf{k}_j$.

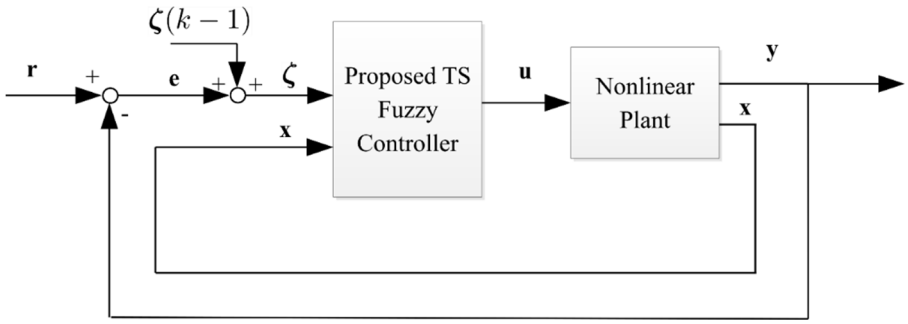

Figure 3-1: Schematic diagram of the closed loop control system.

By defining the following vectors and matrices: $\mathbf{z}(k) = [\mathbf{x}(k)\ \ \boldsymbol{\zeta}(k)]^{\mathrm{T}}$, $\mathbf{K} = [\mathbf{K}_0\ \ \mathbf{k}_0]$, $\mathbf{A} = \begin{bmatrix} \mathbf{A}_0 & 0 \\ -\mathbf{C} & \mathbf{I} \end{bmatrix}$, $\Delta\tilde{\mathbf{A}} = \begin{bmatrix} \Delta\tilde{\mathbf{A}}_0 & 0 \\ -\mathbf{C} & \mathbf{I} \end{bmatrix}$, $\mathbf{B} = \begin{bmatrix} \mathbf{B}_0 & 0 \end{bmatrix}^{\mathrm{T}}$ and $\Delta\tilde{\mathbf{B}} = \begin{bmatrix} \Delta\tilde{\mathbf{B}}_0 & 0 \end{bmatrix}^{\mathrm{T}}$, the closed loop system as in Eq. (3.45) can be rewritten as:

$$\tilde{\mathbf{z}}(k+1) = \left(\mathbf{A} + \Delta\tilde{\mathbf{A}} + (\mathbf{B} + \Delta\tilde{\mathbf{B}})\mathbf{K}\right)\mathbf{z}(k) \tag{3.46}$$

where $\tilde{\mathbf{z}}(k+1)$ is the predicted interval value of the state variable vector **z**.

The following lemma is an expansion of the lemma provided in [59], in which the positive constant α is replaced by a positive definite matrix **Z**.

Lemma 1: *Given matrices* **E**, **F** *and a positive definite matrix* **Z**, *the following inequality can be obtained:*

$$\begin{bmatrix} 0 & \mathbf{E}^{\mathrm{T}}\mathbf{F} \\ \mathbf{F}^{\mathrm{T}}\mathbf{E} & 0 \end{bmatrix} \le \begin{bmatrix} \mathbf{E}^{\mathrm{T}}\mathbf{Z}\mathbf{E} & 0 \\ 0 & \mathbf{F}^{\mathrm{T}}\mathbf{Z}^{-1}\mathbf{F} \end{bmatrix} \tag{3.47}$$

Proof:

The lemma can be proven by using the following property of the matrix norm:

$$\left(\mathbf{G}\mathbf{Z}^{1/2} - \mathbf{H}\mathbf{Z}^{-1/2}\right)\left(\mathbf{G}\mathbf{Z}^{1/2} - \mathbf{H}\mathbf{Z}^{-1/2}\right)^{\mathrm{T}} \ge 0 \tag{3.48}$$

where $\mathbf{G} = \begin{bmatrix} \mathbf{E}^{\mathrm{T}} \\ 0 \end{bmatrix}$, $\mathbf{H} = \begin{bmatrix} 0 \\ \mathbf{F}^{\mathrm{T}} \end{bmatrix}$. The above inequality is equivalent to

$$\mathbf{G}\mathbf{H}^{\mathrm{T}} + \mathbf{H}\mathbf{G}^{\mathrm{T}} \le \mathbf{G}\mathbf{Z}\mathbf{G}^{\mathrm{T}} + \mathbf{H}\mathbf{Z}^{-1}\mathbf{H}^{\mathrm{T}} \tag{3.49}$$

$$\Leftrightarrow \quad \begin{bmatrix} \mathbf{E}^{\mathrm{T}} \\ 0 \end{bmatrix}\begin{bmatrix} 0 & \mathbf{F}^{\mathrm{T}} \end{bmatrix} + \begin{bmatrix} 0 \\ \mathbf{F}^{\mathrm{T}} \end{bmatrix}\begin{bmatrix} \mathbf{E}^{\mathrm{T}} & 0 \end{bmatrix} \le \begin{bmatrix} \mathbf{E}^{\mathrm{T}} \\ 0 \end{bmatrix}\mathbf{Z}\begin{bmatrix} \mathbf{E}^{\mathrm{T}} & 0 \end{bmatrix} + \begin{bmatrix} 0 \\ \mathbf{F}^{\mathrm{T}} \end{bmatrix}\mathbf{Z}^{-1}\begin{bmatrix} 0 & \mathbf{F}^{\mathrm{T}} \end{bmatrix} \tag{3.50}$$

which is equivalent to inequality (3.47). Hence, the lemma is proven. ■

Based on Lemma 1 and the coefficient matrices of the type 2 T-S fuzzy model, the feedback gains of the RTSFC can be found from the solution of the LMI given in Theorem 1.

Theorem 3: Consider a class of nonlinear control systems as described in Eq. (3.1), assume that the nonlinear system can be approximated by a type-2 T-S fuzzy model as described in Eq. (3.39), which is obtained from a type-2 FBFN system as described in Eq. (3.19). If there exists a matrix $\mathbf{Y}$, a positive symmetric matrix $\mathbf{Q}$, positive definite diagonal matrices $\mathbf{Z}_{ij}$, a positive constant α, and the following LMI is satisfied:

$$\begin{bmatrix} -(1-\alpha)\mathbf{Q} & \mathbf{Q}\Delta\mathbf{A}_{im}^{\mathrm{T}} + \mathbf{Y}_j^{\mathrm{T}}\Delta\mathbf{B}_{im}^{\mathrm{T}} & \mathbf{Q}\mathbf{A}_i^{\mathrm{T}} + \mathbf{Y}_j^{\mathrm{T}}\mathbf{B}_i^{\mathrm{T}} \\ \Delta\mathbf{A}_{im}\mathbf{Q} + \Delta\mathbf{B}_{im}\mathbf{Y}_j & -\mathbf{Z}_{ij}^{-1} & 0 \\ \mathbf{A}_i\mathbf{Q} + \mathbf{B}_i\mathbf{Y}_j & 0 & -\mathbf{Q} + \mathbf{Z}_{ij}^{-1} \end{bmatrix} \le 0, \text{ with } i = 1,\ldots M,\ j = 1,\ldots,N \tag{3.51}$$

then the system with a robust T-S fuzzy controller as described in Eq. (3.42) with $\bar{\mathbf{K}}_j = \begin{bmatrix} \mathbf{K}_j & \mathbf{k}_j \end{bmatrix} = \mathbf{Y}_j\mathbf{Q}^{-1}$ is quadratic stable with a convergent rate α.

Proof: Define a Lyapunov function $V(\mathbf{z}(k)) = \mathbf{z}(k)^{\mathrm{T}}\mathbf{P}\mathbf{z}(k)$ where $\mathbf{P}$ is a positive definite matrix. The system is stable with a convergent rate α when

$$\Delta V(\mathbf{z}) + \alpha V(\mathbf{z}) \le 0 \tag{3.52}$$

which is equivalent to

$$\begin{aligned} &\mathbf{z}^{\mathrm{T}}(k+1)\mathbf{P}\mathbf{z}(k+1)-\mathbf{z}^{\mathrm{T}}(k)\mathbf{P}\mathbf{z}(k)+\alpha\mathbf{z}^{\mathrm{T}}(k)\mathbf{P}\mathbf{z}(k)\le 0 \\ \Leftrightarrow\ &\mathbf{z}^{\mathrm{T}}(k)\left[\left((\mathbf{A}+\Delta\tilde{\mathbf{A}})^{\mathrm{T}}+\mathbf{K}^{\mathrm{T}}(\mathbf{B}+\Delta\tilde{\mathbf{B}})^{\mathrm{T}}\right)\mathbf{P}\left((\mathbf{A}+\Delta\tilde{\mathbf{A}})+(\mathbf{B}+\Delta\tilde{\mathbf{B}})\mathbf{K}\right)-(1-\alpha)\mathbf{P}\right]\mathbf{z}(k) \end{aligned} \tag{3.53}$$

The above inequality can be written in the matrix form as:

$$\begin{bmatrix} -(1-\alpha)\mathbf{P} & (\mathbf{A}+\Delta\tilde{\mathbf{A}})^{\mathrm{T}}+\mathbf{K}^{\mathrm{T}}(\mathbf{B}+\Delta\tilde{\mathbf{B}})^{\mathrm{T}} \\ (\mathbf{A}+\Delta\tilde{\mathbf{A}})+(\mathbf{B}+\Delta\tilde{\mathbf{B}})\mathbf{K} & -\mathbf{P}^{-1} \end{bmatrix}\le 0 \tag{3.54}$$

$$\Leftrightarrow \quad \begin{bmatrix} -(1-\alpha)\mathbf{P} & \mathbf{A}^{\mathrm{T}}+\mathbf{K}^{\mathrm{T}}\mathbf{B}^{\mathrm{T}} \\ \mathbf{A}+\mathbf{B}\mathbf{K} & -\mathbf{P}^{-1} \end{bmatrix}+\begin{bmatrix} 0 & \Delta\tilde{\mathbf{A}}^{\mathrm{T}}+\mathbf{K}^{\mathrm{T}}\Delta\tilde{\mathbf{B}}^{\mathrm{T}} \\ \Delta\tilde{\mathbf{A}}+\Delta\tilde{\mathbf{B}}\mathbf{K} & 0 \end{bmatrix}\le 0 \tag{3.55}$$

By applying Lemma 1, the following can be obtained:

$$\begin{bmatrix} 0 & \Delta\tilde{\mathbf{A}}^{\mathrm{T}}+\mathbf{K}^{\mathrm{T}}\Delta\tilde{\mathbf{B}}^{\mathrm{T}} \\ \Delta\tilde{\mathbf{A}}+\Delta\tilde{\mathbf{B}}\mathbf{K} & 0 \end{bmatrix}\le\begin{bmatrix} \left(\Delta\tilde{\mathbf{A}}^{\mathrm{T}}+\mathbf{K}^{\mathrm{T}}\Delta\tilde{\mathbf{B}}^{\mathrm{T}}\right)\mathbf{Z}\left(\Delta\tilde{\mathbf{A}}+\Delta\tilde{\mathbf{B}}\mathbf{K}\right) & 0 \\ 0 & \mathbf{Z}^{-1} \end{bmatrix} \tag{3.56}$$

where $\mathbf{Z}=\sum_{i=1}^{M}\sum_{j=1}^{N}\overline{\mu}_i\overline{v}_j\mathbf{Z}_{ij}$, $\mathbf{Z}_{ij}$ is a positive definite diagonal matrix.

From (3.56), inequality (3.55) is satisfied if

$$\begin{bmatrix} -(1-\alpha)\mathbf{P} & \mathbf{A}^{\mathrm{T}}+\mathbf{K}^{\mathrm{T}}\mathbf{B}^{\mathrm{T}} \\ \mathbf{A}+\mathbf{B}\mathbf{K} & -\mathbf{P}^{-1} \end{bmatrix}+\begin{bmatrix} \left(\Delta\tilde{\mathbf{A}}^{\mathrm{T}}+\mathbf{K}^{\mathrm{T}}\Delta\tilde{\mathbf{B}}^{\mathrm{T}}\right)\mathbf{Z}\left(\Delta\tilde{\mathbf{A}}+\Delta\tilde{\mathbf{B}}\mathbf{K}\right) & 0 \\ 0 & \mathbf{Z}^{-1} \end{bmatrix}\le 0 \tag{3.57}$$

$$\Leftrightarrow \quad \begin{bmatrix} -(1-\alpha)\mathbf{P}+\left(\Delta\tilde{\mathbf{A}}^{\mathrm{T}}+\mathbf{K}^{\mathrm{T}}\Delta\tilde{\mathbf{B}}^{\mathrm{T}}\right)\mathbf{Z}\left(\Delta\tilde{\mathbf{A}}+\Delta\tilde{\mathbf{B}}\mathbf{K}\right) & \mathbf{A}^{\mathrm{T}}+\mathbf{K}^{\mathrm{T}}\mathbf{B}^{\mathrm{T}} \\ \mathbf{A}+\mathbf{B}\mathbf{K} & -\mathbf{P}^{-1}+\mathbf{Z}^{-1} \end{bmatrix}\le 0 \tag{3.58}$$

Since $\mathbf{Z}_{ij}$ is a positive definite diagonal matrix, the following inequality can be obtained:

$$\left(\Delta\tilde{\mathbf{A}}_i^{\mathrm{T}}+\mathbf{K}_j^{\mathrm{T}}\Delta\tilde{\mathbf{B}}_i^{T}\right)\mathbf{Z}_{ij}\left(\Delta\tilde{\mathbf{A}}_i+\Delta\tilde{\mathbf{B}}_i\mathbf{K}_j\right)\le\left(\Delta\mathbf{A}_{im}^{\mathrm{T}}+\mathbf{K}_j^{\mathrm{T}}\Delta\mathbf{B}_{im}^{\mathrm{T}}\right)\mathbf{Z}_{ij}\left(\Delta\mathbf{A}_{im}+\Delta\mathbf{B}_{im}\mathbf{K}_j\right) \tag{3.59}$$

where $\Delta\mathbf{A}_{im}$ and $\Delta\mathbf{B}_{im}$ can be calculated by Eq. (3.38). Hence, inequality (3.58) is satisfied if

$$\begin{bmatrix} -(1-\alpha)\mathbf{P} + \left(\Delta\mathbf{A}_M^T + \mathbf{K}^{\mathrm{T}}\Delta\mathbf{B}_M^{\mathrm{T}}\right)\mathbf{Z}\left(\Delta\mathbf{A}_M + \Delta\mathbf{B}_M\mathbf{K}\right) & \mathbf{A}^{\mathrm{T}} + \mathbf{K}^{\mathrm{T}}\mathbf{B}^{\mathrm{T}} \\ \mathbf{A} + \mathbf{B}\mathbf{K} & -\mathbf{P}^{-1} + \mathbf{Z}^{-1} \end{bmatrix} \le 0 \qquad (3.60)$$

where $\Delta\mathbf{A}_M = \begin{bmatrix} \Delta\mathbf{A}_{0M} & 0 \\ -\mathbf{C} & \mathbf{I} \end{bmatrix}$, $\Delta\mathbf{B}_M = \begin{bmatrix} \Delta\mathbf{B}_{0M} \\ 0 \end{bmatrix}$ with $\Delta\mathbf{A}_{0M} = \sum_{i=1}^{M} \bar{\mu}_i \Delta\mathbf{A}_{im}$ and

$\Delta\mathbf{B}_{0M} = \sum_{i=1}^{M} \bar{\mu}_i \Delta\mathbf{B}_{im}$. By replacing matrix $\mathbf{P}$ by $\mathbf{Q}$ such that $\mathbf{Q} = \mathbf{P}^{-1}$, (3.60) is equivalent to:

$$\begin{bmatrix} -(1-\alpha)\mathbf{Q} & \mathbf{Q}\Delta\mathbf{A}_m^{\mathrm{T}} + \mathbf{Q}\mathbf{K}^{\mathrm{T}}\Delta\mathbf{B}_m^{\mathrm{T}} & \mathbf{Q}\mathbf{A}^{\mathrm{T}} + \mathbf{Q}\mathbf{K}^{\mathrm{T}}\mathbf{B}^{\mathrm{T}} \\ \Delta\mathbf{A}_m\mathbf{Q} + \Delta\mathbf{B}_m\mathbf{K}\mathbf{Q} & -\mathbf{Z}^{-1} & 0 \\ \mathbf{A}\mathbf{Q} + \mathbf{B}\mathbf{K}\mathbf{Q} & 0 & -\mathbf{Q} + \mathbf{Z}^{-1} \end{bmatrix} \le 0 \qquad (3.61)$$

The above inequality can be rewritten as:

$$\sum_{i=1}^{M}\sum_{j=1}^{N} \bar{\mu}_i \bar{v}_j \begin{bmatrix} -(1-\alpha)\mathbf{Q} & \mathbf{Q}\Delta\mathbf{A}_{im}^{\mathrm{T}} + \mathbf{Q}\bar{\mathbf{K}}_j^{\mathrm{T}}\Delta\mathbf{B}_{im}^{T} & \mathbf{Q}\mathbf{A}_i^{\mathrm{T}} + \mathbf{Q}\bar{\mathbf{K}}_j^{\mathrm{T}}\mathbf{B}_i^{\mathrm{T}} \\ \Delta\mathbf{A}_{im}\mathbf{Q} + \Delta\mathbf{B}_{im}\bar{\mathbf{K}}_j\mathbf{Q} & -\mathbf{Z}_{ij}^{-1} & 0 \\ \mathbf{A}_i\mathbf{Q} + \mathbf{B}_i\bar{\mathbf{K}}_j\mathbf{Q} & 0 & -\mathbf{Q} + \mathbf{Z}_{ij}^{-1} \end{bmatrix} \le 0 \qquad (3.62)$$

$$\Leftrightarrow \qquad \sum_{i=1}^{M}\sum_{j=1}^{N} \bar{\mu}_i \bar{v}_j \begin{bmatrix} -(1-\alpha)\mathbf{Q} & \mathbf{Q}\Delta\mathbf{A}_{im}^{\mathrm{T}} + \mathbf{Y}_j^{\mathrm{T}}\Delta\mathbf{B}_{im}^{\mathrm{T}} & \mathbf{Q}\mathbf{A}_i^{\mathrm{T}} + \mathbf{Y}_j^{\mathrm{T}}\mathbf{B}_i^{\mathrm{T}} \\ \Delta\mathbf{A}_{im}\mathbf{Q} + \Delta\mathbf{B}_{im}\mathbf{Y}_j & -\mathbf{Z}_{ij}^{-1} & 0 \\ \mathbf{A}_i\mathbf{Q} + \mathbf{B}_i\mathbf{Y}_j & 0 & -\mathbf{Q} + \mathbf{Z}_{ij}^{-1} \end{bmatrix} \le 0 \qquad (3.63)$$

where $\mathbf{Y}_j = \bar{\mathbf{K}}_j\mathbf{Q}$, $\bar{\mathbf{K}}_j = \begin{bmatrix} \mathbf{K}_j & \mathbf{k}_j \end{bmatrix}$. Since $\bar{\mu}_i\bar{v}_j \ge 0$, the above inequality is satisfied if each term under the summation is negative semi-definite. Hence, the theorem is proven. ■

Theorem 3 provides a method to obtain a robust T-S fuzzy controller that not only guarantees system stability but also can achieve good transient performance. The designer can use the convergent rate to adjust how fast the system converges to steady-state values.

Since the LMI set does not depend on the uncertainty norm but on the linear coefficient matrices of the local linear systems that maximize the Lyapunov function, the stability conditions provided in this paper are much more relaxed than other robust controller's conditions. The result is a robust T-S controller that can achieve performance as good as a T-S controller that is designed for a system without uncertainty.

3.4 Simulation Results on an Electrohydraulic Actuator

In this section, performance comparisons on an electrohydraulic actuator (EHA) between the RTSFC, the robust sliding mode controller [18] and the H∞ sliding mode controller [85] are presented. The electrohydraulic actuator is driven by a bidirectional fixed displacement gear pump. A special symmetrical actuator is connected with the load and the motion of the load is controlled by varying the speed of the electric motor. In [86], a nonlinear model of the hydraulic part of the EHA system was developed as follows:

$$
\begin{aligned}
x_1(k+1) &= x_1(k) + Tx_2(k) + Tw_1(k) \\
x_2(k+1) &= x_2(k) + Tx_3(k) + Tw_2(k) \\
x_3(k+1) &= \left[1 - T\left(\frac{a_2V_0 + M\beta_e C_T}{MV_0}\right)\right]x_3(k) - T\frac{(2A_p^2 + a_2C_T)\beta_e}{MV_0}x_2(k) \\
&\quad - T\frac{2a_1V_0x_2(k)x_3(k)}{MV_0}\operatorname{sgn}(x_2(k)) - T\frac{\beta_c C_T[a_1(x_2(k))^2 + a_3]}{MV_0}\operatorname{sgn}(x_2(k)) \\
&\quad + T\frac{2A_pD_p\beta_e}{MV_0}u(k) + Tw_3(k) \\
y(k+1) &= x_1(k+1)
\end{aligned}
\tag{3.64}
$$

where x_1, x_2 and x_3 are the position (m), velocity (m/s) and acceleration of the load (m/s^2), respectively; $u(k)$ represents the rotation speed of the bidirectional hydraulic pump (rpm),

which is also the control signal of the system. Other parameters can be found in Table Table 3-1.

The uncertainties of the EHA are introduced by time-varying friction effects, which are included in the variations of the coefficients of the nonlinear actuator friction a_1, a_2 and a_3 [18]:

$$\begin{aligned} a_1 &\in \left[a_{1o} - \Delta a_1 \cdot a_{1o} \quad a_{1o} + \Delta a_1 \cdot a_{1o}\right] \\ a_2 &\in \left[a_{2o} - \Delta a_2 \cdot a_{2o} \quad a_{2o} + \Delta a_2 \cdot a_{2o}\right] \\ a_3 &\in \left[a_{3o} - \Delta a_3 \cdot a_{3o} \quad a_{3o} + \Delta a_3 \cdot a_{3o}\right] \end{aligned} \tag{3.65}$$

with $a_{1o} = 2.1\times10^4$, $a_{2o} = -1450$, $a_{3o} = 46$.

Table 3-1: Parameters of the EHA [18], [85], [86].

Symbol	Name	Value
M	Mass of the load	20 kg
A_p	Pressure area in the symmetric actuator	5.05×10^{-4} m^2
D_p	Pump displacement	1.6925×10^{-7} m^3/rad
β_e	Bulk modulus of the hydraulic oil	2.1×10^8 Pa
C_T	Lumped leakage coefficient	5×10^{-13} m^3 / s $\cdot$ Pa
V_0	Mean volume of the hydraulic actuator	6.85×10^{-5} m^3
$\omega_1, \omega_2, \omega_3$	Lumped system noises and disturbances	0.01×10^{-3} m

A type-2 FBFN model is used to approximate the state variable x_3 of the nonlinear system. The structure of rule *j* of the FBFN has the following form:

$$R^j: \quad \text{IF } x_1(k) \text{ is } X_1^j \text{ and } x_2(k) \text{ is } X_2^j \text{ and } x_3(k) \text{ is } X_3^j \text{ and } u(k) \text{ is } U^j \quad \text{THEN } \tilde{x}_3(k+1) = \tilde{G}^j \tag{3.66}$$

where $\tilde{x}_3(k+1)$ is the predicted interval value of the state variable vector x_3. $\tilde{G}^j$ is an interval type-2 fuzzy set with its centroid $\tilde{w}^j$ as an interval set: $\tilde{w}_p^j = [w_l^j, w_r^j]$.

In order to evaluate the performance of the type-2 FBFN for capturing the uncertainties of the data, the type-2 FBFN is trained with training data generated from the nonlinear system, then comparisons between the outputs of the type-2 FBFN and the nonlinear system are conducted. During data generation process, the uncertain parameters in the nonlinear model are assigned with random values within bounded ranges. In this work, the type-2 FBFN model was obtained two times from the same nonlinear model with different amounts of uncertainties represented by the nonlinear friction coefficients a_1, a_2 and a_3. It has been shown that 10% variations of the parameters a_1, a_2 and a_3 can reasonably capture the real friction in the actual system [18]. For each training data, the parameters a_1, a_2 and a_3 were chosen as random numbers within the lower and upper bounds as shown in Eq. (3.65). The values of Δa_1, Δa_2, Δa_3 can be found in Table 3-2.

Table 3-2: Uncertainty cases for the EHA system.

Case	Δa_1	Δa_2	Δa_3
1	0.1	0.1	0.1
2	0	0.1	0

Figure 3-2 shows the non-dimensional error indices (NDEI) during training in two cases. The NDEIs show that the errors observed during the training processes approach steady-state values as the number of hidden nodes is increased. Figure 3-3 shows nominal system responses of the nominal nonlinear system when the input is constant. Figure 3-4 and Figure 3-5 show the response comparison between the type-2 FBFN and the uncertain nonlinear model under two uncertain conditions and input values. It can be seen from the results that the type-2 FBFN models are able to capture all the uncertainties of the nonlinear system very "tightly". The deviations from nominal responses of the type-2 FBFN are also very small, which proves that the type-2 FBFN can accurately approximate the nonlinear system.

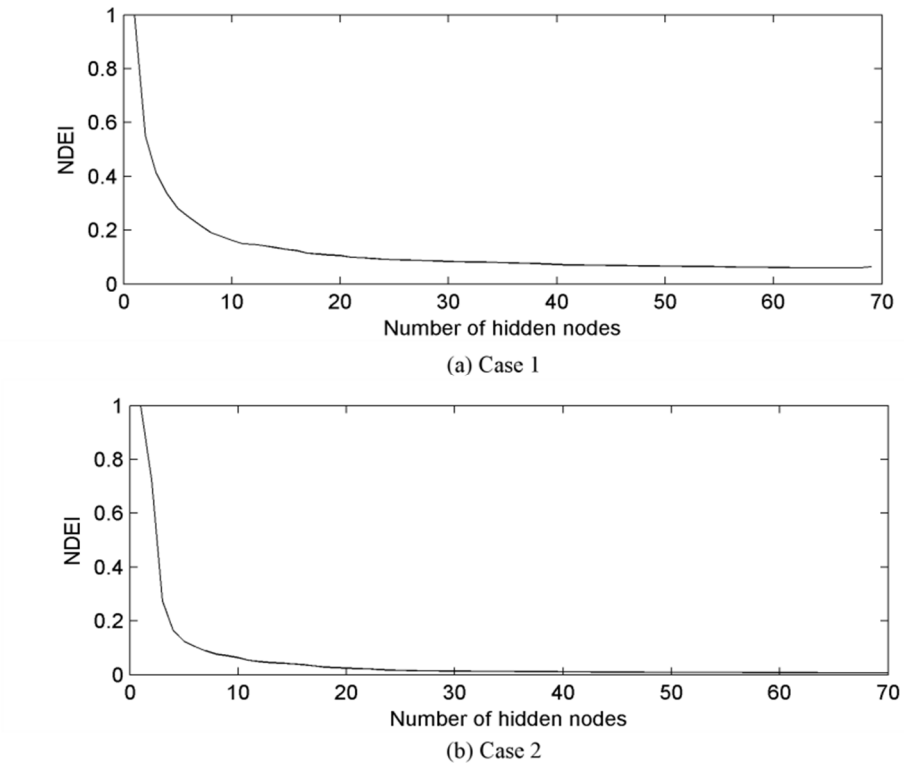

Figure 3-2: NDEI for both cases.

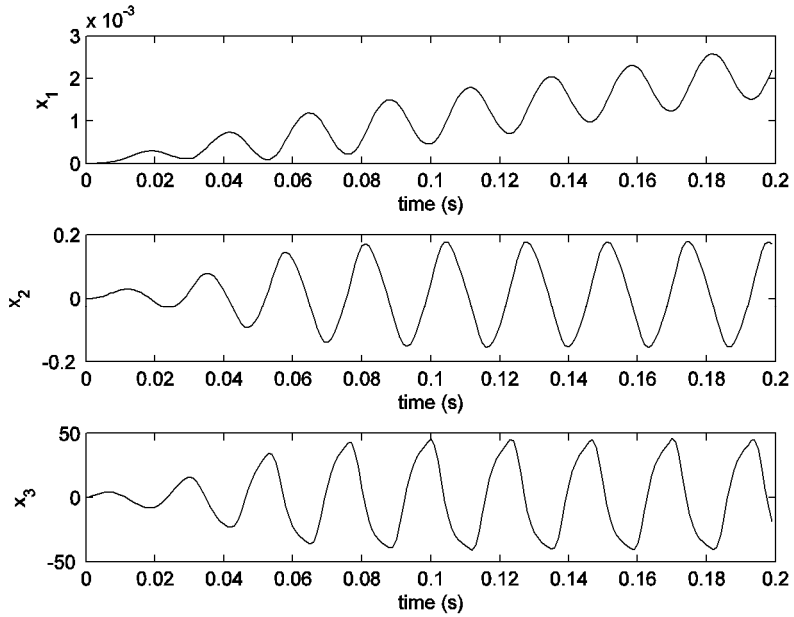

Figure 3-3: Nominal system responses (u = 30 rpm).

From the type-2 FBFN, a type-2 T-S fuzzy model was obtained by using the procedure as described in Section 3.2. The type-2 T-S fuzzy model has four rules, in which each rule has the following form:

$$\begin{aligned} R^i: \quad & \text{IF } x_2(k) \text{ is } X_2^i \text{ and } x_3(k) \text{ is } X_3^i \\ & \text{THEN } \tilde{\mathbf{x}}(k+1) = \tilde{\mathbf{A}}_i \mathbf{x}(k) + \tilde{\mathbf{B}}_i \mathbf{u}(k) \end{aligned} \tag{3.67}$$

where $\tilde{\mathbf{x}}(k+1)$ is the predicted interval value of the state variable vector **x**. The centers of the fuzzy sets X_2^i and X_3^i are chosen as follows:

$$\begin{aligned} c_{X_2^1} = c_{X_2^2} = -0.015 \text{ m/s}, \; c_{X_2^3} = c_{X_2^4} = 0.015 \text{ m/s} \\ c_{X_3^1} = c_{X_3^3} = -0.015 \text{ m/s}, \; c_{X_3^2} = c_{X_3^4} = 0.015 \text{ m/s} \end{aligned} \tag{3.68}$$

The minimum and maximum values of matrices $\tilde{\mathbf{A}}_i$ and $\tilde{\mathbf{B}}_i$ are given in APPENDIX A.

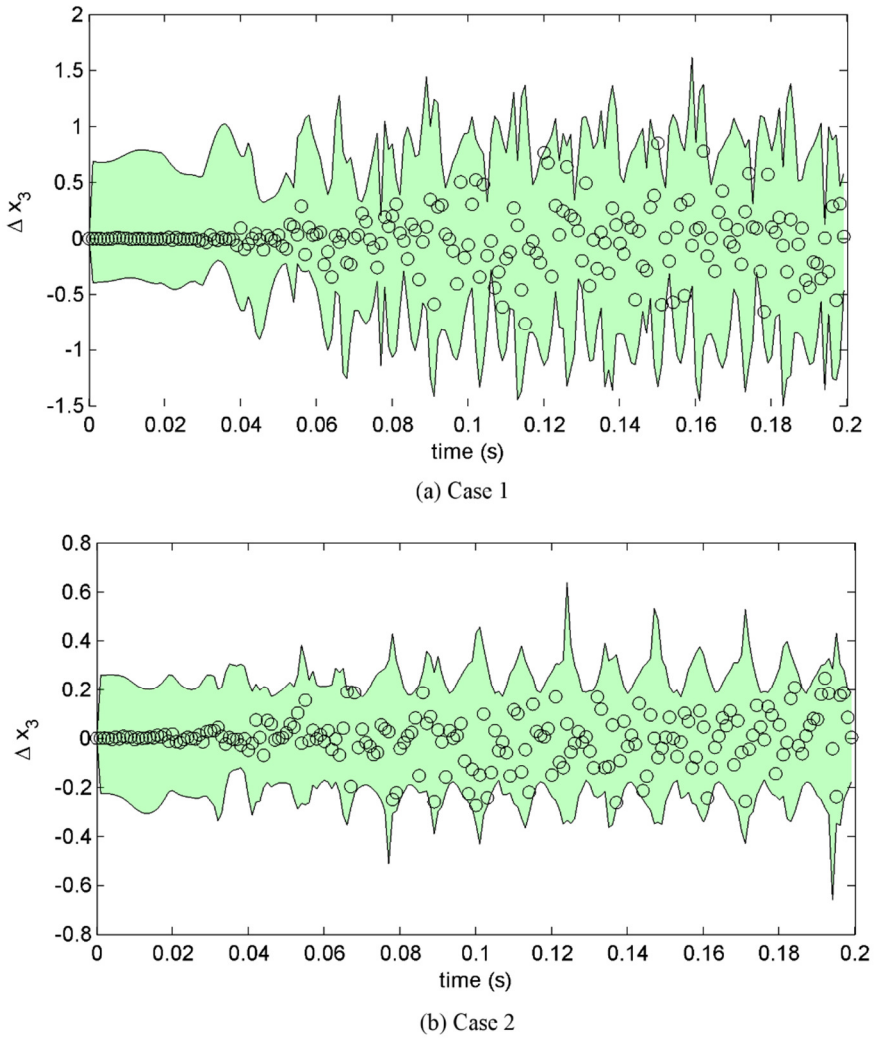

Figure 3-4: Deviations from nominal responses with u = 10 rpm, shaded areas indicate the interval output deviation of the type-2 FBFN model, circle markers represent sampling data measured from the responses of the uncertain nonlinear system.

By solving the LMI given in Theorem 1, a robust T-S fuzzy controller (RTSFC) which has four rules can be found. Each rule of the controller has the following form:

$$\begin{aligned} &\text{Rule } j: \text{IF } x_2(k) \text{ is } X_{02}^i \text{ and } x_3(k) \text{ is } X_{03}^i \\ &\quad \text{THEN } \mathbf{u}(k) = \mathbf{K}_j \mathbf{x}(k) + \mathbf{k}_j \boldsymbol{\zeta}(k), \\ &\quad \boldsymbol{\zeta}(k+1) = \boldsymbol{\zeta}(k) + T\mathbf{e}(k), \quad \mathbf{e}(k) = \mathbf{r}(k) - \mathbf{C}\mathbf{x}(k) \end{aligned} \tag{3.69}$$

where the feedback gains of each rule are given in APPENDIX J.

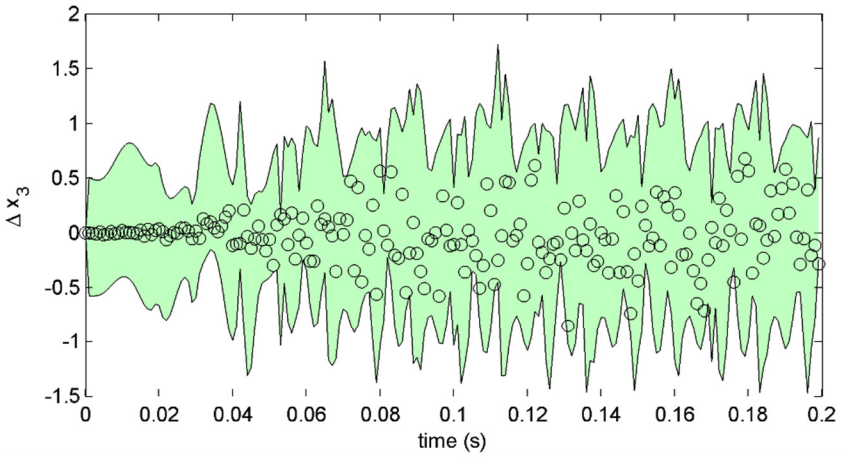

(a) Case 1

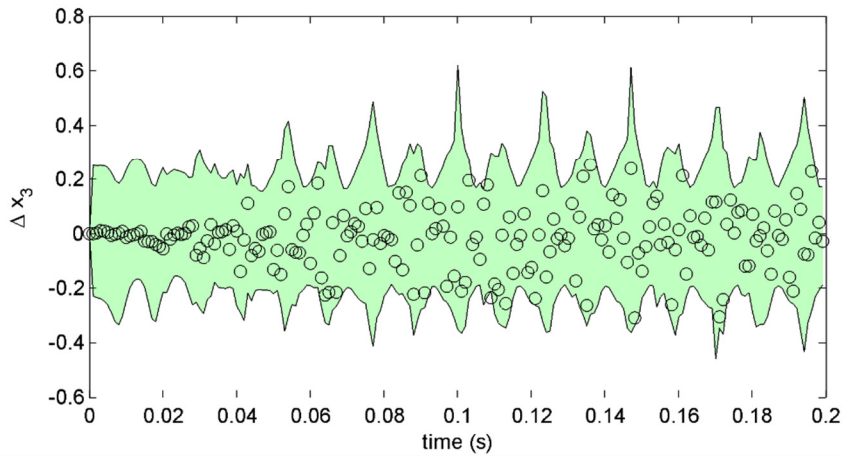

(b) Case 2

Figure 3-5: Deviations from nominal responses with u = 30 rpm, shaded areas indicate the interval output deviation of the type-2 FBFN model, circle markers represent sampling data measured from the responses of the uncertain nonlinear system.

To investigate the performance of the RTSFC when implementing on the hydraulic actuator, simulations were conducted in the MATLAB/SIMULINK environment. The computation time to calculate the output of the RTSFC when using a DELL Optilex 960 PC is 0.01 ms. Hence, the RTSFC is very suitable to be implemented in many real-time

applications with small sampling time. The simulation results of the RTSFC were compared with the system responses of the robust sliding mode controller (RSLMC) [18] and the robust H∞ sliding mode controller (RH∞SLMC) [85] under the same conditions.

Figure 3-6 shows the system response comparisons between the robust sliding mode controller (RSLMC) and the RTSFC with two different convergent rates used. A constant reference signal was used and the simulations were conducted in the MATLAB/SIMULINK environment. The results show that the RTSFC is able to obtain much faster responses than the RSLMC while keeping the output with less oscillation in both cases of convergent rates. The higher the convergent rate, the faster the responses that the RTSFC can achieve. In the first case ($\alpha = 0.05$), the settling time is less than 0.05 s while in the second case ($\alpha = 0.03$), the settling time is about 0.08 s. The control efforts of the RTSFC are shown in Figure 3-7.

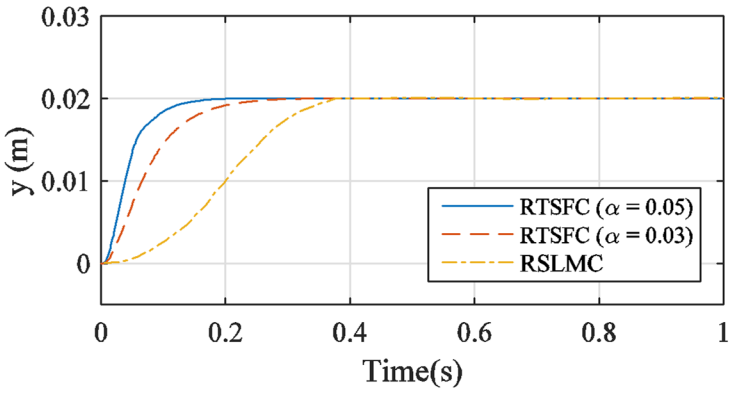

Figure 3-6: System response comparisons with a constant reference signal (r = 0.02m) between the RTSFC and the RSLMC.

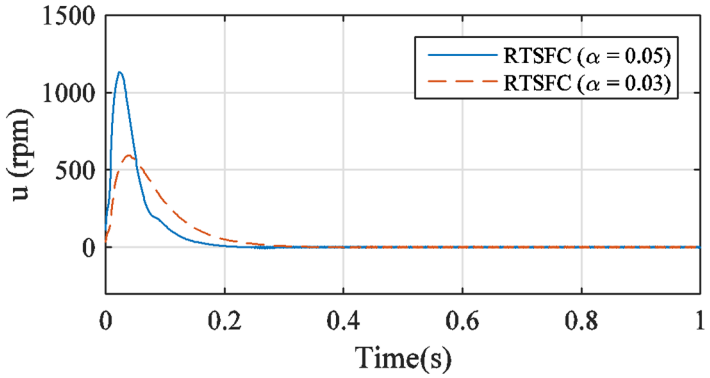

Figure 3-7: Control inputs from the RTSFC under different convergence rates.

Figure 3-8 shows the system response comparisons between the RTSFC and the robust H∞ sliding mode controller (RH∞SLMC) [85] with a sinusoidal reference signal under lump system noises and disturbances. The mean absolute errors between the controllers' responses and the reference signals are shown in Table 3-3. From the results, it can be seen that the RTSFC with a convergent rate $\alpha = 0.2$ can reduce the steady-state error by almost 50 percent compared to the RH∞SLMC.

Table 3-3: Comparison of mean absolute errors between the RTSFC and the RH∞SLMC under sinusoidal reference signal.

Controller	**Mean Absolute Error (m)**
RTSFC α = 0.2	7.7352e-05
RTSFC α = 0.1	1.3222e-04
RH∞SLMC	1.6707e-04

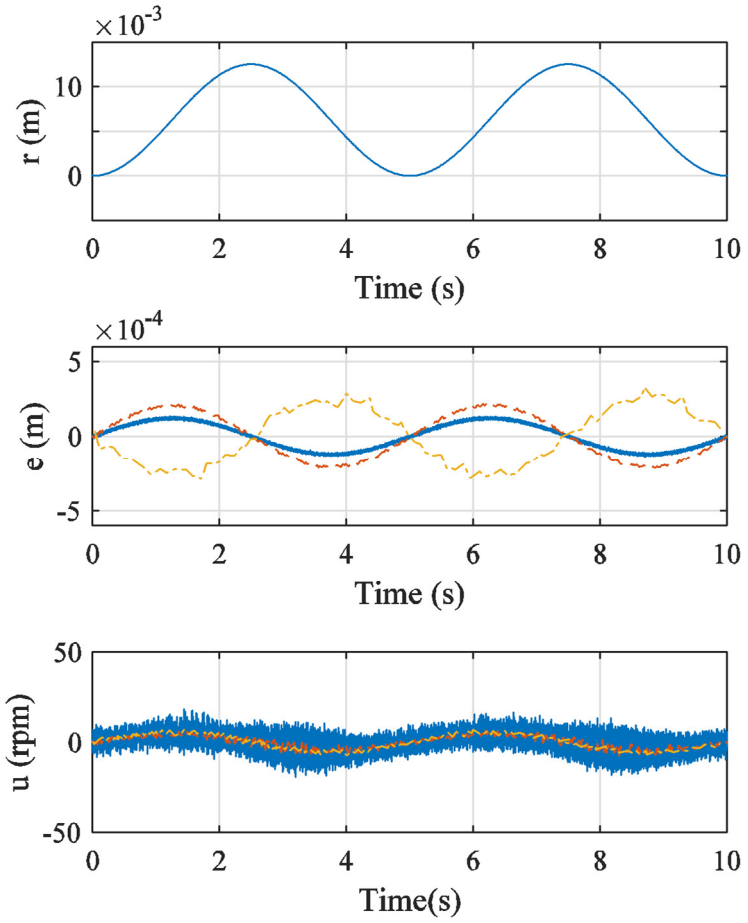

Figure 3-8: System response comparisons between the RTSFC and the RH∞SLMC with a sinusoidal reference signal (solid: RTSFC with $\alpha = 0.2$, dash: RTSFC with $\alpha = 0.1$ dash-dot: RH∞SLMC).

Figure 3-9 shows the system response comparisons between the RTSFC and the robust H∞ sliding mode controller (RH∞SLMC) [85] with a spike reference signal under lump system noises and disturbances. From the results, it can be seen that the RTSFC can follow the reference signal better than RH∞SLMC under very small transient time. The control efforts of the RTSFC can also be found in Figure 3-9.

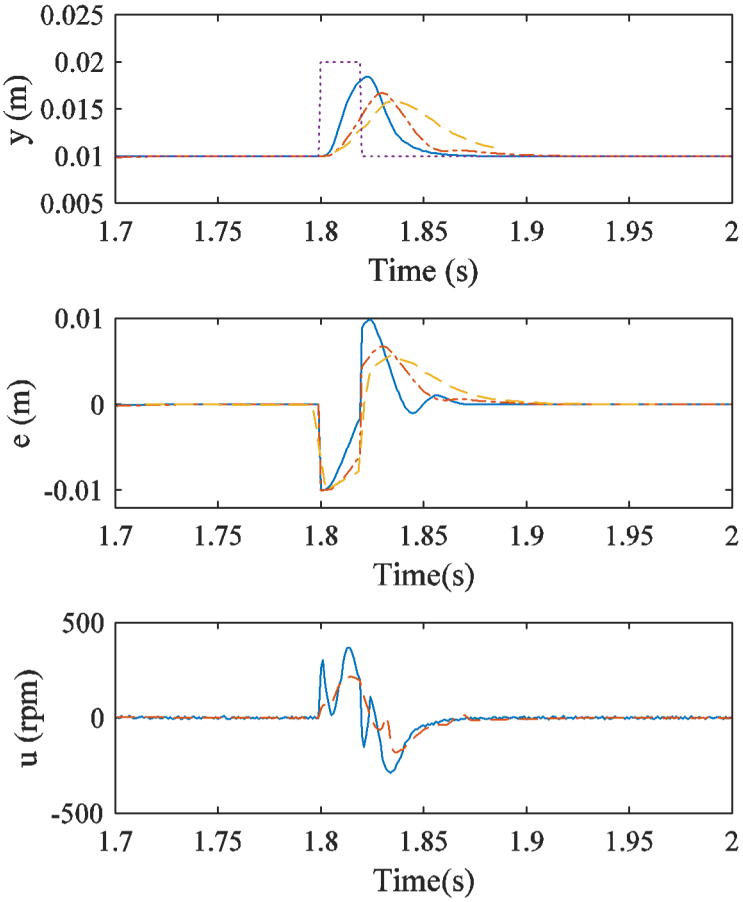

Figure 3-9: System response comparisons between the RTSFC and the RH∞SLMC with a spike reference signal (solid: RTSFC with α = 0.2, dash-dot: RTSFC with α = 0.1, dash: RH∞SLMC, dot: reference signal).

CHAPTER 4. MODELING AND ROBUST CONTROL OF LASER WELDING PROCESS ON HIGH STRENGTH TITANIUM ALLOY USING FUZZY BASIS FUNCTION NETWORKS AND ROBUST TAKAGI SUGENO FUZZY CONTROLLER

This chapter first proposes a new laser keyhole-welding model and an observer to estimate the penetration depth of the keyhole during the welding process. Based on the welding model, a robust Takagi-Sugeno fuzzy controller (RTSFC) was chosen to change the laser power during implementation since the welding process is a nonlinear process with large amounts of uncertainties. Experiments conducted on titanium samples to evaluate the accuracy and effectiveness of the model and the RTSFC are presented at the end of the chapter.

4.1 Introduction

Laser keyhole welding is an important and well-known process for joining metals in many industrial applications. Throughout the process, the laser beam creates a weld with a higher aspect ratio than traditional arc welding processes [87], which is critical to deep penetration welding [88]. In keyhole welding, the penetration depth is the most important feature that needs to be monitored and controlled to ensure that the keyhole is stable and weld quality is good. However, the mathematical relationship between the penetration depth and the welding parameters is very complex [89]–[92] due to the nonlinear nature of the process and process variation that occurs due to the effects of many factors such as

varying assisted gas pressure, uneven surface of the workpiece or fluctuation of the surface absorption of the laser beam. Thus, estimation of keyhole geometry has become the primary objective of many studies. Tan et al. [91] investigated the keyhole and molten pool and proposed a three-dimensional model of the keyhole dynamics, together with the vapor plume and molten pool for the laser welding process when assisted gases are used. Courtois et al. [92] provided a complete model of keyhole and weld pool dynamics, which includes three phases of the matter: the vaporized metal, the liquid phase, and the solid base. The model also shows keyhole oscillation and porosity formed during the laser welding process. In real-time applications, the numerical models used for describing the keyhole dynamics described above cannot be used due to intensive computational requirements. In order to alleviate that problem, data-driven models such as fuzzy systems and neural networks based on experimental data have been built. Since the outputs of these models can be calculated in a short amount of time, they are suitable for control applications. Huang and Kovacevic [93] used a multilayer feedforward neural network and a multiple regression method to obtain a relationship between weld penetration and the acoustic signal measured during the welding process. Singh et al. [94] modeled the weld bed geometry of laser welding by using a counter propagation neural network and feed-forward back-propagation neural network. By using radial basis function neural networks, Luo and Shin [95] proposed static and dynamic models to estimate the keyhole geometry and predict porosity in the laser keyhole welding.

However, the dynamics of the keyhole depend on many factors such as assisted gas pressure or uneven surface conditions. Assisted gases can alter the flow pattern of the molten pool and change the laser energy distribution [96]–[98]. Changes in the focal

diameter due to uneven surfaces can affect the distributions of the energy intensity, which will influence the keyhole geometry [99]. Neural network based models can only predict the keyhole dynamics accurately in a certain set of conditions used to train the network. Changing the welding parameters requires retraining of the model, making it difficult and impractical to use the existing models for applications in industrial settings with uncertainties. To alleviate this limitation and to improve the applicability of data-driven laser welding models, this study uses a type-2 fuzzy basis function network (type-2 FBFN). This fuzzy neural network system can approximate the keyhole geometry while effectively capturing the unstructured uncertainties, which may come from many factors such as varying assisted gas pressure, uneven surface of the workpiece or fluctuation of the laser beam diameter.

The experiments in this study are conducted with titanium alloys. Titanium alloys are widely used in many areas where high performance and reliability are required [100] in the medical, aerospace and nuclear industries. Hence, a robust and efficient method to improve the quality of welding processes is essential to meet the highly demanding requirements of products in these industries. In order to achieve this objective, many studies have investigated the influence of laser welding parameters on the quality of titanium samples [100]–[103]. However, since laser welding is a complex process with many uncertainties, real-time control of the welding quality would be desirable to ensure the consistent quality of the weld in the presence of uncertainties.

The control of the weld joint-penetration in real time for other materials and welding processes has been reported previously. Liu and Zhang [104] used a predictive controller to obtain a desired weld penetration based on a linear model of the Gas Tungsten

Arc Welding (GTAW) process. Sibillano et al. [105] stabilized the penetration depth of the CO_2 laser lap welding process on stainless steel plates by using a proportional-integral controller. However, most of the methods presented in the literature did not provide any stability analysis due to the lack of a mathematical model for the process. Hence, their applications in industry, where a high degree of reliability is required, are still limited.

4.2 Experimental Setup

The laser welding experimental setup (Figure 4-1) used in this study consists of a Mazak VQC-15/40 vertical machining center, a fiber laser (IPG photonics YLS-1000) with a focal diameter of 200 μm, a weld pool monitoring system and a real time computer for controller implementation. The weld pool monitoring system (Figure 4-2) includes a complementary metal–oxide–semiconductor (CMOS) camera with optical filters, a 200 mW focus-adaptable green laser with the wavelength close to 530 nm used as the illuminant for the image processing system, and a computer equipped with the National Instruments (NI) Labview software and the NI vision system toolkit. The CMOS camera (DFK 42BUC03 USB 2.0) is a color industrial camera with a frame rate of 30 frames/s and the image resolution of 1280 x 720 pixels. The estimation of keyhole diameter is conducted based on live images by using the algorithm developed by Luo and Shin [95]. The analog control signal is generated by using the NI real-time computer (PXI 8115) through a data acquisition card (6070E). The fiber laser system accepts an analog signal with voltage between 0 to 12 V. The calibration curve between the voltage and the laser output power is shown in Figure 4-3. High-strength grade 5 titanium (Ti-6Al-4V) is used in this study

as the substrate material. The shielding gas is Argon, which is blown into the weld pool both coaxially and horizontally as shown in Figure 4-2.

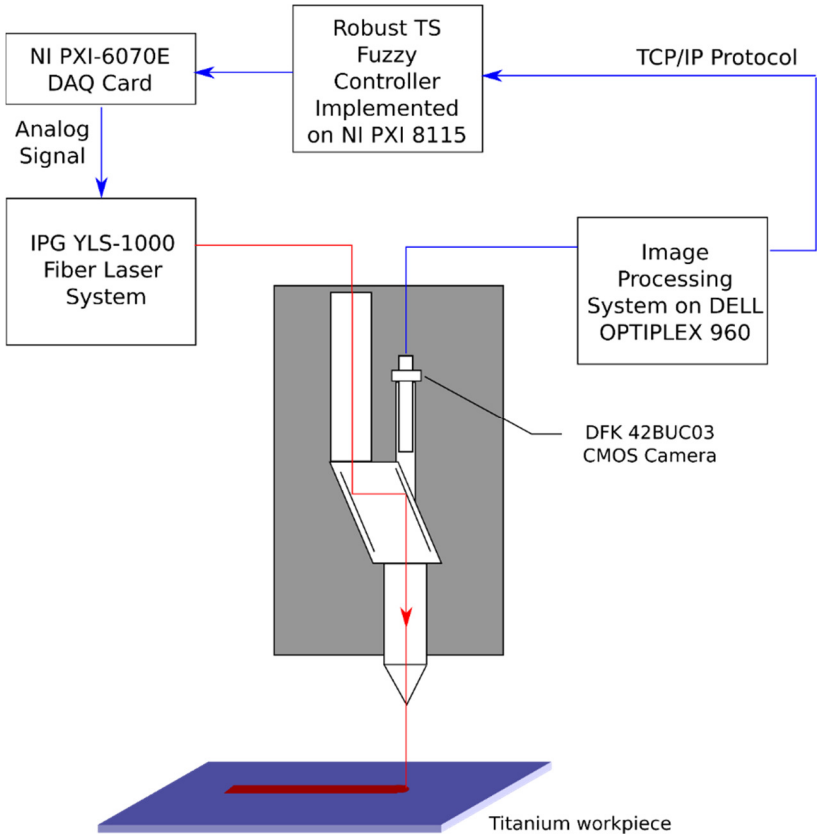

Figure 4-1: Laser Welding Control Experiment Setup.

Figure 4-2: Photo of the Laser Head and The Coaxial Monitoring System on the Mazak Vertical Machining Center.

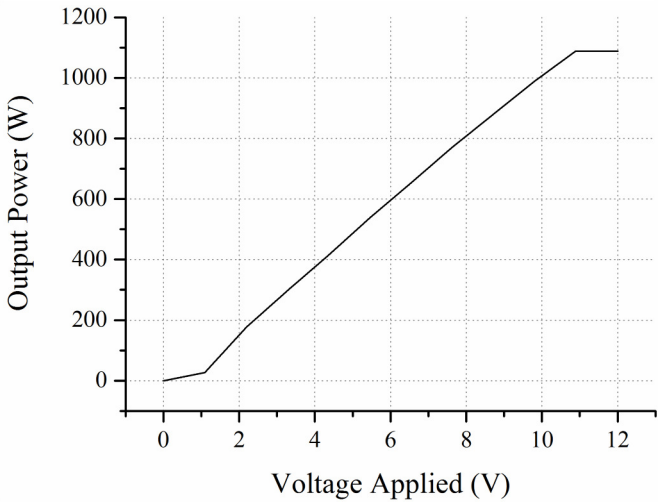

Figure 4-3: Relationship Between the Voltage Applied and the Laser Power [106].

4.3 Estimation of Keyhole Dynamics

In this section, an FBFN-based observer is constructed to estimate the keyhole penetration depth. The observer includes a static keyhole dimeter model, a dynamic keyhole penetration depth model and an adaptive divided difference filter (ADDF).

4.3.1 Keyhole Dynamic Model

The dynamic system (Figure 4-4) of the keyhole welding process can be built by using a type-2 FBFN model. The type-2 FBFN model is chosen since it can capture unstructured uncertainties within the welding process such as fluctuation of the shielding gas pressure, bending of the workpiece due to heat and uneven surface reflectivity. The output of the model is the future value of the keyhole diameter, while the inputs are the current and previous (measured) values of the keyhole diameter, the current laser power and the welding speed. The structure of the type-2 FBFN model includes a set of *M* fuzzy rules, in which the j^{th} rule has the following form:

$$\begin{aligned} R^j: \quad & \text{IF } u_1(k) \text{ is } A_1^j \text{ and } u_2(k) \text{ is } A_2^j \text{ and } x_1(k-1) \text{ is } B_1^j \text{ and } x_1(k) \text{ is } B_2^j \\ & \text{then } \tilde{x}_1(k+1) = \tilde{X}_1^j \end{aligned} \tag{4.1}$$

where x_1, u_1 and u_2 represent the keyhole diameter, the laser power and the welding speed, respectively. A_1^j, A_2^j, B_1^j and B_2^j are type-1 fuzzy sets of rule R^j, characterized by Gaussian membership functions $\mu_{A_p^j}(u_i)$ and $\mu_{B_q^j}(x_j)$ $(p=1,2;\ q=1,2)$ with the centers c_{Ap}^j, c_{Bq}^j and standard deviations σ_{Ap}^j, σ_{Bq}^j:

$$A_p^j = \left(u_p, \mu_{A_p^j}(u_p)\right), \qquad \mu_{A_p^j}(u_p) = \exp\left[-\frac{1}{2}\left(\frac{u_p - c_{Ap}^j}{\sigma_{Ap}^j}\right)^2\right] \tag{4.2}$$

$$B_q^j = \left(x_q, \mu_{B_q^j}(x_q)\right), \qquad \mu_{B_q^j}(x_q) = \exp\left[-\frac{1}{2}\left(\frac{x_q - c_{Bq}^j}{\sigma_{Bq}^j}\right)^2\right] \tag{4.3}$$

$\tilde{X}_1^j$ is a type-2 interval fuzzy set, which is defined by two end points w_l^j and w_r^j.

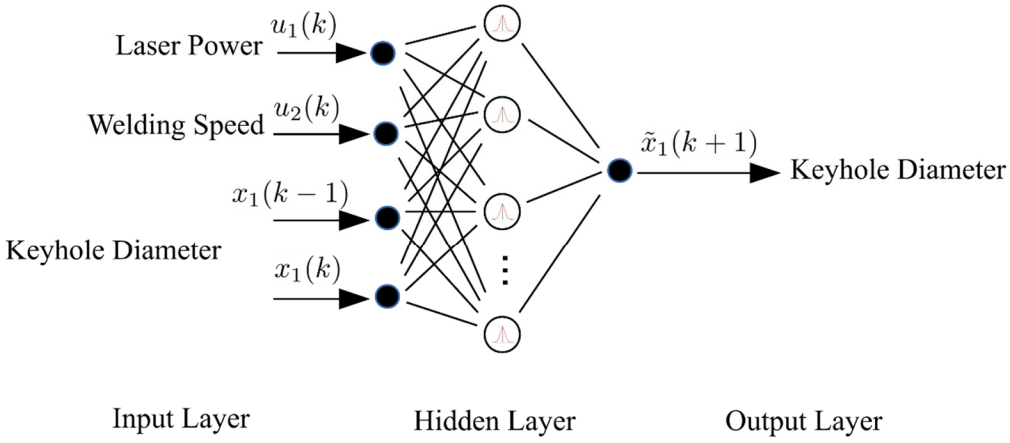

Figure 4-4: FBFN model for the dynamics of keyhole diameter.

The parameters of the model (c_{Ap}^j , c_{Bq}^j , σ_{Ap}^j , σ_{Bq}^j , w_l^j , w_r^j) were obtained by using the adaptive least square and active set method as proposed by Ngo and Shin [73]. The values of the centers and widths of the input membership functions are shown in Table 4-1 and Table 4-2, respectively. Two endpoints of the output membership functions can be found in Table 4-3. With the singleton fuzzier, product inference and centroid defuzzifier used in the inferencing process, the estimated interval keyhole diameter $\tilde{x}_1(k+1)$ can be computed by the interval-type nonlinear mapping $\tilde{f}: u_1(k),\, u_2(k),\, x_1(k-1),\, x_1(k) \subset \Re \rightarrow \tilde{x}_1(k+1) \subset \Re$, which is formulated as follows [107]:

$$\begin{aligned}\tilde{x}_1(k+1) &= \tilde{f}\left(u_1(k), u_2(k), x_1(k-1), x_1(k)\right) \\ &= \frac{\sum_{j=1}^{M}\left(\tilde{w}^j \cdot \mu_{A_1^j}\left[u_1(k)\right] \cdot \mu_{A_2^j}\left[u_2(k)\right] \cdot \mu_{B_1^j}\left[x_1(k-1)\right] \cdot \mu_{B_2^j}\left[x_1(k)\right]\right)}{\sum_{j=1}^{M}\left(\mu_{A_1^j}\left[u_1(k)\right] \cdot \mu_{A_2^j}\left[u_2(k)\right] \cdot \mu_{B_1^j}\left[x_1(k-1)\right] \cdot \mu_{B_2^j}\left[x_1(k)\right]\right)} \\ &= \left[\frac{\sum_{j=1}^{M}\left(w_l^j \cdot \mu_{A_1^j}\left[u_1(k)\right] \cdot \mu_{A_2^j}\left[u_2(k)\right] \cdot \mu_{B_1^j}\left[x_1(k-1)\right] \cdot \mu_{B_2^j}\left[x_1(k)\right]\right)}{\sum_{j=1}^{M}\left(\mu_{A_1^j}\left[u_1(k)\right] \cdot \mu_{A_2^j}\left[u_2(k)\right] \cdot \mu_{B_1^j}\left[x_1(k-1)\right] \cdot \mu_{B_2^j}\left[x_1(k)\right]\right)},\right. \\ &\qquad \left.\frac{\sum_{j=1}^{M}\left(w_r^j \cdot \mu_{A_1^j}\left[u_1(k)\right] \cdot \mu_{A_2^j}\left[u_2(k)\right] \cdot \mu_{B_1^j}\left[x_1(k-1)\right] \cdot \mu_{B_2^j}\left[x_1(k)\right]\right)}{\sum_{j=1}^{M}\left(\mu_{A_1^j}\left[u_1(k)\right] \cdot \mu_{A_2^j}\left[u_2(k)\right] \cdot \mu_{B_1^j}\left[x_1(k-1)\right] \cdot \mu_{B_2^j}\left[x_1(k)\right]\right)}\right]\end{aligned} \tag{4.4}$$

The nominal estimated keyhole diameter $x_1(k+1)$ is defined as the center of the keyhole diameter interval $\tilde{x}_1(k+1)$ and can be calculated as:

$$\begin{aligned}x_1(k+1) &= f\left(u_1(k), u_2(k), x_1(k-1), x_1(k)\right) \\ &= \frac{1}{2}\frac{\sum_{j=1}^{M}\left(w_l^j \cdot \mu_{A_1^j}\left[u_1(k)\right] \cdot \mu_{A_2^j}\left[u_2(k)\right] \cdot \mu_{B_1^j}\left[x_1(k-1)\right] \cdot \mu_{B_2^j}\left[x_1(k)\right]\right)}{\sum_{j=1}^{M}\left(\mu_{A_1^j}\left[u_1(k)\right] \cdot \mu_{A_2^j}\left[u_2(k)\right] \cdot \mu_{B_1^j}\left[x_1(k-1)\right] \cdot \mu_{B_2^j}\left[x_1(k)\right]\right)} \\ &\quad + \frac{1}{2}\frac{\sum_{j=1}^{M}\left(w_r^j \cdot \mu_{A_1^j}\left[u_1(k)\right] \cdot \mu_{A_2^j}\left[u_2(k)\right] \cdot \mu_{B_1^j}\left[x_1(k-1)\right] \cdot \mu_{B_2^j}\left[x_1(k)\right]\right)}{\sum_{j=1}^{M}\left(\mu_{A_1^j}\left[u_1(k)\right] \cdot \mu_{A_2^j}\left[u_2(k)\right] \cdot \mu_{B_1^j}\left[x_1(k-1)\right] \cdot \mu_{B_2^j}\left[x_1(k)\right]\right)}\end{aligned} \tag{4.5}$$

Table 4-1: Centers of the input membership functions of the keyhole diameter model.

Rule R^j	c_{A1}^j	c_{A2}^j	c_{B1}^j	c_{B2}^j
1	1075.09	0.84	1.30	1.61
2	290.62	1.06	0.36	0.94
3	954.07	3.66	1.08	1.73
4	755.97	3.26	0.81	1.49
5	815.46	4.13	1.78	1.35

Table 4-2: Widths of the input membership functions of the keyhole diameter model.

Rule R^j	σ_{A1}^j	σ_{A2}^j	σ_{B1}^j	σ_{B2}^j
1	509.6825	4.620077	3.191627	1.022197
2	3173.063	6.062091	0.941378	0.95564
3	785.979	4.370629	6.416455	1.337549
4	3382.97	10.99296	0.13319	0.16013
5	66.43663	1.578863	0.16013	3.377035

Table 4-3: Endpoints of the output membership functions of the keyhole diameter model.

Rule R^j	w_l^j	w_r^j
1	2.301817	2.882255
2	-0.6872	-0.25375
3	0.82227	1.128243
4	3.347483	8.643222
5	-159.703	-159.703

4.3.2 Keyhole Penetration Model

The penetration depth can be estimated from the values of laser power, welding speed and current keyhole diameter using the structure of the FBFN model shown in Figure 4-5. The model is constructed by l rules, in which the i^{th} rule has the following form:

$$\begin{aligned} R^i: \quad & \text{IF } u_1(k) \text{ is } A_1^i \text{ and } u_2(k) \text{ is } A_2^i \text{ and } x_1(k+1) \text{ is } B_1^i \\ & \text{THEN } x_2(k+1) = X_2^i \end{aligned} \tag{4.6}$$

where x_1, x_2, u_1 and u_2 represent the keyhole diameter, the penetration depth, the laser power and the welding speed, respectively. A_1^i, A_2^i, B_1^i and X_2^i are type-1 fuzzy sets of rule R^i characterized by the Gaussian membership function $\mu(\bullet)$:

$$\mu(x) = \exp\left[-\frac{1}{2}\left(\frac{x-c}{\sigma}\right)^2\right] \tag{4.7}$$

where c is the center and σ is the standard deviation.

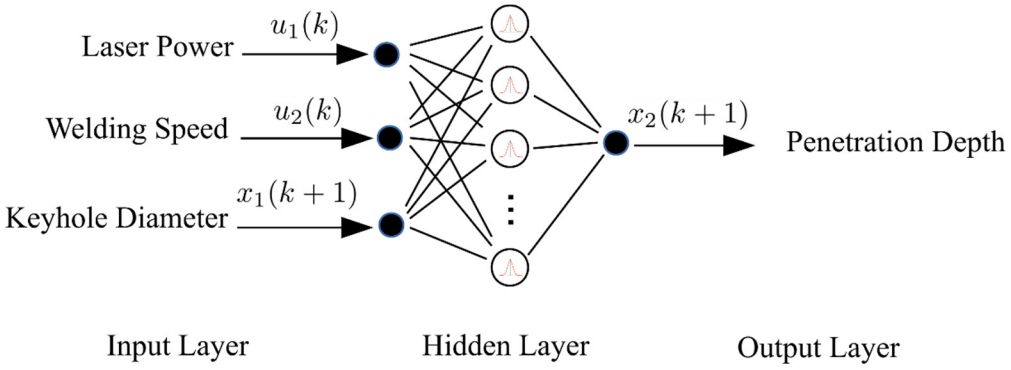

Figure 4-5: Static FBFN model for the keyhole penetration depth.

By using singleton fuzzification, product inference and centroid defuzzification methods, the nonlinear mapping $g: u_1(k), u_2(k) \subset \Re, x_1(k+1) \subset \Re \rightarrow x_2(k+1) \subset \Re$ of the FBFN is formulated as follows:

$$x_2(k+1) = g\left(u_1(k), u_2(k), x_1(k+1)\right) = \frac{\sum_{i=1}^{l}\left(b^i \cdot \mu_{A_1^i}\left[u_1(k)\right] \cdot \mu_{A_2^i}\left[u_2(k)\right] \cdot \mu_{B_1^i}\left[x_1(k+1)\right]\right)}{\sum_{i=1}^{l}\left(\mu_{A_1^i}\left[u_1(k)\right] \cdot \mu_{A_2^i}\left[u_2(k)\right] \cdot \mu_{B_1^i}\left[x_1(k+1)\right]\right)} \tag{4.8}$$

The parameters of the model (c, σ and b) (Table 4-4) were obtained by using the adaptive least square and genetic training algorithm as proposed by Lee and Shin [73].

Table 4-4: Parameters of the keyhole static FBFN model.

Rule R^i	c_{A1}^i	c_{A2}^i	c_{B1}^i	σ_{A1}^i	σ_{A2}^i	σ_{A2}^i	b
1	9.6332	3.4077	1.4129	253.87	2.8516	0.54574	2.9875
2	8.4658	2.0949	1.9656	290.36	1.9638	4.3209	-0.098572

4.3.3 Adaptive Divided Difference Filter Based Observer

Since the penetration depth of the welding process cannot be measured in real time during the welding process, an observer is designed based on the adaptive divided difference filter [108] to estimate penetration depth and filter out noises. The welding system that includes a keyhole diameter and a penetration depth model described in Eq. (4.1) and Eq. (4.6), respectively, can be written in the following form:

$$\begin{aligned} \mathbf{x}(k+1) &= \mathbf{f}(\mathbf{x}(k), \mathbf{u}(k)) + \mathbf{w}(k) \\ y(k+1) &= x_2(k+1) = g\left(u_1(k), u_2(k), x_1(k+1)\right) + v(k) \end{aligned} \tag{4.9}$$

where $\mathbf{x}(k) = [x_1(k-1) \quad x_1(k)]^{\mathrm{T}}$ is the state variable vector which includes the current and past values of the keyhole diameter, $\mathbf{u}(k) = \left[u_1(k) \quad u_2(k)\right]^{\mathrm{T}}$ is the input vector which includes the welding power and welding speed. $\mathbf{w}(k) = \left[0 \quad w(k)\right]^{\mathrm{T}}$, where $w(k)$ is the Gaussian random noises with covariance $Q(k)$. In Eq. (4.9), $v(k)$ is also the Gaussian random noise with covariance. The nonlinear mapping vector $\mathbf{f}(\mathbf{x}(k), \mathbf{u}(k))$ is defined as:

$$\mathbf{f}(\mathbf{x}(k), \mathbf{u}(k)) = \left[x_1(k) \quad f\left(u_1(k),\, u_2(k), x_1(k-1),\, x_1(k)\right)\right]^{\mathrm{T}} \tag{4.10}$$

where f is the nominal nonlinear mapping of the dynamic FBFNs representing the keyhole diameter, and g is the nonlinear mapping of the static FBFN representing the penetration depth. f and g are defined by Eq. (4.5) and Eq. (4.8), respectively.

Let $\hat{\mathbf{P}}(k)=\hat{\mathbf{S}}_{\mathbf{x}}(k)\hat{\mathbf{S}}_{\mathbf{x}}^{\mathrm{T}}(k)$ denote the *a posteriori* state covariance estimate. Also define temporary matrices $\mathbf{S}_{\mathbf{x}\hat{\mathbf{x}}}^{(1)}(k)$ and $\mathbf{S}_{\mathbf{x}\hat{\mathbf{x}}}^{(2)}(k)$ whose p^{th} columns are calculated as:

$$\mathbf{S}_{\mathbf{x}\hat{\mathbf{x}}}^{(1)}(k)_{(p)}=\frac{1}{2T}\left\{\mathbf{f}\left(\hat{\mathbf{x}}(k)+T\hat{\mathbf{s}}_{\mathbf{x},p},\mathbf{u}(k)\right)-\mathbf{f}\left(\hat{\mathbf{x}}(k)-T\hat{\mathbf{s}}_{\mathbf{x},p},\mathbf{u}(k)\right)\right\} \tag{4.11}$$

$$\mathbf{s}_{\mathbf{x}\hat{\mathbf{x}}}^{(2)}(k)_{(p)}=\frac{\sqrt{T^2-1}}{2T^2}\left\{\mathbf{f}\left(\hat{\mathbf{x}}(k)+T\hat{\mathbf{s}}_{\mathbf{x},p},\mathbf{u}(k)\right)-\mathbf{f}\left(\hat{\mathbf{x}}(k)-T\hat{\mathbf{s}}_{\mathbf{x},p},\mathbf{u}(k)\right)-2\mathbf{f}\left(\hat{\mathbf{x}}(k),\mathbf{u}(k)\right)\right\} \tag{4.12}$$

where $\hat{\mathbf{x}}(k)$ is the previous *a posteriori* estimate, $\hat{\mathbf{s}}_{\mathbf{x},p}$ is the p^{th} column of $\hat{\mathbf{S}}_{\mathbf{x}}(k)$, and T is the sampling time. The *a priori* state estimate is computed as:

$$\overline{\mathbf{x}}(k+1)=\frac{T^2-n}{T^2}\mathbf{f}\left(\hat{\mathbf{x}}(k),\mathbf{u}(k)\right)+\frac{1}{2T^2}\left\{\sum_{p=1}^{n}\mathbf{f}\left(\hat{\mathbf{x}}(k)+T\hat{\mathbf{s}}_{\mathbf{x},p},\mathbf{u}(k)\right)+\mathbf{f}\left(\hat{\mathbf{x}}(k)-T\hat{\mathbf{s}}_{\mathbf{x},p},\mathbf{u}(k)\right)\right\} \tag{4.13}$$

where n is the number of state variables.

From that, the *a posteriori* estimate of the state variables and the future penetration depth of the welding process can be determined by the following equation:

$$\hat{\mathbf{x}}(k+1)=\overline{\mathbf{x}}(k+1)-\mathbf{L}(k+1)\left[\overline{\mathbf{x}}(k+1)-\mathbf{x}(k+1)\right] \tag{4.14}$$

$$x_2(k+1)=g\left(u_1(k),u_2(k),\mathbf{c}\cdot\mathbf{f}\left(\overline{\mathbf{x}}(k)-\mathbf{L}(k)\left[\overline{\mathbf{x}}(k)-\mathbf{x}(k)\right],\mathbf{u}(k)\right)\right) \tag{4.15}$$

where $\mathbf{x}(k)$ is the measured state variable vector, $\mathbf{c}=\begin{bmatrix}1 & 0\end{bmatrix}$. The filter gain $\mathbf{L}(k)$ can be computed in real time by using the algorithm provided by Subrahmanya and Shin [108] as follows:

$$\mathbf{L}(k+1)=\overline{\mathbf{S}}_{\mathbf{x}}^{u}(k+1)\overline{\mathbf{S}}_{\mathbf{x}}^{u}(k+1)^{\mathrm{T}}\times\left(\overline{\mathbf{S}}_{\mathbf{x}}^{u}(k+1)\overline{\mathbf{S}}_{\mathbf{x}}^{u}(k+1)^{\mathrm{T}}+\mathbf{R}(k+1)\right)^{-1} \tag{4.16}$$

where

$$\overline{\mathbf{S}}_{\mathbf{x}}^{u}(k+1) = HT\left(\left[\sqrt{\lambda_k}\overline{\mathbf{S}}_{\mathbf{x}}(k+1) \quad \sqrt{\alpha \,\mathrm{Trace}\left(\hat{\mathbf{P}}^{u}(k)\right)}\mathbf{I} \quad \sqrt{\beta}\mathbf{I}\right]\right) \tag{4.17}$$

In Eq. (4.17), *HT* is the Householder transformation, α and β are the parameters that can be calculated offline, and $\lambda(k)$ is the age weighting factor. $\overline{\mathbf{S}}_{\mathbf{x}}(k+1)$ and $\hat{\mathbf{P}}^{u}(k)$ can be computed as [108]:

$$\overline{\mathbf{S}}_{\mathbf{x}}(k+1) = HT\left[\mathbf{S}_{\mathbf{x}\hat{\mathbf{x}}}^{(1)}(k) \quad \mathbf{S}_{\mathbf{x}\hat{\mathbf{x}}}^{(2)}(k) \quad \mathbf{S}_{\mathbf{w},k}\right] \tag{4.18}$$

$$\overline{\mathbf{P}}^{u}(k+1) = \lambda(k)\overline{\mathbf{P}}^{u}(k+1) + \alpha \,\mathrm{Trace}\left(\overline{\mathbf{P}}^{u}(k)\right)\mathbf{I} + \beta\mathbf{I} \tag{4.19}$$

4.3.4 Converting type-2 FBFN welding model to type-2 T-S welding model

The following part describes the process of converting the type-2 FBFN to the interval type-2 T-S fuzzy model [107], which was used to design the robust T-S fuzzy controller in the next section. During the controlled welding process, the power is used as the only control variable while the welding speed is set at a constant value of 2 m/min. Consider $\mathbf{x}(k) = [x_1(k-1),\ x_1(k)]^{\mathrm{T}}$ as the vector of measured state variables. When $\mathbf{x}(k)$ and $u_1(k)$ are around a certain operating condition:

$$\mathbf{x}(k) \approx \boldsymbol{\chi}_i = [\chi_i^{(1)},\ \chi_i^{(2)}]^{\mathrm{T}},\ u_1(k) \approx \upsilon_i,\ u_2(k) = 2 \text{ m/min} \tag{4.20}$$

fuzzy rules of the interval type-2 T-S fuzzy model of the welding system can be constructed from the local linear models as follows:

R^i: IF $x_1(k-1)$ is X_1^i and $x_1(k)$ is X_2^i and $u_1(k)$ is U_1^i

$$\text{THEN } \tilde{\mathbf{x}}(k+1) = \boldsymbol{\chi}_i + \tilde{\mathbf{A}}_i\left(\boldsymbol{\chi}_i, \upsilon_i\right)\left[\mathbf{x}(k) - \boldsymbol{\chi}_i\right] + \tilde{\mathbf{B}}_i\left(\boldsymbol{\chi}_i, \boldsymbol{\upsilon}_i\right)\left[u_1(k) - \upsilon_i\right] \tag{4.21}$$

$$\tilde{y}(k) = \tilde{x}_2(k) = \mathbf{C}_i\tilde{\mathbf{x}}(k) \qquad i = 1, \ldots, M$$

where $\boldsymbol{\upsilon}_i = [0 \quad \upsilon_i]$. X_1^i, X_2^i and U_1^i are type-1 fuzzy sets with triangular membership functions that describe the operating condition. Each element of vector $\tilde{\mathbf{A}}_i(\boldsymbol{\chi}_i, \upsilon_i)$ and $\tilde{\mathbf{B}}_i(\boldsymbol{\chi}_i, \boldsymbol{\upsilon}_i)$ is an interval number. Based on the FBFN-based welding models, by using the converting algorithm provided in [107], the type-2 T-S fuzzy model of the dynamic process was obtained with five rules. The parameters of the model for each rule can be found in APPENDIX K.

By defining the following matrices:

$$\mathbf{A}_i = \frac{\mathbf{A}_{i\max} + \mathbf{A}_{i\min}}{2},\ \mathbf{B}_i = \frac{\mathbf{B}_{i\min} + \mathbf{B}_{i\max}}{2},\ \Delta\tilde{\mathbf{A}}_i = \tilde{\mathbf{A}}_i - \mathbf{A}_i,\ \Delta\tilde{\mathbf{B}}_i = \tilde{\mathbf{B}}_i - \mathbf{B}_i\ , \tag{4.22}$$

the predicted output of the T-S fuzzy model can be derived by using the T-S interference mechanism as follows:

$$\begin{aligned}\tilde{\mathbf{x}}(k+1) &= \sum_{i=1}^{M} \bar{\mu}_i(\mathbf{x}(k), \mathbf{u}(k)) \cdot \left\{\tilde{\mathbf{A}}_i \mathbf{x}(k) + \tilde{\mathbf{B}}_i \mathbf{u}(k)\right\} \\ &= \sum_{i=1}^{M} \bar{\mu}_i(\mathbf{x}(k), \mathbf{u}(k)) \cdot \left\{(\mathbf{A}_i + \Delta\tilde{\mathbf{A}}_i)\mathbf{x}(k) + (\mathbf{B}_i + \Delta\tilde{\mathbf{B}}_i)\mathbf{u}(k)\right\} \\ \tilde{y}(k) &= \tilde{x}_2(k) = \mathbf{C}_i \tilde{\mathbf{x}}(k)\end{aligned} \tag{4.23}$$

where $\bar{\mu}_i$ is the normalized weighting function:

$$\bar{\mu}_i(\mathbf{x}(k), \mathbf{u}(k)) = \frac{\mu_{X_1^i}(x_1(k-1))\,\mu_{X_2^i}(x_1(k))\,\mu_{U_1^i}(u_1(k))}{\sum_{i=1}^{M}\left[\mu_{X_1^i}(x_1(k-1))\,\mu_{X_2^i}(x_1(k))\,\mu_{U_1^i}(u_1(k))\right]}, \tag{4.24}$$

$\mu_{X_1^i}(x(k-1))$, $\mu_{X_2^i}(x(k))$ and $\mu_{U_1^i}(u_1(k))$ are the membership functions of $x(k-1)$, $x(k)$ and $u(k)$, respectively.

4.4 Robust T-S Fuzzy Control of Laser Keyhole Welding Process

In this section, the robust T-S fuzzy controller (RTSFC) is implemented to maintain constant penetration depth of the keyhole laser welding process since the process is nonlinear with large amounts of uncertainties. Figure 4-6 shows the schematic diagram of the control system. In the figure, *r* is the reference signal, *e* is the error, x_1 is the measured keyhole diameter, $\hat{x}_2$ is the estimated penetration depth, u_1 is the laser power and u_2 is the welding speed. The structure of rule R^j of the fuzzy controller is described as follows:

$$\begin{aligned} R^j: \quad & \text{IF } x_1(k) \text{ is } X^j \text{ THEN } u_1(k) = \mathbf{K}_j \mathbf{x}(k) + k_j \zeta(k), \\ & \zeta(k) = \zeta(k-1) + Te(k), \quad e(k) = r(k) - x_2(k) \end{aligned} \tag{4.25}$$

where $\mathbf{x}(k) = [x_1(k-1) \quad x_1(k)]^{\mathrm{T}}$, $\zeta(k)$ is the integral signal of the error at time *k*, *r*(*k*) is the reference penetration depth, $\mathbf{K}_j$ and k_j are the proportional and integral gain, respectively. By using the T-S inference mechanism, the control effort $u_1(k)$ can be calculated as:

$$u_1(k) = \sum_{j=1}^{N} \overline{v}_j(\mathbf{x}(k)) \cdot \{\mathbf{K}_j \mathbf{x}(k) + k_j \zeta(k)\} \tag{4.26}$$

where $\overline{v}_j$ is the normalized firing strength of the j^{th} rule:

$$\overline{v}_j(\mathbf{x}(k)) = \frac{v_{X^j}(x_1(k))}{\sum_{j=1}^{N} v_{X^j}(x_1(k))}, \tag{4.27}$$

and $v_{X^j}(x_1(k))$ is the membership functions of $x_1(k)$. By substituting Eq. (3.43) into Eq. (3.40), the closed loop equations can be obtained:

$$\tilde{\mathbf{x}}(k+1)=\sum_{i=1}^{M}\sum_{j=1}^{N}\left[\bar{\mu}_i\left(\mathbf{x}(k),\mathbf{u}(k)\right)\cdot\bar{v}_j\left(\mathbf{x}(k)\right)\cdot\left\{\left(\mathbf{A}_i+\Delta\tilde{\mathbf{A}}_i+\mathbf{B}_i\mathbf{K}_j\right)\mathbf{x}(k)+\mathbf{B}_i k_j\zeta(k)+\Delta\tilde{\mathbf{B}}_i u_1(k)\right\}\right]$$

$$\zeta(k)=\zeta(k-1)+r(k-1)-\mathbf{C}_i\mathbf{x}(k-1)$$

(4.28)

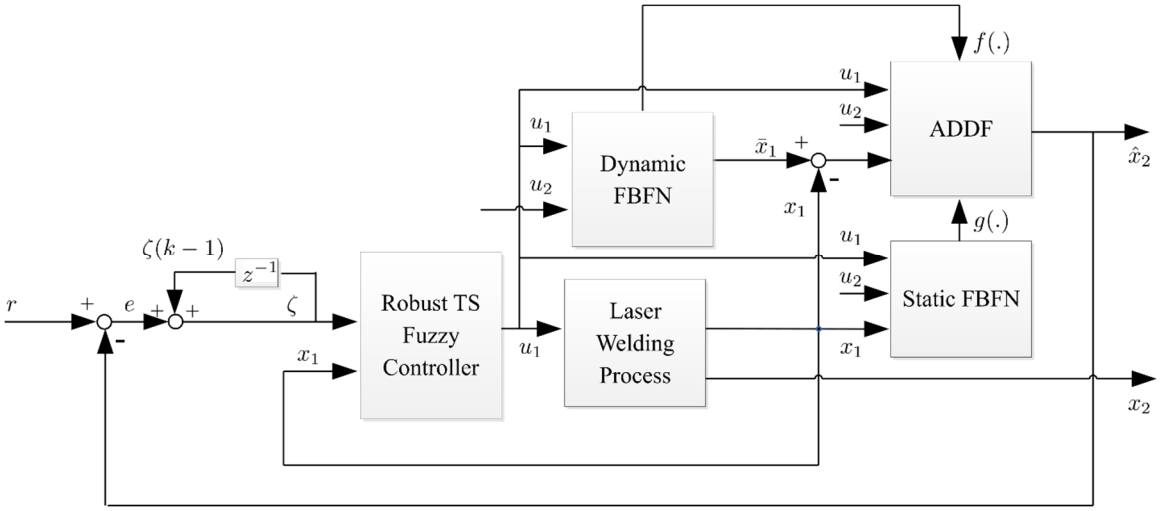

Figure 4-6: Laser keyhole welding control system schematic diagram.

The parameters of the RTSFC can be obtained by solving the linear matrix inequalities (LMIs) given in Theorem 3. In addition to the LMI given in Theorem 3, the following conditions were added to limit the control effort by an upper bound value $\| u_1(t) \| \leq \mu$ [109]:

$$\begin{bmatrix}\mathbf{Q} & \mathbf{Y}_j^{\mathrm{T}}\\ \mathbf{Y}_j & \mu^2\mathbf{I}\end{bmatrix}\geq 0 \tag{4.29}$$

where $\mathbf{Q}$ and $\mathbf{Y}_j$ are defined in Theorem 3. By solving the combination of the LMIs given in Theorem 3 and the above LMIs with $\alpha = 0.1$ and $\mu^2 = 1000$, the positive definite matrix $\mathbf{Q}$ was found as follows:

$$\mathbf{Q} = \begin{bmatrix} 0.5763 & 0.0059 & 7.3347\times10^{-4} \\ 0.0059 & 0.0608 & 0.0013 \\ 7.3347\times10^{-4} & 0.0013 & 3.3041\times10^{-4} \end{bmatrix} \tag{4.30}$$

Then, the feedback gains of the RTSFC (Table 4-5) can be calculated from $\mathbf{Q}$ and $\mathbf{Y}_j$:

$$\bar{\mathbf{K}}_j = \begin{bmatrix} \mathbf{K}_j & k_j \end{bmatrix} = \mathbf{Y}_j \mathbf{Q}^{-1} \tag{4.31}$$

Table 4-5: Feedback gains of the RTSFC.

Rule R^j	$\mathbf{Y}_j$	$\mathbf{K}_j$	k_j
1	[–4.7892 –1.9878 0.4620]	[-9.765 -67.394]	1682.890
2	[–3.3997 –1.7753 0.4760]	[–7.415 -64.694]	1709.644
3	[2.5165 –0.7105 0.5050]	[2.681 -48.183]	1710.383
4	[1.3710 0.8107 0.5480]	[0.394 -23.810]	1750.568
5	[0.5000 1.2974 0.5545]	[–1.191 -15.455]	1741.026

4.5 Experimental Results

4.5.1 Obtaining Keyhole Laser Welding Models

A set of experimental parameters (Table 4-6) were chosen to obtain the best FBFN representation of the nonlinear system. The results of the experiments were used for training both the static and dynamic FBFN models.

Table 4-6: Experiment parameters for training the welding model FBFNs.

Exp. no	Power (W)	Speed (m/min)	Exp. no	Power (W)	Speed (m/min)
1	1000	2.66	15	900	0.5
2	1000	3.153	16	1000	4
3	1000	3.73	17	900	2
4	900	2.23	18	900	4
5	900	2.678	19	800	0.5
6	900	3.21	20	800	2
7	800	1.739	21	1000	5
8	800	2.146	22	1000	3.75
9	800	2.649	23	1000	2.5
10	1000	2.86	24	900	5
11	1000	2.7545	25	900	3.5
12	800	1.433	26	900	2
13	800	1.586	27	800	5
14	1000	0.5	28	800	3.125

For the static welding model (to estimate the keyhole penetration depth), an FBFN was obtained with four hidden nodes by using the genetic algorithm and adaptive least square technique [73]. Based on the dynamic data, a dynamic type-2 FBFN model was also constructed with eight hidden nodes. To evaluate the accuracy of the welding models under two different conditions, experimental and estimation data were collected from the experiments and from the welding models. Measured and predicted (from type-2 FBFN model) keyhole diameters versus time are shown in Figure 4-7 and Figure 4-8. Measured and predicted (from type-1 FBFN model) penetration depths versus time are shown in Figure 4-9 and Figure 4-10. It can be seen that the FBFNs provide not only an accurate

estimation of the state variables but also the uncertainty information for the controller design purpose.

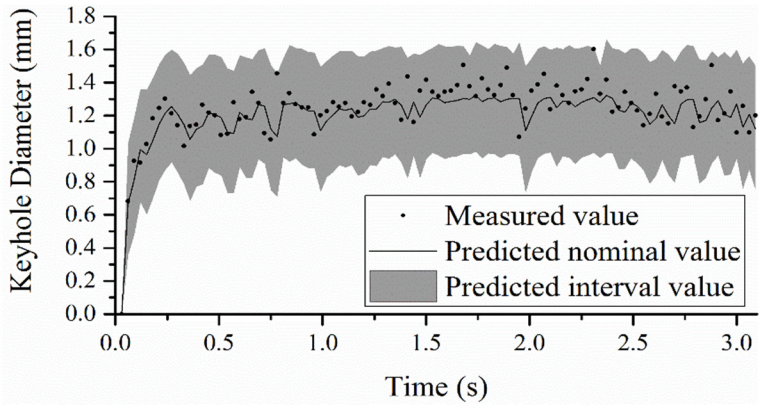

Figure 4-7: Keyhole diameter with 800 W power and 1.433 m/min welding speed.

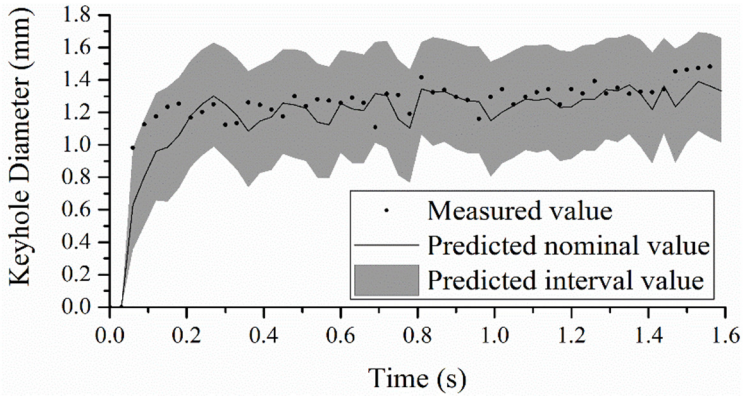

Figure 4-8: Keyhole diameter with 1000 W power and 2.86 m/min welding speed.

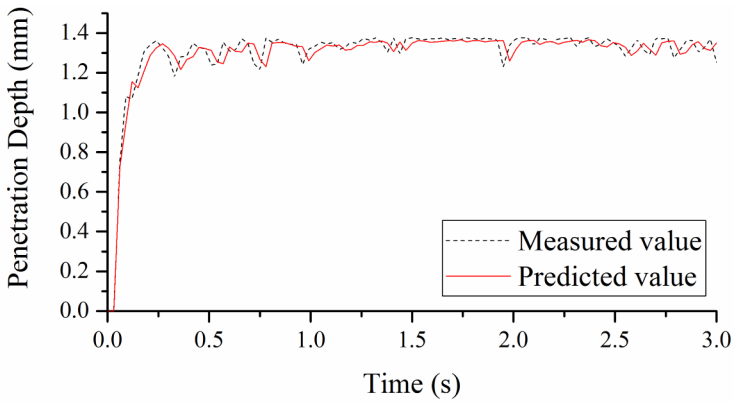

Figure 4-9: Penetration depth with 800 W power and 1.433 m/min welding speed.

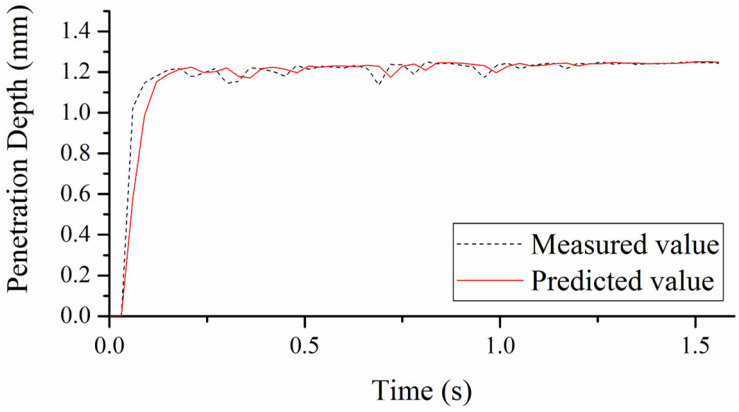

Figure 4-10: Penetration depth 1000 W power and 2.86 m/min welding speed.

4.5.2 Controller Implementation

In order to evaluate the performance of the RTSFC, experiments were conducted on the laser welding process to control the penetration depth of the keyhole. The control input is the welding speed while the estimated output is the penetration depth. Each case includes both controlled (closed-loop) and un-controlled (open-loop) experiments. The experiment parameters with laser powers used for the open-loop system and the open-loop powers are shown in Table 4-7. The open-loop laser powers were calculated from the welding model represented by the FBFNs. Cases 1 and 2 were conducted with the same

condition to check the repeatability of the experiments. Although the focus of the paper is on lap welding, case 4 was added to evaluate the effects of zero gap on the welding processes.

Table 4-7: Experiment parameters for controlling laser keyhole welding processes.

Case	Penetration depth (mm)	Join type	Open-loop power (W)
1	1.2	Lap welding	850
2	1.2	Lap welding	850
3	1.0	Lap welding	776
4	1.2	One plate	850

In lap welding, since the strength of the weld spot depends greatly on how deep the welding pool is on the second plate, the penetration depth was measured without including the gap distance. To verify the accuracy of the controller, four cross-sectional surfaces of each welding sample were cut, polished and etched by a solution of hydrofluoric acid and nitric acid. Figure 4-11 and Figure 4-12 show examples of the microscopic images of the cross-sectional surfaces under the open-loop and the closed-loop system, respectively. The remaining microscopic images can be found in APPENDIX L. In each figure, the keyhole shapes formed by both lap welding and one-plate welding are presented. For the open-loop system, due to the presence of the gap, it can be seen from Figure 4-11 that the penetration depth under the lap-welding process is much smaller compared with that under the one-plate welding. In the closed-loop system (Figure 4-12), the penetration depths of both processes are much more similar. Figure 4-13 and Figure 4-14 show the penetration depth responses of the open-loop and closed-loop systems. It can be seen that the keyhole

penetration depth varied significantly with respect to time when implemented without a controller. Figure 4-15 to Figure 4-18 show the comparisons of the system responses between the welding processes conducted with and without the RTSFC for all four cases. The RTSFC reduced the transient time and the steady-state error significantly in the lap-welding processes. The performances of the closed-loop and open-loop systems in one-plate welding are less different than those in lap-welding since there is less uncertainty (zero gap) in the system. The mean absolute errors (MAE) (Table 4-8) between the estimated penetration depth and the reference signal were calculated by the following formula:

$$MAE = \frac{1}{N}\sum_{k=1}^{N}\left|x_2(k) - r\right| \tag{4.32}$$

where N is the number of measurements collected, $x_2(k)$ is the penetration depth at time instant k, and r is the reference signal. The microscopic results from the samples indicate that the welding observer was able to estimate the welding penetration depth accurately. The specimens of the controlled welding process show closer penetration depth to the target value and are more consistent than the uncontrolled specimens. The inconsistencies of the uncontrolled welding processes can be explained by the variation of the welding gap and the bending of the workpiece due to high temperature during the process.

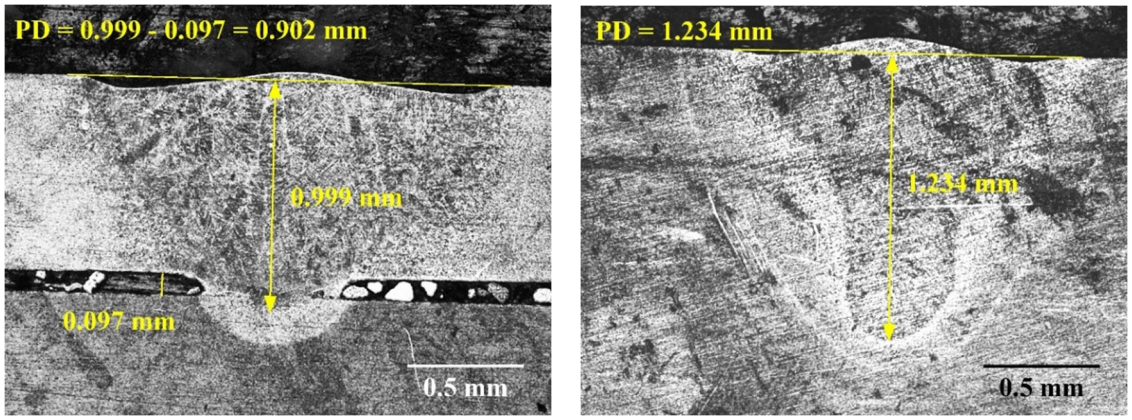

(a) Lap welding (b) One-plate welding

Figure 4-11: Microscopic images of the cross-sectional samples produced by the open-loop system with desired penetration depth of 1.2 mm.

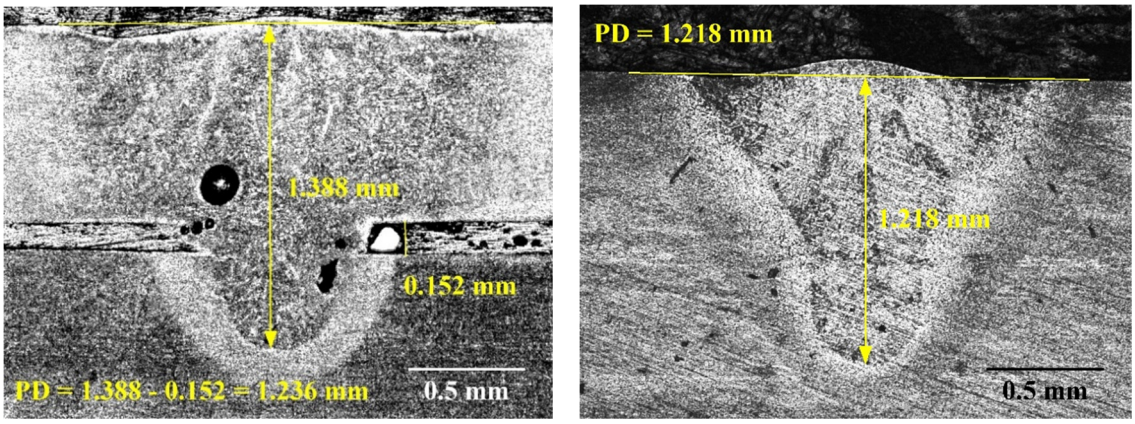

(a) Lap welding (b) One-plate welding

Figure 4-12: Microscopic images of the cross-sectional sample produced by the closed-loop system with desired penetration depth of 1.2 mm.

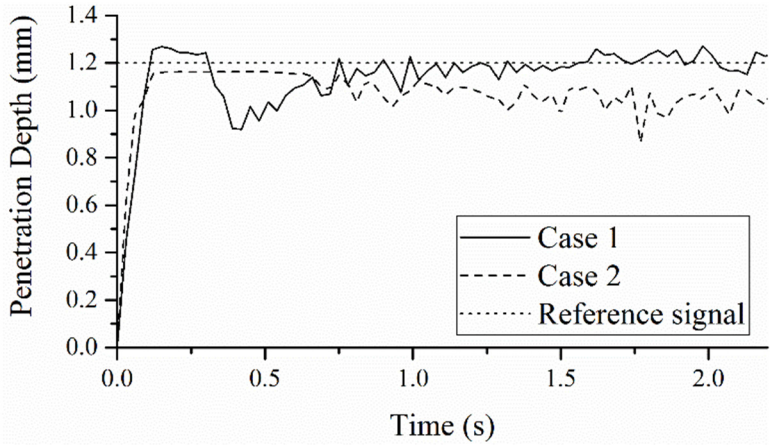

Figure 4-13: Penetration depth responses of the open-loop laser welding system.

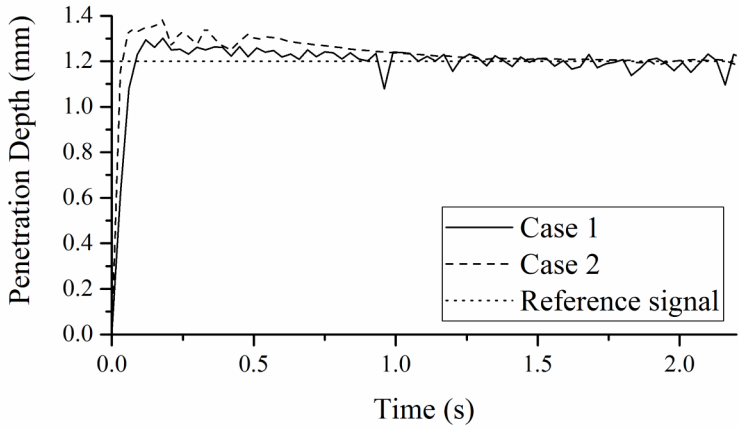

Figure 4-14: Penetration depth responses of the closed-loop laser welding system.

Table 4-8: Mean absolute error of the estimated penetration depth.

Case	Closed-loop error (mm)	Open-loop error (mm)
1	0.056	0.090
2	0.061	0.136
3	0.073	0.120
4	0.070	0.091

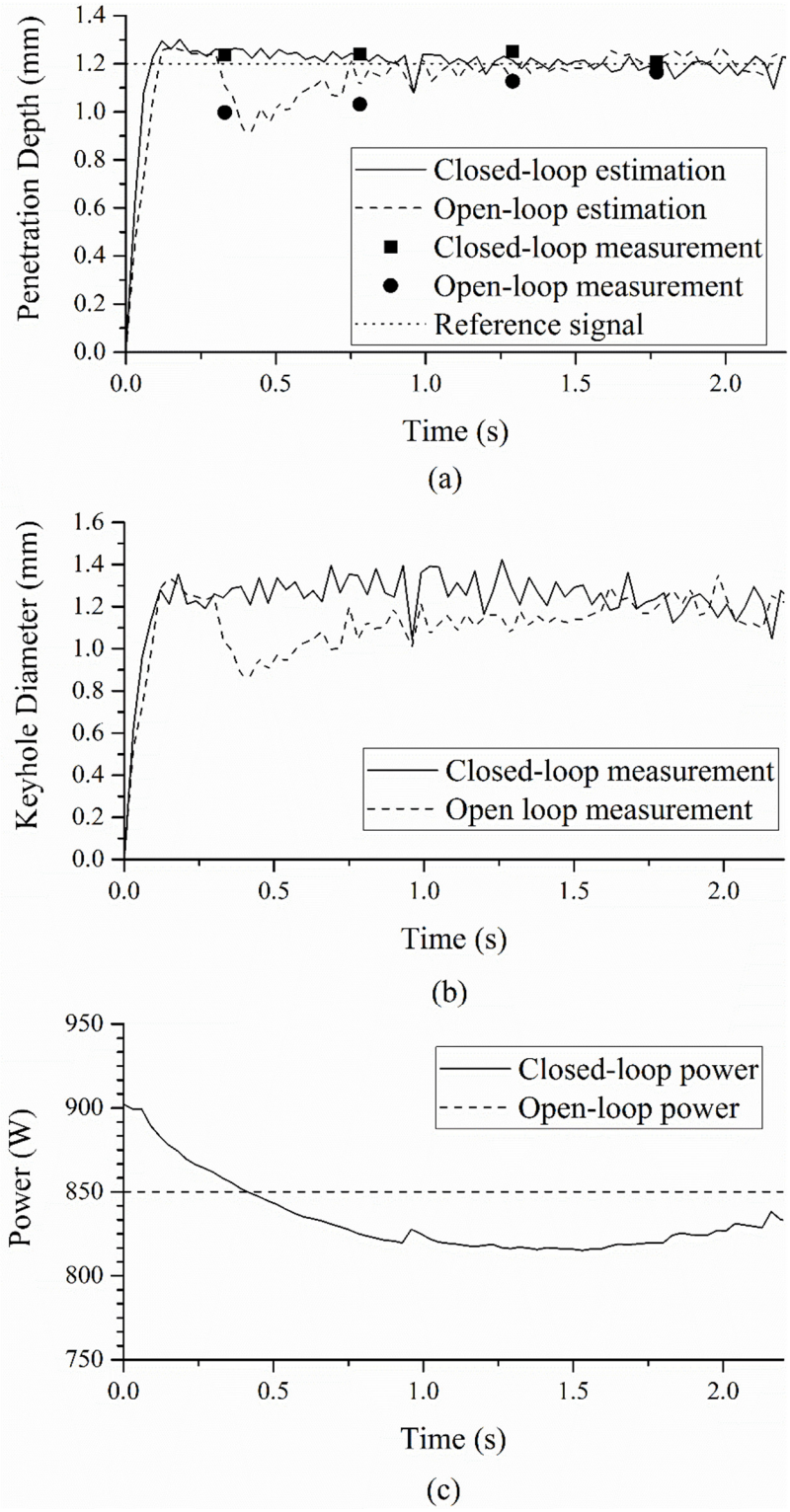

Figure 4-15: Closed-loop and open-loop system responses in case 1. (a) Estimated and measured penetration depth. (b) Measured keyhole diameter. (c) Power signal.

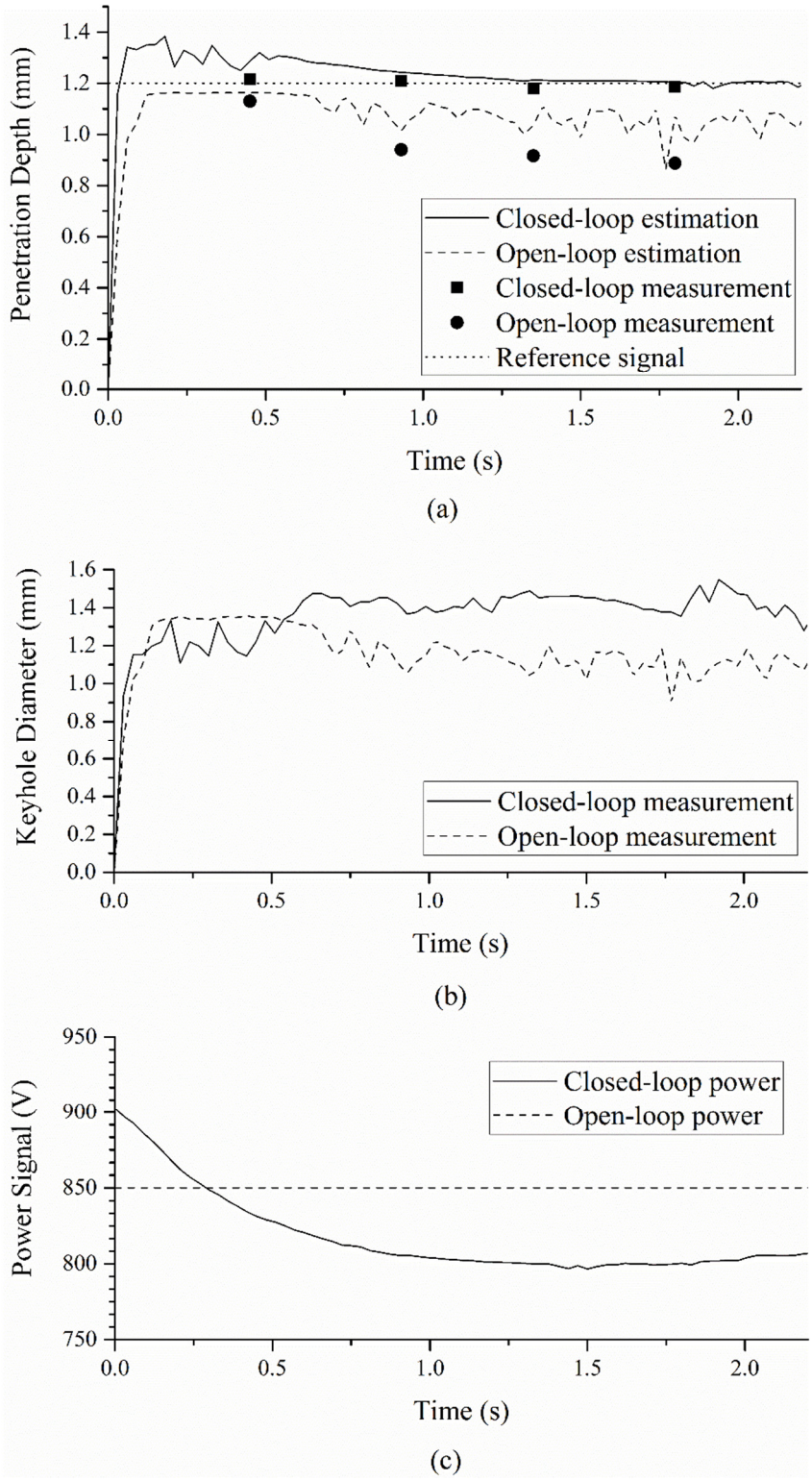

Figure 4-16: Closed-loop and open-loop system responses in case 2. (a) Estimated and measured penetration depth. (b) Measured keyhole diameter. (c) Power signal.

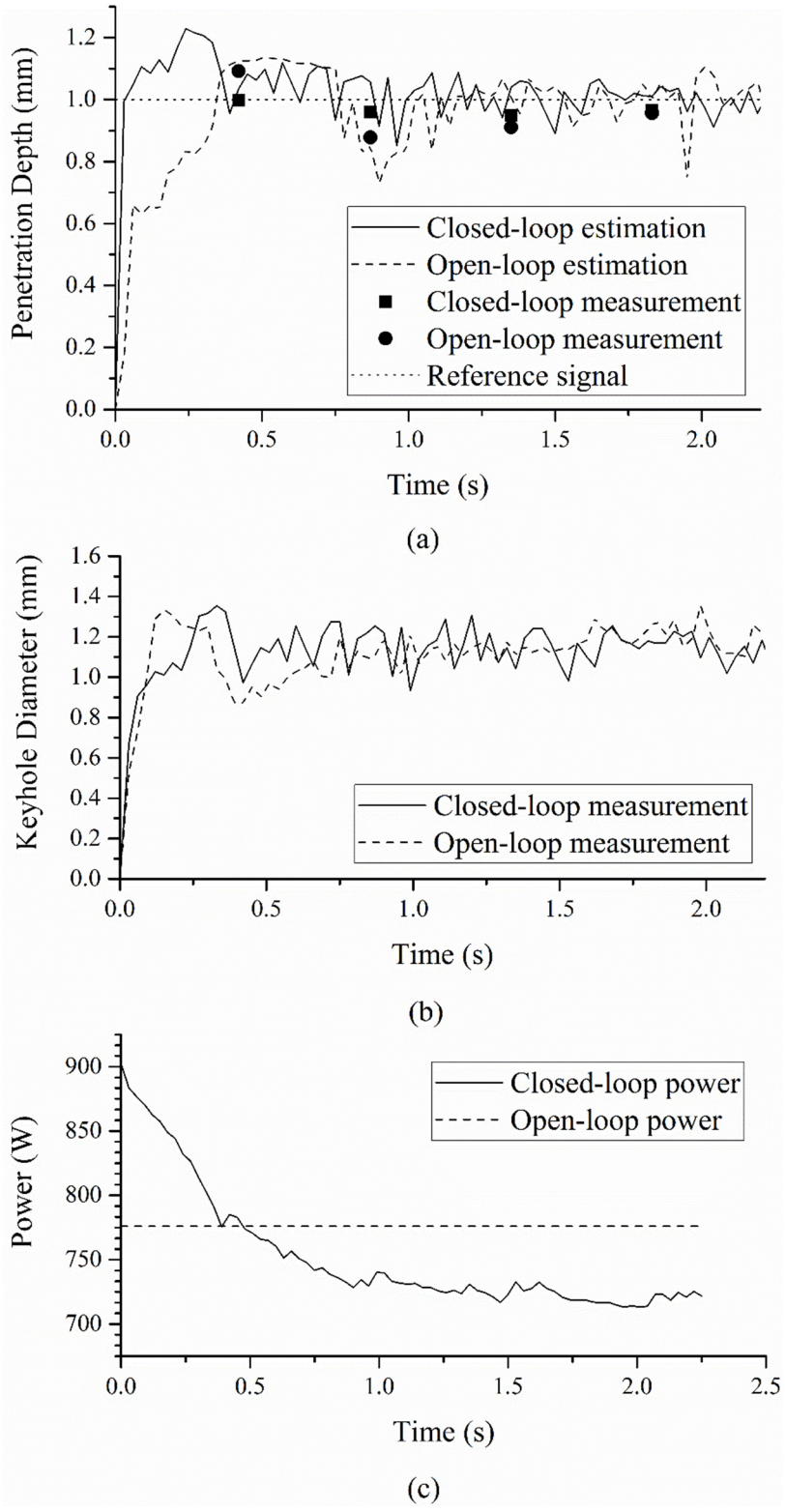

Figure 4-17: Closed-loop and open-loop system responses in case 3. (a) Estimated and measured penetration depth. (b) Measured keyhole diameter. (c) Power signal.

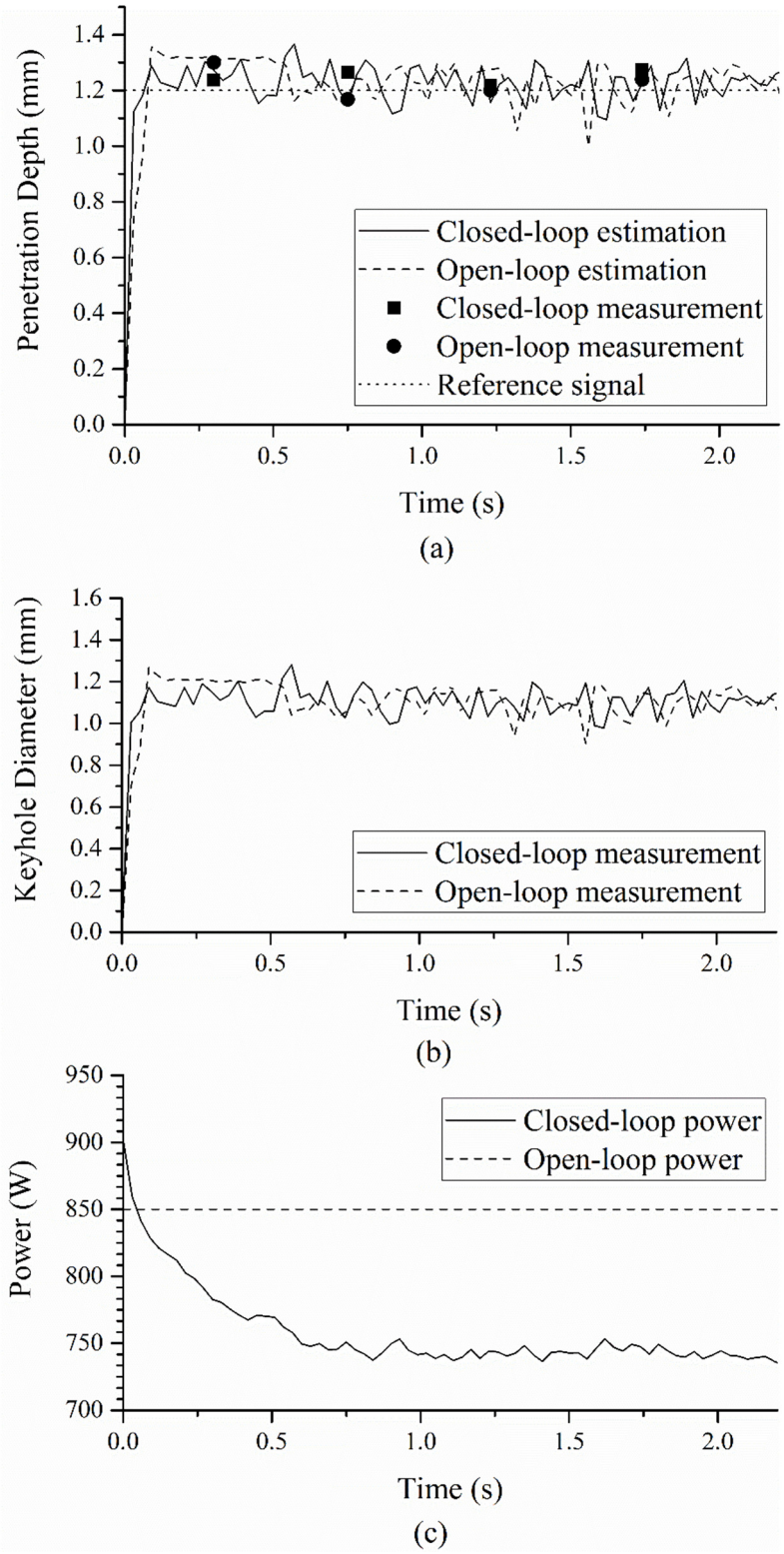

Figure 4-18: Closed-loop and open-loop system responses in case 4. (a) Estimated and measured penetration depth. (b) Measured keyhole diameter. (c) Power signal.

CHAPTER 5. CONCLUSION

In this work, new theories were developed to provide a framework for modeling and control of a class of unknown nonlinear systems based on input and output data. Both single-input and single-output systems were considered. Novel stability analyses were provided to guarantee the stability while maintaining good performance of the control systems under unstructured uncertainties. Simulations and experiments were also conducted to demonstrate the effectiveness of the models and controllers for actual nonlinear uncertain systems.

First, a new stability analysis was derived for a class of nonlinear proportional-integral fuzzy control systems by using the small gain theorem. A new technique to estimate the dynamic gains of the systems was presented and a multilevel fuzzy controller was proposed with a mechanism to tune the output scaling-factor. From the proposed stability analysis, the only design parameter that is needed for a stable fuzzy control system is the maximum output scaling-factor of the fuzzy controller. Simulations conducted on a tower crane system demonstrated the superior performance of the proposed multilevel fuzzy controller over the robust adaptive fuzzy controller. With the self-tuning ability of the controller's output scaling-factor, the control systems remained within the stable condition. The simulation results showed that the responses of the proposed multilevel

fuzzy controller produced a better output transient performance in terms of oscillation and settling time.

Next, a new method of training an interval type-2 fuzzy basis function network is presented. The antecedents of the fuzzy basis function network are obtained by using the adaptive least square with the genetic algorithm method, while the interval values of the consequents are obtained by the active set method. Moreover, a new technique was proposed to convert the interval type-2 fuzzy basis function network to an interval type-2 T-S fuzzy model. Based on the proposed methods, a robust controller for a class of multi-input and multi-output nonlinear systems is designed based on a set of linear matrix inequalities that represent a relaxed stability condition of the closed-loop system. The convergence rate allows the controller to be more flexible. Simulation results on an electrohydraulic actuator demonstrate the robustness and better performance of the proposed controller in comparison with the other robust sliding mode controllers.

The type-2 fuzzy basis function network and RTSFC were implemented for modeling and control of the keyhole laser welding process. The welding process was represented by a static type-1 fuzzy basis function network model and a dynamic type-2 fuzzy basis function network model. During the process, the penetration depth was estimated in real time by using an adaptive-divided-difference-filter-based observer. Based on the welding process models, a robust Takagi-Sugeno fuzzy controller was implemented to control the penetration depth. Experimental results demonstrated the effectiveness of the models and the robustness of the robust Takagi-Sugeno fuzzy controller. The penetration depth error in the closed-loop system was reduced significantly compared to the open-loop system. The penetration depth of the system implemented with the robust Takagi-Sugeno

fuzzy controller is also more stable and less varied. Hence, the accuracy and quality of the weld was improved by using the robust Takagi-Sugeno fuzzy controller.

Modeling unstable nonlinear systems is not an easy task due to limited training data available and the difficult convergence of system parameters. Therefore, a new effective method to generate input and output data and model unstable systems based on the current frameworks by using measured input and output data can be investigated to expand the applications of the developed controllers.

LIST OF REFERENCES

LIST OF REFERENCES

[1] T. Takagi and M. Sugeno, "Fuzzy identification of systems and its applications to modeling and control," *IEEE Trans. Syst. Man Cybern.*, vol. SMC-15, no. 1, pp. 116–132, 1985.

[2] L.-X. Wang and J. Mendel, "Fuzzy basis functions, universal approximation, and orthogonal least-squares learning," *IEEE Trans. Neural Networks*, vol. 3, no. 5, pp. 807–814, 1992.

[3] J. B. Kiszka, M. M. Gupta, and P. N. Nikiforuk, "Energetistic stability of fuzzy dynamic systems," *IEEE Trans. Syst. Man. Cybern.*, no. 6, pp. 783–792, 1985.

[4] E. Furutani, M. Saeki, and M. Araki, "Shifted Popov criterion and stability analysis of fuzzy control systems," in *Proceedings of the 31st IEEE Conference on Decision and Control*, 1992, pp. 2790–2795.

[5] G. Chen, T. Pham, and J. Weiss, "Fuzzy modeling of control systems," *IEEE Trans. Aerospance Electron. Syst.*, vol. 31, no. 1, 1995.

[6] B. Soualmi, C. Sentouh, J. C. Popieul, and S. Debernard, "Fuzzy Takagi-Sugeno LQ controller for lateral control assistance of a vehicle," in *IEEE Intelligent Vehicles Symposium*, 2012, pp. 377–382.

[7] H.-N. Wu, "Reliable LQ fuzzy control for nonlinear discrete-time systems via LMIs," *IEEE Trans. Syst. Man, Cybern. Part B Cybern.*, vol. 34, no. 2, pp. 1270–1275, 2004.

[8] R. Precup, M. Tomescu, and Å. Preitl, "Fuzzy logic control system stability analysis based on Lyapunov's direct method," *Int. J. Comput. Commun. Control*, vol. IV, no. 4, pp. 415–426, 2009.

[9] C. Xu and Y. C. Shin, "Design of a multilevel fuzzy controller for nonlinear systems and stability analysis," *IEEE Trans. Fuzzy Syst.*, vol. 13, no. 6, pp. 761–778, Dec. 2005.

[10] H. Jiang, J. Yu, and C. Zhou, “Stable adaptive fuzzy control of nonlinear systems using small-gain theorem and LMI approach,” *J. Control Theory Appl.*, vol. 8, no. 4, pp. 527–532, May 2010.

[11] Y. Yang, “Direct robust adaptive fuzzy control (DRAFC) for uncertain nonlinear systems using small gain theorem,” *Fuzzy Sets Syst.*, vol. 151, no. 1, pp. 79–97, Apr. 2005.

[12] G. Calcev, R. Gorez, and M. D. E. Neyer, “Passivity Approach to Fuzzy Control Systems,” *Automatica*, vol. 34, no. 3, pp. 339–344, 1998.

[13] G. Chen and H. Ying, “Stability analysis of nonlinear fuzzy PI control systems,” in *Third International Conference on industrial Fuzzy Control and Intelligent Systems*, 1993, pp. 128–133.

[14] Z.-H. Xiu and G. Ren, “Stability analysis and systematic design of Takagi–Sugeno fuzzy control systems,” *Fuzzy Sets Syst.*, vol. 151, no. 1, pp. 119–138, 2005.

[15] W. W. Chang and C. Ku, “Fuzzy Control with Passivity Constraint for Discrete Affine T-S Fuzzy Systems,” *First Int. Conf. Innov. Comput. Inf. Control - Vol. I*, vol. 2, pp. 187–190, 2006.

[16] W. W.-J. Chang, C.-C. Ku, and P.-H. Huang, “Fuzzy controller design for passive continuous-time affine T-S fuzzy models with relaxed stability conditions,” *ISA Trans.*, vol. 48, no. 3, pp. 295–303, Jul. 2009.

[17] C. Sloth, T. Esbensen, M. O. K. Niss, J. Stoustrup, and P. F. Odgaard, “Robust LMI-based control of wind turbines with parametric uncertainties,” in *18th IEEE International Conference on Control Applications*, 2009, pp. 776–781.

[18] Y. Lin, Y. Shi, and R. Burton, “Modeling and robust discrete-time sliding-mode control design for a fluid power electrohydraulic actuator (EHA) system,” *IEEE/ASME Trans. Mechatronics*, vol. 18, no. 1, pp. 1–10, Feb. 2013.

[19] M. Sato, “Robust model-following controller design for LTI systems affected by parametric uncertainties: a design example for aircraft motion,” *Int. J. Control*, vol. 82, no. 4, pp. 689–704, Apr. 2009.

[20] H. J. Lee, J. B. Park, and G. Chen, “Robust fuzzy control of nonlinear systems with parametric uncertainties,” *IEEE Trans. Fuzzy Syst.*, vol. 9, no. 2, pp. 369–379, Apr. 2001.

[21] Q. Gao, X.-J. Zeng, G. Feng, Y. Wang, and J. Qiu, "T-S-fuzzy-model-based approximation and controller design for general nonlinear systems.," *IEEE Trans. Syst. Man, Cybern. Part B, Cybern.*, vol. 42, no. 4, pp. 1143–1154, Mar. 2012.

[22] M. Balas and V. Balas, "World Knowledge for Control Applications by Fuzzy-Interpolative Systems," *Int. J. Comput. Commun. Control*, vol. III, pp. 28–32, 2008.

[23] A. Bazoula, M. Djouadi, and H. Maaref, "Formation control of multi-robots via fuzzy logic technique," *Int. J. Comput. Commun. Control*, vol. III, pp. 179–184, 2008.

[24] A. Marwan, F. Nagi, K. Sahari, and H. S, "Robust Fuzzy MIMO Bang-Bang Controller for two Links Robot Manipulators," *Aust. J. Basic Appl. Sci.*, vol. 5, no. 12, pp. 2071–2083, 2011.

[25] Y. Tarng and S. Cheng, "Fuzzy control of feed rate in end milling operations," *Int. J. Mach. Tools Manuf.*, vol. 33, no. 4, pp. 643–650, Aug. 1993.

[26] A. Haj-Ali and H. Ying, "Structural analysis of fuzzy controllers with nonlinear input fuzzy sets in relation to nonlinear PID control with variable gains," *Automatica*, vol. 40, no. 9, pp. 1551–1559, Sep. 2004.

[27] R. Arya, "Analytical structures and analysis of simplest fuzzy PD controller with asymmetrical/symmetrical, trapezoidal/triangular/singleton output membership function," *Int. J. Comput. Cogn.*, vol. 5, no. 2, pp. 10–24, 2007.

[28] R. Mudi and N. R. Pal, "A robust self-tuning scheme for PI and PD-type fuzzy controllers," *IEEE Trans. Fuzzy Syst.*, vol. 7, no. 1, pp. 2–16, 1999.

[29] C. Chen, C. Lin, and C. Lin, "Nonlinear system control using adaptive neural fuzzy networks based on a modified differential evolution," *IEEE Trans. Syst. Man, Cybern. Part C Appl. Rev.*, vol. 39, no. 4, pp. 459–473, Jul. 2009.

[30] H. Mingzhi, W. Jinquan, M. Yongwen, W. Yan, L. Weijiang, and S. Xiaofei, "Control rules of aeration in a submerged biofilm wastewater treatment process using fuzzy neural networks," *Expert Syst. Appl.*, vol. 36, no. 7, pp. 10428–10437, Sep. 2009.

[31] C.-J. Lin and Y.-J. Xu, "A novel genetic reinforcement learning for nonlinear fuzzy control problems," *Neurocomputing*, vol. 69, no. 16–18, pp. 2078–2089, Oct. 2006.

[32] J. Spooner and K. Passino, "Stable adaptive control using fuzzy systems and neural networks," *IEEE Trans. Fuzzy Syst.*, vol. 4, no. 3, pp. 339–359, 1996.

[33] R. Ordonez, J. Zumberge, J. T. Spooner, and K. M. Passino, "Adaptive fuzzy control: experiments and comparative analyses," *IEEE Trans. Fuzzy Syst.*, vol. 5, no. 2, pp. 167–188, 1997.

[34] C. Wang, H. Liu, and T.-C. Lin, "Direct adaptive fuzzy-neural control with state observer and supervisory controller for unknown nonlinear dynamical systems," *IEEE Trans. Fuzzy Syst.*, vol. 10, no. 1, pp. 39–49, 2002.

[35] H. Chekireb, M. Tadjine, and D. Bouchaffra, "Direct adaptive fuzzy control of nonlinear system class with application," *Control Intell. Syst.*, vol. 31, no. 2, pp. 1–11, 2003.

[36] R. Qi and M. A. Brdys, "Indirect adaptive controller based on a self-structuring fuzzy system for nonlinear modeling and control," *Int. J. Appl. Math. Comput. Sci.*, vol. 19, no. 4, pp. 619–630, Dec. 2009.

[37] T.-C. Lin, "Observer-based robust adaptive interval type-2 fuzzy tracking control of multivariable nonlinear systems," *Eng. Appl. Artif. Intell.*, vol. 23, no. 3, pp. 386–399, Apr. 2010.

[38] C.-W. Park and Y.-W. Cho, "T-S model based indirect adaptive fuzzy control using online parameter estimation.," *IEEE Trans. Syst. Man, Cybern. Part B, Cybern.*, vol. 34, no. 6, pp. 2293–302, Dec. 2004.

[39] C. Wong and S. Feng, "A switching type of fuzzy controller," in *Proceedings of the Third IEEE Conference on Fuzzy Systems*, 1994, pp. 30–34.

[40] Z.-W. Woo, H.-Y. Chung, and J.-J. Lin, "A PID type fuzzy controller with self-tuning scaling factors," *Fuzzy Sets Syst.*, vol. 115, no. 2, pp. 321–326, Oct. 2000.

[41] H. Ying, "Practical design of nonlinear fuzzy controllers with stability analysis for regulating processes with unknown mathematical models," *Automatica*, vol. 30, no. 7, pp. 1185–1195, 1994.

[42] H. Li and S. Tong, "A hybrid adaptive fuzzy control for a class of nonlinear MIMO systems," *IEEE Trans. Fuzzy Syst.*, vol. 11, no. 1, pp. 24–34, Feb. 2003.

[43] A. Boubakir, S. Labiod, and F. Boudjema, “A stable self-tuning proportional-integral-derivative controller for a class of multi-input multi-output nonlinear systems,” *J. Vib. Control*, vol. 18, no. 2, pp. 228–239, Jul. 2011.

[44] G. Pellegrinetti and J. Bentsman, “Nonlinear control oriented boiler modeling- A benchmark problem for controller design,” *IEEE Trans. Control Syst. Technol.*, vol. 4, no. 1, pp. 57–64, 1996.

[45] T. A. Davis, P. D. Ngo, and Y. C. Shin, “Multi-level fuzzy control of friction stir welding power,” *Int. J. Adv. Manuf. Technol.*, vol. 59, no. 5–8, pp. 559–567, Jul. 2011.

[46] P. D. Ngo and Y. C. Shin, “Milling contour error control using multilevel fuzzy controller,” *Int. J. Adv. Manuf. Technol.*, vol. 66, no. 9–12, pp. 1641–1655, Aug. 2012.

[47] G. Leng, T. M. McGinnity, and G. Prasad, “An approach for on-line extraction of fuzzy rules using a self-organising fuzzy neural network,” *Fuzzy Sets Syst.*, vol. 150, no. 2, pp. 211–243, Mar. 2005.

[48] H.-K. Chiang, C.-T. Chu, and Y.-T. Jhou, “Fuzzy control with fuzzy basis function neural network in magnetic bearing system,” in *International Symposium on Industrial Electronics*, 2012, pp. 846–851.

[49] C. W. Lee and Y. C. Shin, “Construction of fuzzy basis function networks using adaptive least squares method,” in *IFSA World Congress and 20th NAFIPS International Conference*, 2001, pp. 2630–2635.

[50] N. N. Karnik, J. M. Mendel, and Q. Liang, “Type-2 fuzzy logic systems,” *IEEE Trans. Fuzzy Syst.*, vol. 7, no. 6, pp. 643–658, 1999.

[51] G. M. Méndez and M. de los Angeles Hernandez, “Hybrid learning for interval type-2 fuzzy logic systems based on orthogonal least-squares and back-propagation methods,” *Inf. Sci. (Ny).*, vol. 179, no. 13, pp. 2146–2157, 2009.

[52] A. Rubio-Solis and G. Panoutsos, “Interval type-2 radial basis function neural network: a modeling framework,” *IEEE Trans. Fuzzy Syst.*, vol. 23, no. 2, pp. 457–473, Apr. 2015.

[53] H. Lee and M. Tomizuka, “Robust adaptive control using a universal approximator for SISO nonlinear systems,” *IEEE Trans. Fuzzy Syst.*, vol. 8, no. 1, pp. 95–106, 2000.

[54] H. Lee, “Robust adaptive fuzzy control by backstepping for a class of MIMO nonlinear systems,” *IEEE Trans. Fuzzy Syst.*, vol. 19, no. 2, pp. 265–275, Apr. 2011.

[55] V. Goyal, V. K. Deolia, and T. N. Sharma, “Robust sliding mode control for nonlinear discrete-time delayed systems based on neural network,” *Intell. Control Autom.*, vol. 06, no. 01, pp. 75–83, 2015.

[56] M. Chadli and T. M. Guerra, “LMI solution for robust static output feedback control of discrete Takagi-Sugeno fuzzy models,” *IEEE Trans. Fuzzy Syst.*, vol. 20, no. 6, pp. 1160–1165, 2012.

[57] J. Yao, Z. Jiao, and D. Ma, “Extended-state-observer-based output feedback nonlinear robust control of hydraulic systems with backstepping,” *IEEE Trans. Ind. Electron.*, vol. 61, no. 11, pp. 6285–6293, 2014.

[58] J. Hu, Z. Wang, H. Gao, and L. K. Stergioulas, “Robust sliding mode control for discrete stochastic systems with mixed time delays, randomly occurring uncertainties, and randomly occurring nonlinearities,” *IEEE Trans. Ind. Electron.*, vol. 59, no. 7, pp. 3008–3015, 2012.

[59] X. Wang, E. E. Yaz, and J. Long, “Robust and resilient state-dependent control of discrete-time nonlinear systems with general performance criteria,” *Syst. Sci. Control Eng.*, vol. 2, no. 1, pp. 48–54, Dec. 2014.

[60] S.-C. Tong, X.-L. He, and H.-G. Zhang, “A combined backstepping and small-gain approach to robust adaptive fuzzy output feedback control,” *IEEE Trans. Fuzzy Syst.*, vol. 17, no. 5, pp. 1059–1069, Oct. 2009.

[61] Y. Li, S. Tong, Y. Liu, and T. Li, “Adaptive fuzzy robust output feedback control of nonlinear systems with unknown dead zones based on a small-gain approach,” *IEEE Trans. Fuzzy Syst.*, vol. 22, no. 1, pp. 164–176, 2014.

[62] Z. Liu, F. Wang, Y. Zhang, X. Chen, and C. L. Phillip Chen, “Adaptive fuzzy output-feedback controller design for nonlinear systems via backstepping and small-gain approach,” *IEEE Trans. Cybern.*, vol. 44, no. 10, pp. 1714–1725, 2014.

[63] C. Xu and Y. C. Shin, “A self-tuning fuzzy controller for a class of multi-input multi-output nonlinear systems,” *Eng. Appl. Artif. Intell.*, vol. 24, no. 2, pp. 238–250, Mar. 2011.

[64] M. Nikolaou and V. Manousiouthakis, “A hybrid approach to nonlinear system stability and performance,” *AIChE J.*, vol. 35, no. 4, pp. 559–572, Apr. 1989.

[65] A. van der Schaft, "L2-gain analysis of nonlinear systems and nonlinear state-feedback H∞ control," *IEEE Trans. Automat. Contr.*, vol. 37, no. 6, pp. 770–784, 1992.

[66] N. Bruinsma and M. Steinbuch, "A fast algorithm to compute the H∞-norm of a transfer function matrix," *Syst. Control Lett.*, vol. 14, no. 4, pp. 287–293, 1990.

[67] M. Nikolaou and V. Manousiouthakis, "A hybrid approach to nonlinear system theory," in *26th IEEE Conference on Decision and Control*, 1987, vol. 26, pp. 2127–2132.

[68] M. Gerdts, "A nonsmooth Newton's method for control-state constrained optimal control problems," *Math. Comput. Simul.*, vol. 79, no. 4, pp. 925–936, Dec. 2008.

[69] M. Dahleh and G. Verghese, "Lectures on dynamic systems and control discrete-time linear state-space models," *MIT*, 2011. [Online]. Available: http://ocw.mit.edu/courses/electrical-engineering-and-computer-science/6-241j-dynamic-systems-and-control-spring-2011/readings/.

[70] C. Desoer and M. Vidyasagar, *Feedback Systems: Input–Output Properties*. New York: Academic Press, 1975.

[71] A. Haj-Ali and H. Ying, "Input-output structural relationship between fuzzy controllers using nonlinear input fuzzy sets and PI or PD control," *Int. J. Fuzzy Syst.*, vol. 5, no. 60–65, 2003.

[72] K. Wu, M. Karkoub, and T. Wu, "Robust adaptive fuzzy control design for 3-D tower crane with time delayed states," in *International Conference on Systems, Control and Informatics*, 2013, pp. 193–200.

[73] C. W. Lee and Y. C. Shin, "Construction of fuzzy systems using least-squares method and genetic algorithm," *Fuzzy Sets Syst.*, vol. 137, no. 3, pp. 297–323, Aug. 2003.

[74] C.-K. Lin, "Robust adaptive critic control of nonlinear systems using fuzzy basis function networks: An LMI approach," *Inf. Sci. (Ny).*, vol. 177, no. 22, pp. 4934–4946, 2007.

[75] P. D. Ngo and Y. C. Shin, "Gain estimation of nonlinear dynamic systems modeled by an FBFN and the maximum output scaling factor of a self-tuning PI fuzzy controller," *Eng. Appl. Artif. Intell.*, vol. 42, pp. 1–15, 2015.

[76] X. Jin and Y. C. Shin, "Nonlinear discrete time optimal control based on Fuzzy Models (in press)," *J. Intell. Fuzzy Syst.*, 2015.

[77] H. Khalil, *Nonlinear Systems*. New Jersey: Prentice Hall, 2002.

[78] Q. Liang and J. M. Mendel, "Interval type-2 fuzzy logic systems: theory and design," *IEEE Trans. Fuzzy Syst.*, vol. 8, no. 5, pp. 535–550, 2000.

[79] P. E. Gill, W. Murray, and M. H. Wright, *Numerical linear algebra and optimization, Volume 1*. Addison Wesley, 1991.

[80] P. E. Gill, W. Murray, M. a. Saunders, and M. H. Wright, "Procedures for optimization problems with a mixture of bounds and general linear constraints," *ACM Trans. Math. Softw.*, vol. 10, no. 3, pp. 282–298, 1984.

[81] MathWorks, "MATLAB optimization toolbox: User's Guide (r2015a)," 2015. [Online]. Available: http://www.mathworks.com/help/pdf_doc/optim/optim_tb.pdf. [Accessed: 06-Feb-2015].

[82] G. B. Dantzig, A. Orden, and P. Wolfe, "The generalized simplex method for minimizing a linear form under linear inequality restraints," *Pacific J. Math.*, vol. 5, no. 2, pp. 183–195, 1955.

[83] S. Mehrotra, "On the Implementation of a Primal-Dual Interior Point Method," *SIAM J. Optim.*, vol. 2, no. 4, pp. 575–601, 1992.

[84] Y. Zhang, "Solving large-scale linear programs by interior-point methods under the Matlab Environment," *Optim. Methods Softw.*, vol. 10, no. 1, pp. 1–31, 1998.

[85] H. Zhang, X. Liu, J. Wang, and H. R. Karimi, "Robust H∞ sliding mode control with pole placement for a fluid power electrohydraulic actuator (EHA) system," *Int. J. Adv. Manuf. Technol.*, vol. 73, no. 5–8, pp. 1095–1104, 2014.

[86] S. Wang, S. Habibi, and R. Burton, "Sliding mode control for an electrohydraulic actuator system with discontinuous non-linear friction," *Proc. Inst. Mech. Eng. Part I J. Syst. Control Eng.*, vol. 222, no. 8, pp. 799–815, Aug. 2008.

[87] A. Matsunawa, J.-D. Kim, N. Seto, M. Mizutani, and S. Katayama, "Dynamics of keyhole and molten pool in laser welding," *J. Laser Appl.*, vol. 10, no. 6, pp. 247–254, 1998.

[88] H. Ki, P. S. Mohanty, and J. Mazumder, “Modeling of laser keyhole welding: Part I. Mathematical modeling, numerical methodology, role of recoil pressure, multiple reflections, and free surface evolution,” *Metall. Mater. Trans. A*, vol. 33, no. June, pp. 1817–1830, 2002.

[89] X. Jin, L. Li, and Y. Zhang, “A heat transfer model for deep penetration laser welding based on an actual keyhole,” *Int. J. Heat Mass Transf.*, vol. 46, no. 1, pp. 15–22, 2003.

[90] R. P. Wang, Y. P. Lei, and Y. W. Shi, “Keyhole modeling during laser deep penetration welding,” *Appl. Mech. Mater.*, vol. 29–32, pp. 252–257, 2010.

[91] W. Tan, N. S. Bailey, and Y. C. Shin, “Investigation of keyhole plume and molten pool based on a three-dimensional dynamic model with sharp interface formulation,” *J. Phys. D. Appl. Phys.*, vol. 46, no. 5, p. 55501, 2013.

[92] M. Courtois, M. Carin, P. Le Masson, S. Gaied, and M. Balabane, “A complete model of keyhole and melt pool dynamics to analyze instabilities and collapse during laser welding,” *J. Laser Appl.*, vol. 26, no. 4, p. 042001, 2014.

[93] W. Huang and R. Kovacevic, “A neural network and multiple regression method for the characterization of the depth of weld penetration in laser welding based on acoustic signatures,” *J. Intell. Manuf.*, vol. 22, no. 2, pp. 131–143, 2011.

[94] A. Singh, D. E. Cooper, N. J. Blundell, D. K. Pratihar, and G. J. Gibbons, “Modelling of weld-bead geometry and hardness profile in laser welding of plain carbon steel using neural networks and genetic algorithms,” *Int. J. Comput. Integr. Manuf.*, vol. 27, no. 7, pp. 656–674, 2014.

[95] M. Luo and Y. C. Shin, “Estimation of keyhole geometry and prediction of welding defects during laser welding based on a vision system and a radial basis function neural network,” *Int. J. Adv. Manuf. Technol.*, vol. 81, no. 1–4, pp. 263–276, Oct. 2015.

[96] R. Fabbro, S. Slimani, I. Doudet, F. Coste, and F. Briand, “Experimental study of the dynamical coupling between the induced vapour plume and the melt pool for Nd–Yag CW laser welding,” *J. Phys. D. Appl. Phys.*, vol. 39, no. 2, pp. 394–400, 2006.

[97] L. Zhang, J. Zhang, G. Zhang, W. Bo, and S. Gong, "An investigation on the effects of side assisting gas flow and metallic vapour jet on the stability of keyhole and molten pool during laser full-penetration welding," *J. Phys. D. Appl. Phys.*, vol. 44, no. 13, p. 135201, 2011.

[98] T. Mościcki, J. Hoffman, and Z. Szymanski, "Modeling of plasma plume induced during laser welding," in *AIP Conference Proceedings*, 2006, vol. 812, no. 2006, pp. 165–168.

[99] J. Volpp, "Investigation on the influence of different laser beam intensity distributions on keyhole geometry during laser welding," *Phys. Procedia*, vol. 39, pp. 17–26, 2012.

[100] E. Akman, A. Demir, T. Canel, and T. Sinmazçelik, "Laser welding of Ti6Al4V titanium alloys," *J. Mater. Process. Technol.*, vol. 209, no. 8, pp. 3705–3713, 2009.

[101] X.-L. Gao, L.-J. Zhang, J. Liu, and J.-X. Zhang, "Effects of weld cross-section profiles and microstructure on properties of pulsed Nd:YAG laser welding of Ti6Al4V sheet," *Int. J. Adv. Manuf. Technol.*, vol. 72, no. 5–8, pp. 895–903, 2014.

[102] A. Lisiecki, "Welding of titanium alloy by disk laser," in *Laser Technology 2012: Applications of Lasers*, 2013, vol. 8703, pp. 87030T–1 – 87030T–12.

[103] S. S. Shirguppikar, V. S. Ganachari, P. S. Dhaingade, and A. D. Apte, "Study of laser welding technique for titanium alloy sheet," *Int. J. Adv. Engg Res.Studies*, vol. III, no. Jan-Mar 2014, pp. 20–22, 2014.

[104] Y. Liu and Y. Zhang, "Weld penetration control in gas tungsten arc welding (GTAW) process," in *IECON Proceedings (Industrial Electronics Conference)*, 2013, pp. 3842–3847.

[105] T. Sibillano, D. Rizzi, F. P. Mezzapesa, P. M. Lugarà, A. R. Konuk, R. Aarts, B. H. in 'T Veld, and A. Ancona, "Closed loop control of penetration depth during CO2 laser lap welding processes," *Sensors*, vol. 12, no. 12, pp. 11077–11090, 2012.

[106] IPG-Photonics, "High power fiber laser: User guide." Oxford, MA, MA, 2011.

[107] P. D. Ngo and Y. C. Shin, "Modelling of unstructured uncertainties and robust controlling of nonlinear dynamic systems based on type-2 fuzzy basis function networks (submitted)," *Eng. Appl. Artif. Intell.*, 2016.

[108] N. Subrahmanya and Y. C. Shin, “Adaptive divided difference filtering for simultaneous state and parameter estimation,” *Automatica*, vol. 45, no. 7, pp. 1686–1693, 2009.

[109] B. Stephen, E. G. Laurent, F. Eric, and B. Venkataramanan, *Linear Matrix Inequalities in System and Control Theory*. Philadelphia, PA: Society for Industrial and Applied Mathematics, 1994.

APPENDICES

APPENDIX A. GAIN CALCULATION OF THE MAMDANI PI FUZZY CONTROLLER IN CASE 1

The conditions of the error and the time rate of change of error relative to the activated membership functions for case 1 (Figure A-1) are given by:

$$L\left(p+\frac{1}{2}\right)<\bar{e}<L(p+1)\ \text{AND}\ L\left(q+\frac{1}{2}\right)<\bar{r}<L(q+1)\ \text{AND}\ \bar{e}-L\left(p+\frac{1}{2}\right)<\bar{r}-L\left(q+\frac{1}{2}\right) \tag{A.1}$$

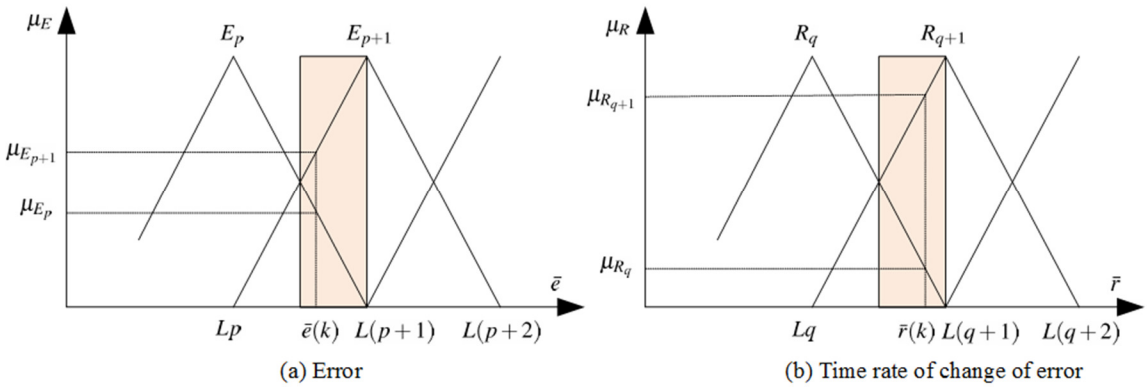

Figure A-1: Error and the time rate of change of the error in case 1.

By assuming that E_p, E_{p+1}, R_q, and R_{q+1} are four non-zero input membership functions of the error and the time rate of change of the error, the membership values can be found as follows:

$$\mu_{E_{\{p\}}}=\frac{L(p+1)-K_e e}{L},\ \mu_{E_{\{p+1\}}}=\frac{K_e e-Lp}{L} \tag{A.2}$$

$$\mu_{R_{\{q\}}}=\frac{L(q+1)-K_r r}{L},\ \mu_{R_{\{q+1\}}}=\frac{K_r r-Lq}{L} \tag{A.3}$$

The premises $H_{i,j}$ ($i = p, p+1$ and $j = q, q+1$) of the four activated rules for case 1 are calculated by using the minimum operations:

$$H_{p,q} = \min\left(\mu_{E_p}(e), \mu_{R_q}(r)\right) = \mu_{R_q}(r) = \frac{L(q+1) - K_r r}{L} \tag{A.4}$$

$$H_{p+1,q} = \min\left(\mu_{E_{p+1}}(e), \mu_{R_q}(r)\right) = \mu_{R_q}(r) = \frac{L(q+1) - K_r r}{L} \tag{A.5}$$

$$H_{p,q+1} = \min\left(\mu_{E_p}(e), \mu_{R_{q+1}}(r)\right) = \mu_{E_p}(e) = \frac{L(p+1) - K_e e}{L} \tag{A.6}$$

$$H_{p+1,q+1} = \min\left(\mu_{E_{p+1}}(e), \mu_{R_{q+1}}(r)\right) = \mu_{E_{p+1}}(e) = \frac{K_e e - Lp}{L} \tag{A.7}$$

The change in control output $\Delta u(k)$ can be calculated by using singleton fuzzification, minimum inference, and centroid defuzzification methods:

$$\Delta u(k) = \frac{\sum_{i,j} U_{i,j} \cdot \min\left[\mu_{E_i}(\bar{e}), \mu_{E_j}(\bar{r})\right]}{\sum_{i,j} \min\left[\mu_{E_i}(\bar{e}), \mu_{E_j}(\bar{r})\right]} = \frac{\sum_{i,j} U_{i,j} \cdot H_{i,j}}{\sum_{i,j} H_{i,j}}, \quad (i = p, p+1 \text{ and } j = q, q+1)$$

$$= \frac{\dfrac{U_{p,q}\left(L(q+1) - K_r r\right) + U_{p+1,q}\left(L(q+1) - K_r r\right) + U_{p,q+1}\left(L(p+1) - K_e e\right) + U_{p+1,q+1}\left(K_e e - Lp\right)}{L}}{\dfrac{L(q+1) - K_r r}{L} + \dfrac{L(q+1) - K_r r}{L} + \dfrac{L(p+1) - K_e e}{L} + \dfrac{K_e e - Lp}{L}}$$

$$\left(-U_{p,q+1} + U_{p+1,q+1}\right) K_e e + \left(-U_{p,q} - U_{p+1,q}\right) K_r r +$$

$$= \frac{qL\left(U_{p,q} + U_{p+1,q}\right) + pL\left(U_{p,q+1} - U_{p+1,q+1}\right) + L\left(U_{p,q} + U_{p+1,q} + U_{p,q+1}\right)}{2qL + 3L - 2K_r r} \tag{A.8}$$

In Case 1, since $K_r r < L(q+1)$, the following inequalities can be obtained:

$$D = 2qL + 3L - 2K_r r > L > 0 \text{ and} \tag{A.9}$$

$$\left(G_e K_e + \frac{G_r K_r}{T}\right)e(k) - \frac{G_r K_r}{T}e(k-1) + C \le \left|G_e K_e + \frac{G_r K_r}{T}\right|\left|e_1(k)\right| + \left|-\frac{G_r K_r}{T}e(k-1) + C\right|$$

$$\le \frac{T\left|G_e K_e\right| + \left|G_r K_r\right|}{T}\left|e_1(k)\right| + \frac{T\left|C\right| + \left|G_r K_r\right|\left|e(k-1)\right|}{T} \tag{A.10}$$

As the output membership functions $U_{i,j}$ are bounded by $[-1,1]$, the following were used:

$$\begin{aligned} \left|-U_{p,q+1} + U_{p+1,q+1}\right| &\le \left|U_{p,q+1}\right| + \left|U_{p+1,q+1}\right| \le 2 \\ \left|U_{p,q} - U_{p+1,q}\right| &\le \left|U_{p,q}\right| + \left|U_{p+1,q}\right| \le 2 \end{aligned} \tag{A.11}$$

From the definition of $S_1(e_1(k))$ in Eq. (2.32) and the above inequalities, the upper bound of $S_1(e_1(k))$ can be computed as follows:

$$\begin{aligned} S_1(e_1(k)) &= T\frac{\left(G_e K_e + \frac{G_r K_r}{T}\right)e(k) - \frac{G_r K_r}{T}e(k-1) + C}{2qL + 3L - 2K_r r} \\ &\le \frac{T\left|G_e K_e\right| + \left|G_r K_r\right|}{L}\left|e_1(k)\right| + \frac{T\left|C\right| + \left|G_r K_r\right|\left|e(k-1)\right|}{L} \\ &= \frac{TK_e\left|-U_{p,q+1} + U_{p+1,q+1}\right| + K_r\left|U_{p,q} - U_{p+1,q}\right|}{L}\left|e_1(k)\right| + \frac{T\left|C\right| + \left|G_r K_r\right|M_e}{L} \\ &\le \frac{2\left(K_e T + K_r\right)}{L}\left|e_1(k)\right| + \frac{T\left|C\right| + \left|G_r K_r\right|M_e}{L} = \gamma_1\left|e_1(k)\right| + \beta_1 \end{aligned} \tag{A.12}$$

where M_e is the maximum magnitude of the error signal, $M_e = \sup_{k\ge 0}\left|e(k)\right|$, and

$$\gamma_1 = \frac{2\left(K_e T + K_r\right)}{L}, \qquad \beta_1 = \frac{T\left|C\right| + \left|G_r K_r\right|M_e}{L} \tag{A.13}$$

Hence, the gain of the operator S_1 in case 1 is $\left\|S_1\right\|_p = \gamma_1$.

APPENDIX B . GAIN CALCULATION OF THE MAMDANI PI FUZZY CONTROLLER IN CASE 2

The conditions of the error and the time rate of change of error relative to the activated membership functions for case 2 (Figure B-1) are given by:

$$L\left(p+\frac{1}{2}\right)<\bar{e}<L(p+1) \text{ AND } L\left(q+\frac{1}{2}\right)<\bar{r}<L(p+1) \text{ AND } \bar{e}-L\left(p+\frac{1}{2}\right)>\bar{r}-L\left(q+\frac{1}{2}\right) \tag{B.1}$$

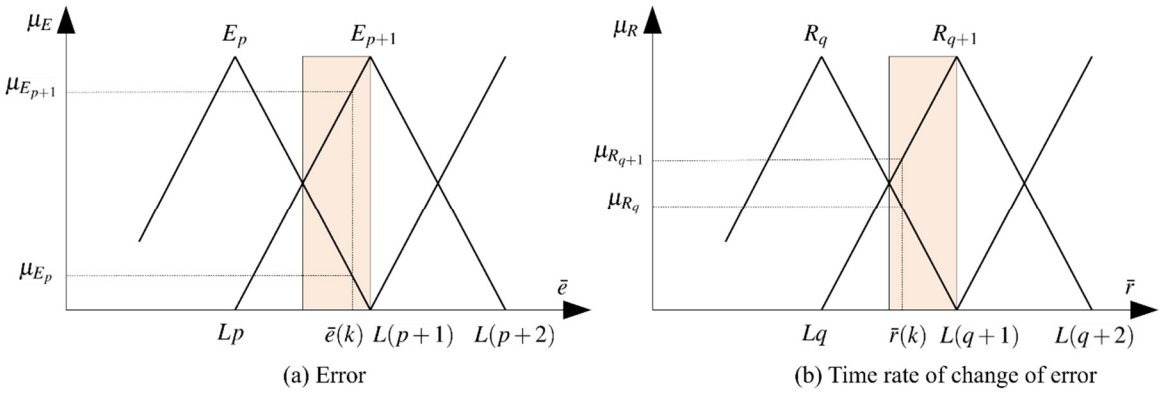

Figure B-1: Error and the time rate of change of the error in case 2.

By assuming that E_p, E_{p+1}, R_q, and R_{q+1} are four non-zero input membership functions of the error and the time rate of change of the error, the membership values can be found as follows:

$$\mu_{E_{\{p\}}}=\frac{L(p+1)-K_e e}{L}, \mu_{E_{\{p+1\}}}=\frac{K_e e-Lp}{L} \tag{B.2}$$

$$\mu_{R_{\{q\}}}=\frac{L(q+1)-K_r r}{L}, \mu_{R_{\{q+1\}}}=\frac{K_r r-Lq}{L} \tag{B.3}$$

The premises $H_{i,j}$ ($i = p, p+1$ and $j = q, q+1$) of the four activated rules for case 2 are calculated by using the minimum operations:

$$H_{p,q} = \min\left(\mu_{E_p}(e), \mu_{R_q}(r)\right) = \mu_{E_p}(e) = \frac{L(p+1) - K_e e}{L} \tag{B.4}$$

$$H_{p+1,q} = \min\left(\mu_{E_{p+1}}(e), \mu_{R_q}(r)\right) = \mu_{R_q}(r) = \frac{L(q+1) - K_r r}{L} \tag{B.5}$$

$$H_{p,q+1} = \min\left(\mu_{E_p}(e), \mu_{R_{q+1}}(r)\right) = \mu_{E_p}(e) = \frac{L(p+1) - K_e e}{L} \tag{B.6}$$

$$H_{p+1,q+1} = \min\left(\mu_{E_{p+1}}(e), \mu_{R_{q+1}}(r)\right) = \mu_{R_{q+1}}(r) = \frac{K_r r - Lq}{L} \tag{B.7}$$

The change in control output $\Delta u(k)$ can be calculated by using singleton fuzzification, minimum inference, and centroid defuzzification methods:

$$\Delta u(k) = \frac{\sum_{i,j} U_{i,j} \cdot \min\left[\mu_{E_i}(\bar{e}), \mu_{E_j}(\bar{r})\right]}{\sum_{i,j} \min\left[\mu_{E_i}(\bar{e}), \mu_{E_j}(\bar{r})\right]} = \frac{\sum_{i,j} U_{i,j} \cdot H_{i,j}}{\sum_{i,j} H_{i,j}}, \quad (i = p, p+1 \text{ and } j = q, q+1)$$

$$= \frac{\dfrac{U_{p,q}\left(L(p+1) - K_e e\right) + U_{p+1,q}\left(L(q+1) - K_r r\right) + U_{p,q+1}\left(L(p+1) - K_e e\right) + U_{p+1,q+1}\left(K_r r - Lq\right)}{L}}{\dfrac{L(p+1) - K_e e}{L} + \dfrac{L(q+1) - K_r r}{L} + \dfrac{L(p+1) - K_e e}{L} + \dfrac{K_r r - Lq}{L}}$$

$$\left(-U_{p,q} - U_{p,q+1}\right) K_e e + \left(-U_{p+1,q} + U_{p+1,q+1}\right) K_r r +$$

$$= \frac{qL\left(U_{p+1,q} - U_{p+1,q+1}\right) + pL\left(U_{p,q} + U_{p,q+1}\right) + L\left(U_{p,q} + U_{p+1,q} + U_{p,q+1}\right)}{2Lp + 3L - 2K_e e} \tag{B.8}$$

In case 2, since $K_e e < L(p+1)$, the following inequalities can be obtained:

$$D = 2Lp + 3L - 2K_e e > L > 0 \text{ and} \tag{B.9}$$

$$\left(G_e K_e + \frac{G_r K_r}{T}\right) e(k) - \frac{G_r K_r}{T} e(k-1) + C \le \left|G_e K_e + \frac{G_r K_r}{T}\right| \left|e_1(k)\right| + \left|-\frac{G_r K_r}{T} e(k-1) + C\right|$$

$$\le \frac{T\left|G_e K_e\right| + \left|G_r K_r\right|}{T} \left|e_1(k)\right| + \frac{T\left|C\right| + \left|G_r K_r\right| \left|e(k-1)\right|}{T} \tag{B.10}$$

As the output membership functions $U_{i,j}$ are bounded by $[-1,1]$, the following were used:

$$\begin{aligned} \left|-U_{p,q} - U_{p,q+1}\right| &\le \left|-U_{p,q}\right| + \left|-U_{p,q+1}\right| \le 2 \\ \left|-U_{p+1,q} + U_{p+1,q+1}\right| &\le \left|-U_{p+1,q}\right| + \left|U_{p+1,q+1}\right| \le 2 \end{aligned} \tag{B.11}$$

From the definition of $S_1(e_1(k))$ in Eq. (2.32) and the above inequalities, the upper bound of $S_1(e_1(k))$ can be computed as follows:

$$\begin{aligned} S_1(e_1(k)) &= T \frac{\left(G_e K_e + \frac{G_r K_r}{T}\right) e(k) - \frac{G_r K_r}{T} e(k-1) + C}{2qL + 3L - 2K_r r} \\ &\le \frac{T\left|G_e K_e\right| + \left|G_r K_r\right|}{L} \left|e_1(k)\right| + \frac{T\left|C\right| + \left|G_r K_r\right| \left|e(k-1)\right|}{L} \\ &= \frac{TK_e \left|-U_{p,q} - U_{p,q+1}\right| + K_r \left|-U_{p+1,q} + U_{p+1,q+1}\right|}{L} \left|e_1(k)\right| + \frac{T\left|C\right| + \left|G_r K_r\right| M_e}{L} \\ &\le \frac{2\left(K_e T + K_r\right)}{L} \left|e_1(k)\right| + \frac{T\left|C\right| + \left|G_r K_r\right| M_e}{L} = \gamma_1 \left|e_1(k)\right| + \beta_1 \end{aligned} \tag{B.12}$$

where M_e is the maximum magnitude of the error signal, $M_e = \sup_{k \ge 0} \left|e(k)\right|$, and

$$\gamma_1 = \frac{2\left(K_e T + K_r\right)}{L}, \qquad \beta_1 = \frac{T\left|C\right| + \left|G_r K_r\right| M_e}{L} \tag{B.13}$$

Hence, the gain of the operator S_1 in case 2 is $\left\|S_1\right\|_p = \gamma_1$.

APPENDIX C . GAIN CALCULATION OF THE MAMDANI PI FUZZY CONTROLLER IN CASE 3

The conditions of the error and the time rate of change of error relative to the activated membership functions for case 3 (Figure C-1) are given by:

$$Lp < \bar{e} < L\left(p+\frac{1}{2}\right) \text{AND } L\left(q+\frac{1}{2}\right) < \bar{r} < L(q+1) \text{ AND } L\left(p+\frac{1}{2}\right) - \bar{e} < \bar{r} - L\left(q+\frac{1}{2}\right) \tag{C.1}$$

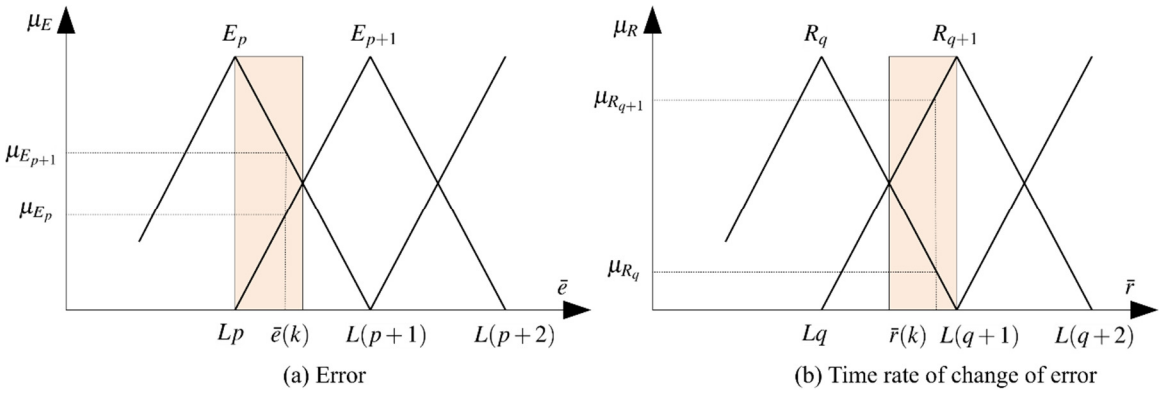

Figure C-1: Error and the time rate of change of the error in case 3.

By assuming that E_p, E_{p+1}, R_q, and R_{q+1} are four non-zero input membership functions of the error and the time rate of change of the error, the membership values can be found as follows:

$$\mu_{E_{\{p\}}} = \frac{L(p+1) - K_e e}{L}, \mu_{E_{\{p+1\}}} = \frac{K_e e - Lp}{L} \tag{C.2}$$

$$\mu_{R_{\{q\}}} = \frac{L(q+1) - K_r r}{L}, \ \mu_{R_{\{q+1\}}} = \frac{K_r r - Lq}{L} \tag{C.3}$$

The premises $H_{i,j}$ ($i = p, p+1$ and $j = q, q+1$) of the four activated rules for case 3 are calculated by using the minimum operations:

$$H_{p,q} = \min\left(\mu_{E_p}(e), \mu_{R_q}(r)\right) = \mu_{R_q}(r) = \frac{L(q+1) - K_r r}{L} \tag{C.4}$$

$$H_{p+1,q} = \min\left(\mu_{E_{p+1}}(e), \mu_{R_q}(r)\right) = \mu_{R_q}(r) = \frac{L(q+1) - K_r r}{L} \tag{C.5}$$

$$H_{p,q+1} = \min\left(\mu_{E_p}(e), \mu_{R_{q+1}}(r)\right) = \mu_{E_p}(e) = \frac{L(p+1) - K_e e}{L} \tag{C.6}$$

$$H_{p+1,q+1} = \min\left(\mu_{E_{p+1}}(e), \mu_{R_{q+1}}(r)\right) = \mu_{E_{p+1}}(e) = \frac{K_e e - Lp}{L} \tag{C.7}$$

The change in control output $\Delta u(k)$ can be calculated by using singleton fuzzification, minimum inference, and centroid defuzzification methods:

$$\Delta u(k) = \frac{\sum_{i,j} U_{i,j} \cdot \min\left[\mu_{E_i}(\bar{e}), \mu_{E_j}(\bar{r})\right]}{\sum_{i,j} \min\left[\mu_{E_i}(\bar{e}), \mu_{E_j}(\bar{r})\right]} = \frac{\sum_{i,j} U_{i,j} \cdot H_{i,j}}{\sum_{i,j} H_{i,j}}, \quad (i = p, p+1 \text{ and } j = q, q+1)$$

$$= \frac{\dfrac{U_{p,q}\left(L(q+1) - K_r r\right) + U_{p+1,q}\left(L(q+1) - K_r r\right) + U_{p,q+1}\left(L(p+1) - K_e e\right) + U_{p+1,q+1}\left(K_e e - Lp\right)}{L}}{\dfrac{L(p+1) - K_e e}{L} + \dfrac{L(q+1) - K_r r}{L} + \dfrac{L(p+1) - K_e e}{L} + \dfrac{K_e e - Lp}{L}}$$

$$\left(-U_{p,q+1} + U_{p+1,q+1}\right) K_e e + \left(-U_{p,q} - U_{p+1,q}\right) K_r r +$$

$$= \frac{qL\left(U_{p,q} + U_{p+1,q}\right) + pL\left(U_{p,q+1} - U_{p+1,q+1}\right) + L\left(U_{p,q} + U_{p+1,q} + U_{p,q+1}\right)}{2qL + 3L - 2K_r r} \tag{C.8}$$

In case 3, the following inequalities can be obtained:

$$D = 2qL + 3L - 2K_r r > L > 0 \text{ (since } K_r r < L(q+1)\text{) and} \tag{C.9}$$

$$\left(G_e K_e + \frac{G_r K_r}{T}\right) e(k) - \frac{G_r K_r}{T} e(k-1) + C \le \left|G_e K_e + \frac{G_r K_r}{T}\right| \left|e_1(k)\right| + \left|-\frac{G_r K_r}{T} e(k-1) + C\right|$$

$$\le \frac{T\left|G_e K_e\right| + \left|G_r K_r\right|}{T} \left|e_1(k)\right| + \frac{T\left|C\right| + \left|G_r K_r\right| \left|e(k-1)\right|}{T} \tag{C.10}$$

As the output membership functions $U_{i,j}$ are bounded by $[-1,1]$, the following were used:

$$\begin{aligned} \left|U_{p,q} + U_{p+1,q}\right| &\le \left|U_{p,q}\right| + \left|U_{p+1,q}\right| \le 2 \\ \left|U_{p,q+1} - U_{p+1,q+1}\right| &\le \left|U_{p,q+1}\right| + \left|-U_{p+1,q+1}\right| \le 2 \end{aligned} \tag{C.11}$$

From the definition of $S_1(e_1(k))$ in Eq. (2.32) and the above inequalities, the upper bound of $S_1(e_1(k))$ can be computed as follows:

$$\begin{aligned} S_1(e_1(k)) &= T \frac{\left(G_e K_e + \frac{G_r K_r}{T}\right) e(k) - \frac{G_r K_r}{T} e(k-1) + C}{2qL + 3L - 2K_r r} \\ &\le \frac{T\left|G_e K_e\right| + \left|G_r K_r\right|}{L} \left|e_1(k)\right| + \frac{T\left|C\right| + \left|G_r K_r\right| \left|e(k-1)\right|}{L} \\ &= \frac{TK_e \left|U_{p,q} + U_{p+1,q}\right| + K_r \left|U_{p,q+1} - U_{p+1,q+1}\right|}{L} \left|e_1(k)\right| + \frac{T\left|C\right| + \left|G_r K_r\right| M_e}{L} \\ &\le \frac{2\left(K_e T + K_r\right)}{L} \left|e_1(k)\right| + \frac{T\left|C\right| + \left|G_r K_r\right| M_e}{L} = \gamma_1 \left|e_1(k)\right| + \beta_1 \end{aligned} \tag{C.12}$$

where M_e is the maximum magnitude of the error signal, $M_e = \sup_{k \ge 0} \left|e(k)\right|$, and

$$\gamma_1 = \frac{2\left(K_e T + K_r\right)}{L}, \qquad \beta_1 = \frac{T\left|C\right| + \left|G_r K_r\right| M_e}{L} \tag{C.13}$$

Hence, the gain of the operator S_1 in case 3 is $\left\|S_1\right\|_p = \gamma_1$.

APPENDIX D. GAIN CALCULATION OF THE MAMDANI PI FUZZY CONTROLLER IN CASE 4

The conditions of the error and the time rate of change of error relative to the activated membership functions for case 4 (Figure D-1) are given by:

$$Lp < \bar{e} < L\left(p+\frac{1}{2}\right) \text{AND } L\left(q+\frac{1}{2}\right) < \bar{r} < L(q+1) \text{ AND } L\left(p+\frac{1}{2}\right) - \bar{e} > \bar{r} - L\left(q+\frac{1}{2}\right) \tag{D.1}$$

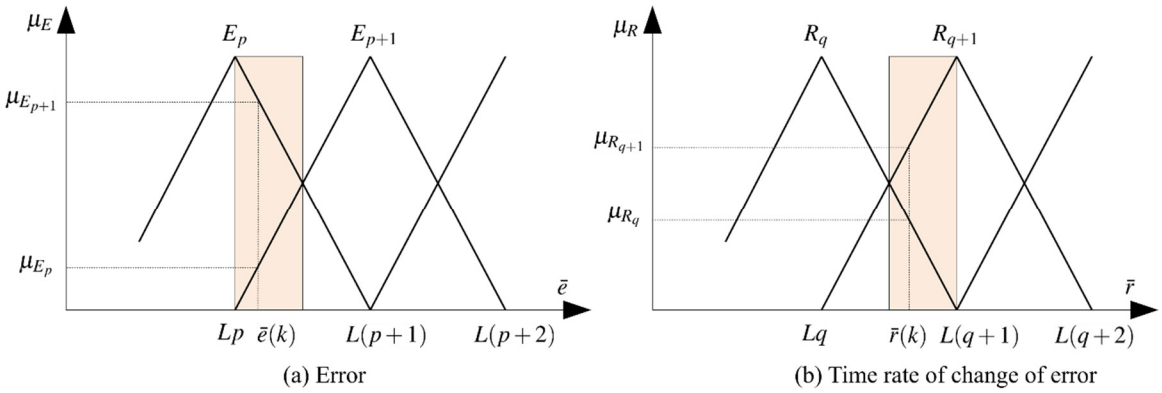

Figure D-1: Error and the time rate of change of the error in case 4.

By assuming that E_p, E_{p+1}, R_q, and R_{q+1} are four non-zero input membership functions of the error and the time rate of change of the error, the membership values can be found as follows:

$$\mu_{E_{\{p\}}} = \frac{L(p+1) - K_e e}{L}, \mu_{E_{\{p+1\}}} = \frac{K_e e - Lp}{L} \tag{D.2}$$

$$\mu_{R_{\{q\}}} = \frac{L(q+1) - K_r r}{L}, \ \mu_{R_{\{q+1\}}} = \frac{K_r r - Lq}{L} \tag{D.3}$$

The premises $H_{i,j}$ ($i = p, p+1$ and $j = q, q+1$) of the four activated rules for case 4 are calculated by using the minimum operations:

$$H_{p,q} = \min\left(\mu_{E_p}(e), \mu_{R_q}(r)\right) = \mu_{R_q}(r) = \frac{L(q+1) - K_r r}{L} \tag{D.4}$$

$$H_{p+1,q} = \min\left(\mu_{E_{p+1}}(e), \mu_{R_q}(r)\right) = \mu_{E_{p+1}}(e) = \frac{K_e e - Lp}{L} \tag{D.5}$$

$$H_{p,q+1} = \min\left(\mu_{E_p}(e), \mu_{R_{q+1}}(r)\right) = \mu_{R_{q+1}}(r) = \frac{K_r r - Lq}{L} \tag{D.6}$$

$$H_{p+1,q+1} = \min\left(\mu_{E_{p+1}}(e), \mu_{R_{q+1}}(r)\right) = \mu_{E_{p+1}}(e) = \frac{K_e e - Lp}{L} \tag{D.7}$$

The change in control output $\Delta u(k)$ can be calculated by using singleton fuzzification, minimum inference, and centroid defuzzification methods:

$$\Delta u(k) = \frac{\sum_{i,j} U_{i,j} \cdot \min\left[\mu_{E_i}(\bar{e}), \mu_{E_j}(\bar{r})\right]}{\sum_{i,j} \min\left[\mu_{E_i}(\bar{e}), \mu_{E_j}(\bar{r})\right]} = \frac{\sum_{i,j} U_{i,j} \cdot H_{i,j}}{\sum_{i,j} H_{i,j}}, \quad (i = p, p+1 \text{ and } j = q, q+1)$$

$$= \frac{\frac{U_{p,q}\left(L(q+1) - K_r r\right)}{L} + \frac{U_{p+1,q}\left(K_e e - Lp\right)}{L} + \frac{U_{p,q+1}\left(K_r r - Lq\right)}{L} + \frac{U_{p+1,q+1}\left(K_e e - Lp\right)}{L}}{\frac{L(q+1) - K_r r}{L} + \frac{K_e e - Lp}{L} + \frac{K_r r - Lq}{L} + \frac{K_e e - Lp}{L}}$$

$$= \frac{\begin{array}{l}\left(U_{p+1,q} + U_{p+1,q+1}\right) K_e e + \left(-U_{p,q} + U_{p,q+1}\right) K_r r + \\ qL\left(U_{p,q} - U_{p,q+1}\right) + pL\left(-U_{p+1,q} - U_{p+1,q+1}\right) + LU_{p,q}\end{array}}{2K_e e + L - 2Lp} \tag{D.8}$$

In case 4, the following inequalities can be obtained:

$$D = 2K_e e + L - 2Lp > L > 0 \text{ (since } K_e e > Lp \text{) and} \tag{D.9}$$

$$\left(G_e K_e + \frac{G_r K_r}{T}\right)e(k) - \frac{G_r K_r}{T}e(k-1) + C \le \left|G_e K_e + \frac{G_r K_r}{T}\right|\left|e_1(k)\right| + \left|-\frac{G_r K_r}{T}e(k-1) + C\right|$$
$$\le \frac{T\left|G_e K_e\right| + \left|G_r K_r\right|}{T}\left|e_1(k)\right| + \frac{T\left|C\right| + \left|G_r K_r\right|\left|e(k-1)\right|}{T} \tag{D.10}$$

As the output membership functions $U_{i,j}$ are bounded by $[-1,1]$, the following were used:

$$\begin{aligned} \left|U_{p+1,q} + U_{p+1,q+1}\right| &\le \left|U_{p+1,q}\right| + \left|U_{p+1,q+1}\right| \le 2 \\ \left|-U_{p,q} + U_{p,q+1}\right| &\le \left|-U_{p,q}\right| + \left|U_{p,q+1}\right| \le 2 \end{aligned} \tag{D.11}$$

From the definition of $S_1(e_1(k))$ in Eq. (2.32) and the above inequalities, the upper bound of $S_1(e_1(k))$ can be computed as follows:

$$\begin{aligned} S_1(e_1(k)) &= T\frac{\left(G_e K_e + \frac{G_r K_r}{T}\right)e(k) - \frac{G_r K_r}{T}e(k-1) + C}{2qL + 3L - 2K_r r} \\ &\le \frac{T\left|G_e K_e\right| + \left|G_r K_r\right|}{L}\left|e_1(k)\right| + \frac{T\left|C\right| + \left|G_r K_r\right|\left|e(k-1)\right|}{L} \\ &= \frac{TK_e\left|U_{p+1,q} + U_{p+1,q+1}\right| + K_r\left|-U_{p,q} + U_{p,q+1}\right|}{L}\left|e_1(k)\right| + \frac{T\left|C\right| + \left|G_r K_r\right|M_e}{L} \\ &\le \frac{2\left(K_e T + K_r\right)}{L}\left|e_1(k)\right| + \frac{T\left|C\right| + \left|G_r K_r\right|M_e}{L} = \gamma_1\left|e_1(k)\right| + \beta_1 \end{aligned} \tag{D.12}$$

where M_e is the maximum magnitude of the error signal, $M_e = \sup_{k\ge 0}\left|e(k)\right|$, and

$$\gamma_1 = \frac{2\left(K_e T + K_r\right)}{L}, \qquad \beta_1 = \frac{T\left|C\right| + \left|G_r K_r\right|M_e}{L} \tag{D.13}$$

Hence, the gain of the operator S_1 in case 4 is $\left\|S_1\right\|_p = \gamma_1$.

APPENDIX E . GAIN CALCULATION OF THE MAMDANI PI FUZZY CONTROLLER IN CASE 5

The conditions of the error and the time rate of change of error relative to the activated membership functions for case 5 (Figure E-1) are given by:

$$L\left(p+\frac{1}{2}\right)<\bar{e}<L(p+1)\ \text{AND}\ Lq<\bar{r}<L\left(q+\frac{1}{2}\right)\text{AND}\ \bar{e}-L\left(p+\frac{1}{2}\right)<L\left(q+\frac{1}{2}\right)-\bar{r} \tag{E.1}$$

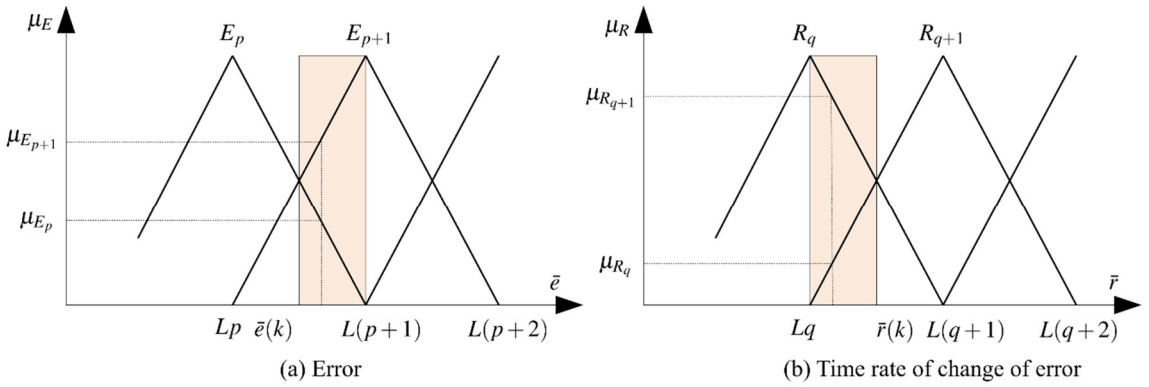

Figure E-1: Error and the time rate of change of the error in case 5.

By assuming that E_p, E_{p+1}, R_q, and R_{q+1} are four non-zero input membership functions of the error and the time rate of change of the error, the membership values can be found as follows:

$$\mu_{E_{\{p\}}}=\frac{L(p+1)-K_e e}{L},\ \mu_{E_{\{p+1\}}}=\frac{K_e e-Lp}{L} \tag{E.2}$$

$$\mu_{R_{\{q\}}}=\frac{L(q+1)-K_r r}{L},\ \mu_{R_{\{q+1\}}}=\frac{K_r r-Lq}{L} \tag{E.3}$$

The premises $H_{i,j}$ $(i = p, p+1$ and $j = q, q+1)$ of the four activated rules for case 5 are calculated by using the minimum operations:

$$H_{p,q} = \min\left(\mu_{E_p}(e), \mu_{R_q}(r)\right) = \mu_{E_p}(e) = \frac{L(p+1) - K_e e}{L} \tag{E.4}$$

$$H_{p+1,q} = \min\left(\mu_{E_{p+1}}(e), \mu_{R_q}(r)\right) = \mu_{E_{p+1}}(e) = \frac{K_e e - Lp}{L} \tag{E.5}$$

$$H_{p,q+1} = \min\left(\mu_{E_p}(e), \mu_{R_{q+1}}(r)\right) = \mu_{R_{q+1}}(r) = \frac{K_r r - Lq}{L} \tag{E.6}$$

$$H_{p+1,q+1} = \min\left(\mu_{E_{p+1}}(e), \mu_{R_{q+1}}(r)\right) = \mu_{R_{q+1}}(r) = \frac{K_r r - Lq}{L} \tag{E.7}$$

The change in control output $\Delta u(k)$ can be calculated by using singleton fuzzification, minimum inference, and centroid defuzzification methods:

$$\Delta u(k) = \frac{\sum_{i,j} U_{i,j} \cdot \min\left[\mu_{E_i}(\bar{e}), \mu_{E_j}(\bar{r})\right]}{\sum_{i,j} \min\left[\mu_{E_i}(\bar{e}), \mu_{E_j}(\bar{r})\right]} = \frac{\sum_{i,j} U_{i,j} \cdot H_{i,j}}{\sum_{i,j} H_{i,j}}, \quad (i = p, p+1 \text{ and } j = q, q+1)$$

$$= \frac{\frac{U_{p,q}\left(L(p+1) - K_e e\right)}{L} + \frac{U_{p+1,q}\left(K_e e - Lp\right)}{L} + \frac{U_{p,q+1}\left(K_r r - Lq\right)}{L} + \frac{U_{p+1,q+1}\left(K_r r - Lq\right)}{L}}{\frac{L(p+1) - K_e e}{L} + \frac{K_e e - Lp}{L} + \frac{K_r r - Lq}{L} + \frac{K_r r - Lq}{L}}$$

$$= \frac{\begin{array}{l}\left(-U_{p,q} + U_{p+1,q}\right) K_e e + \left(U_{p,q+1} + U_{p+1,q+1}\right) K_r r + \\ qL\left(-U_{p,q+1} - U_{p+1,q+1}\right) + pL\left(U_{p,q} - U_{p+1,q}\right) + LU_{p,q}\end{array}}{2K_r r - 2qL + L} \tag{E.8}$$

In case 5, the following inequalities can be obtained:

$$D = 2qL + 3L - 2K_r r > L > 0 \ \ (\text{since } K_r r < L(q+1)), \tag{E.9}$$

$$\left(G_eK_e+\frac{G_rK_r}{T}\right)e(k)-\frac{G_rK_r}{T}e(k-1)+C\le\left|G_eK_e+\frac{G_rK_r}{T}\right|\left|e_1(k)\right|+\left|-\frac{G_rK_r}{T}e(k-1)+C\right|$$
$$\le\frac{T\left|G_eK_e\right|+\left|G_rK_r\right|}{T}\left|e_1(k)\right|+\frac{T\left|C\right|+\left|G_rK_r\right|\left|e(k-1)\right|}{T} \tag{E.10}$$

As the output membership functions $U_{i,j}$ are bounded by $[-1,1]$, the following were used:

$$\begin{aligned}\left|-U_{p,q+1}-U_{p+1,q+1}\right|&\le\left|-U_{p,q+1}\right|+\left|-U_{p+1,q+1}\right|\le 2\\ \left|U_{p,q+1}+U_{p+1,q+1}\right|&\le\left|U_{p,q+1}\right|+\left|U_{p+1,q+1}\right|\le 2\end{aligned} \tag{E.11}$$

From the definition of $S_1(e_1(k))$ in Eq. (2.32) and the above inequalities, the upper bound of $S_1(e_1(k))$ can be computed as follows:

$$\begin{aligned}S_1(e_1(k))&=T\frac{\left(G_eK_e+\frac{G_rK_r}{T}\right)e(k)-\frac{G_rK_r}{T}e(k-1)+C}{2qL+3L-2K_rr}\\ &\le\frac{T\left|G_eK_e\right|+\left|G_rK_r\right|}{L}\left|e_1(k)\right|+\frac{T\left|C\right|+\left|G_rK_r\right|\left|e(k-1)\right|}{L}\\ &=\frac{TK_e\left|-U_{p,q+1}-U_{p+1,q+1}\right|+K_r\left|U_{p,q+1}+U_{p+1,q+1}\right|}{L}\left|e_1(k)\right|+\frac{T\left|C\right|+\left|G_rK_r\right|M_e}{L}\\ &\le\frac{2\left(K_eT+K_r\right)}{L}\left|e_1(k)\right|+\frac{T\left|C\right|+\left|G_rK_r\right|M_e}{L}=\gamma_1\left|e_1(k)\right|+\beta_1\end{aligned} \tag{E.12}$$

where M_e is the maximum magnitude of the error signal, $M_e=\sup_{k\ge0}\left|e(k)\right|$, and

$$\gamma_1=\frac{2\left(K_eT+K_r\right)}{L},\qquad \beta_1=\frac{T\left|C\right|+\left|G_rK_r\right|M_e}{L} \tag{E.13}$$

Hence, the gain of the operator S_1 in case 5 is $\left\|S_1\right\|_p=\gamma_1$.

APPENDIX F . GAIN CALCULATION OF THE MAMDANI PI FUZZY CONTROLLER IN CASE 6

The conditions of the error and the time rate of change of error relative to the activated membership functions for case 6 (Figure F-1) are given by:

$$L\left(p+\frac{1}{2}\right)<\bar{e}<L(p+1) \text{ AND } Lq<\bar{r}<L\left(q+\frac{1}{2}\right) \text{ AND } \bar{e}-L\left(p+\frac{1}{2}\right)>L\left(q+\frac{1}{2}\right)-\bar{r} \tag{F.1}$$

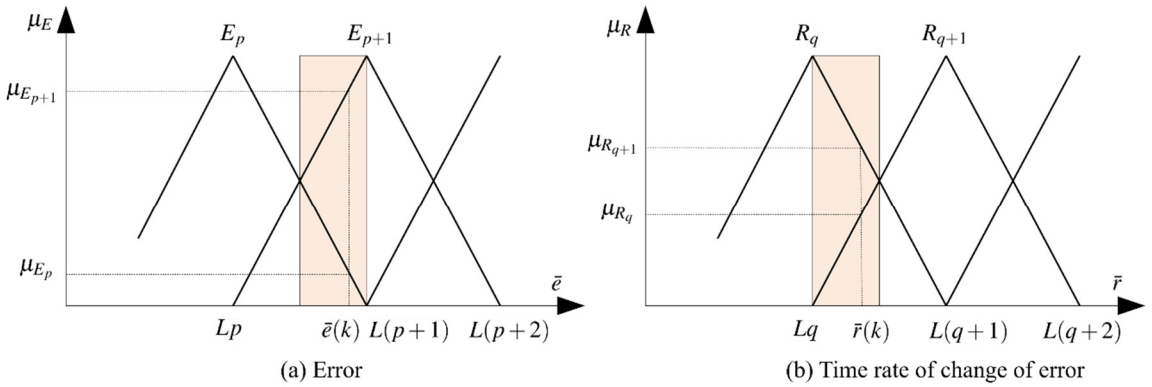

Figure F-1: Error and the time rate of change of the error in case 6.

By assuming that E_p, E_{p+1}, R_q, and R_{q+1} are four non-zero input membership functions of the error and the time rate of change of the error, the membership values can be found as follows:

$$\mu_{E_{\{p\}}}=\frac{L(p+1)-K_e e}{L}, \mu_{E_{\{p+1\}}}=\frac{K_e e-Lp}{L} \tag{F.2}$$

$$\mu_{R_{\{q\}}}=\frac{L(q+1)-K_r r}{L}, \mu_{R_{\{q+1\}}}=\frac{K_r r-Lq}{L} \tag{F.3}$$

The premises $H_{i,j}$ ($i = p, p+1$ and $j = q, q+1$) of the four activated rules for case 6 are calculated by using the minimum operations:

$$H_{p,q} = \min\left(\mu_{E_p}(e), \mu_{R_q}(r)\right) = \mu_{E_p}(e) = \frac{L(p+1) - K_e e}{L} \tag{F.4}$$

$$H_{p+1,q} = \min\left(\mu_{E_{p+1}}(e), \mu_{R_q}(r)\right) = \mu_{R_q}(r) = \frac{L(q+1) - K_r r}{L} \tag{F.5}$$

$$H_{p,q+1} = \min\left(\mu_{E_p}(e), \mu_{R_{q+1}}(r)\right) = \mu_{E_p}(e) = \frac{L(p+1) - K_e e}{L} \tag{F.6}$$

$$H_{p+1,q+1} = \min\left(\mu_{E_{p+1}}(e), \mu_{R_{q+1}}(r)\right) = \mu_{R_{q+1}}(r) = \frac{K_r r - Lq}{L} \tag{F.7}$$

The change in control output $\Delta u(k)$ can be calculated by using singleton fuzzification, minimum inference, and centroid defuzzification methods:

$$\Delta u(k) = \frac{\sum_{i,j} U_{i,j} \cdot \min\left[\mu_{E_i}(\bar{e}), \mu_{E_j}(\bar{r})\right]}{\sum_{i,j} \min\left[\mu_{E_i}(\bar{e}), \mu_{E_j}(\bar{r})\right]} = \frac{\sum_{i,j} U_{i,j} \cdot H_{i,j}}{\sum_{i,j} H_{i,j}}, \quad (i = p, p+1 \text{ and } j = q, q+1)$$

$$= \frac{\dfrac{U_{p,q}\left(L(p+1) - K_e e\right) + U_{p+1,q}\left(L(q+1) - K_r r\right) + U_{p,q+1}\left(L(p+1) - K_e e\right) + U_{p+1,q+1}\left(K_r r - Lq\right)}{L}}{\dfrac{L(p+1) - K_e e}{L} + \dfrac{L(q+1) - K_r r}{L} + \dfrac{L(p+1) - K_e e}{L} + \dfrac{K_r r - Lq}{L}}$$

$$\left(-U_{p,q} - U_{p,q+1}\right) K_e e + \left(-U_{p+1,q} + U_{p+1,q+1}\right) K_r r +$$

$$= \frac{qL\left(U_{p+1,q} - U_{p+1,q+1}\right) + pL\left(U_{p,q} - U_{p,q+1}\right) + L\left(U_{p,q} + U_{p+1,q} + U_{p,q+1}\right)}{2Lp + 3L - 2K_e e} \tag{F.8}$$

In case 6, the following inequalities can be obtained:

$$D = 2Lp + 3L - 2K_e e > L > 0 \text{ (since } K_e e < L(p+1)\text{)}, \tag{F.9}$$

$$\left(G_e K_e + \frac{G_r K_r}{T}\right)e(k) - \frac{G_r K_r}{T}e(k-1) + C \le \left|G_e K_e + \frac{G_r K_r}{T}\right|\left|e_1(k)\right| + \left|-\frac{G_r K_r}{T}e(k-1) + C\right|$$
$$\le \frac{T\left|G_e K_e\right| + \left|G_r K_r\right|}{T}\left|e_1(k)\right| + \frac{T\left|C\right| + \left|G_r K_r\right|\left|e(k-1)\right|}{T} \tag{F.10}$$

As the output membership functions $U_{i,j}$ are bounded by $[-1,1]$, the following were used:

$$\begin{aligned} \left|-U_{p,q} - U_{p,q+1}\right| &\le \left|-U_{p,q}\right| + \left|-U_{p,q+1}\right| \le 2 \\ \left|-U_{p+1,q} + U_{p+1,q+1}\right| &\le \left|-U_{p+1,q}\right| + \left|U_{p+1,q+1}\right| \le 2 \end{aligned} \tag{F.11}$$

From the definition of $S_1(e_1(k))$ in Eq. (2.32) and the above inequalities, the upper bound of $S_1(e_1(k))$ can be computed as follows:

$$\begin{aligned} S_1(e_1(k)) &= T\frac{\left(G_e K_e + \frac{G_r K_r}{T}\right)e(k) - \frac{G_r K_r}{T}e(k-1) + C}{2qL + 3L - 2K_r r} \\ &\le \frac{T\left|G_e K_e\right| + \left|G_r K_r\right|}{L}\left|e_1(k)\right| + \frac{T\left|C\right| + \left|G_r K_r\right|\left|e(k-1)\right|}{L} \\ &= \frac{TK_e\left|-U_{p,q} - U_{p,q+1}\right| + K_r\left|-U_{p+1,q} + U_{p+1,q+1}\right|}{L}\left|e_1(k)\right| + \frac{T\left|C\right| + \left|G_r K_r\right|M_e}{L} \\ &\le \frac{2\left(K_e T + K_r\right)}{L}\left|e_1(k)\right| + \frac{T\left|C\right| + \left|G_r K_r\right|M_e}{L} = \gamma_1\left|e_1(k)\right| + \beta_1 \end{aligned} \tag{F.12}$$

where M_e is the maximum magnitude of the error signal $M_e = \sup_{k\ge 0}\left|e(k)\right|$, and

$$\gamma_1 = \frac{2\left(K_e T + K_r\right)}{L}, \qquad \beta_1 = \frac{T\left|C\right| + \left|G_r K_r\right|M_e}{L} \tag{F.13}$$

Hence, the gain of the operator S_1 in case 6 is $\left\|S_1\right\|_p = \gamma_1$.

APPENDIX G. GAIN CALCULATION OF THE MAMDANI PI FUZZY CONTROLLER IN CASE 7

The conditions of the error and the time rate of change of error relative to the activated membership functions for case 7 (Figure G-1) are given by:

$$Lp < \bar{e} < L\left(p+\frac{1}{2}\right) \text{ AND } Lq < \bar{r} < L\left(q+\frac{1}{2}\right) \text{ AND } \bar{e} - Lp < \bar{r} - Lq \tag{G.1}$$

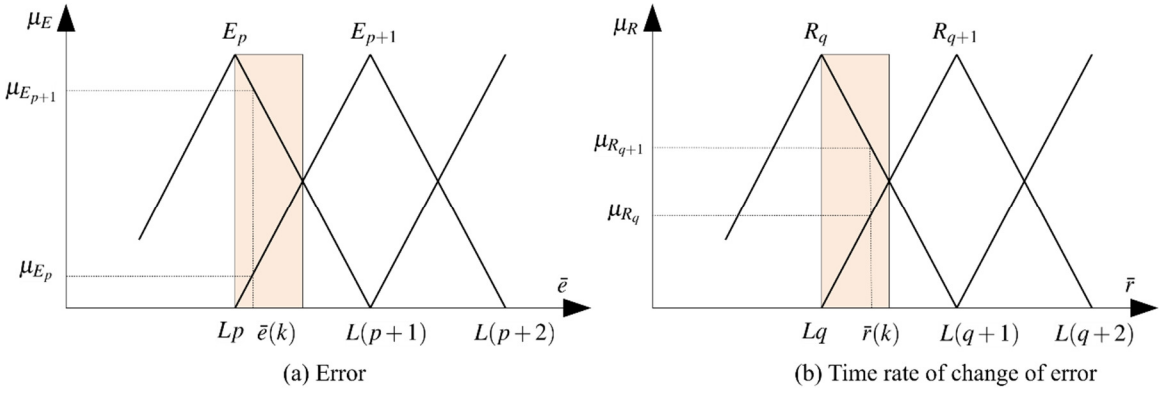

Figure G-1: Error and the time rate of change of the error in case 7.

By assuming that E_p, E_{p+1}, R_q, and R_{q+1} are four non-zero input membership functions of the error and the time rate of change of the error, the membership values can be found as follows:

$$\mu_{E_{\{p\}}} = \frac{L(p+1) - K_e e}{L}, \mu_{E_{\{p+1\}}} = \frac{K_e e - Lp}{L} \tag{G.2}$$

$$\mu_{R_{\{q\}}} = \frac{L(q+1) - K_r r}{L}, \mu_{R_{\{q+1\}}} = \frac{K_r r - Lq}{L} \tag{G.3}$$

The premises $H_{i,j}$ ($i = p, p+1$ and $j = q, q+1$) of the four activated rules for case 6 are calculated by using the minimum operations:

$$H_{p,q} = \min\left(\mu_{E_p}(e), \mu_{R_q}(r)\right) = \mu_{R_q}(r) = \frac{L(q+1) - K_r r}{L} \tag{G.4}$$

$$H_{p+1,q} = \min\left(\mu_{E_{p+1}}(e), \mu_{R_q}(r)\right) = \mu_{E_{p+1}}(e) = \frac{K_e e - Lp}{L} \tag{G.5}$$

$$H_{p,q+1} = \min\left(\mu_{E_p}(e), \mu_{R_{q+1}}(r)\right) = \mu_{R_{q+1}}(r) = \frac{K_r r - Lq}{L} \tag{G.6}$$

$$H_{p+1,q+1} = \min\left(\mu_{E_{p+1}}(e), \mu_{R_{q+1}}(r)\right) = \mu_{E_{p+1}}(e) = \frac{K_e e - Lp}{L} \tag{G.7}$$

The change in control output $\Delta u(k)$ can be calculated by using singleton fuzzification, minimum inference, and centroid defuzzification methods:

$$\Delta u(k) = \frac{\sum_{i,j} U_{i,j} \cdot \min\left[\mu_{E_i}(\bar{e}), \mu_{E_j}(\bar{r})\right]}{\sum_{i,j} \min\left[\mu_{E_i}(\bar{e}), \mu_{E_j}(\bar{r})\right]} = \frac{\sum_{i,j} U_{i,j} \cdot H_{i,j}}{\sum_{i,j} H_{i,j}}, \quad (i = p, p+1 \text{ and } j = q, q+1)$$

$$= \frac{\frac{U_{p,q}\left(L(q+1) - K_r r\right)}{L} + \frac{U_{p+1,q}\left(K_e e - Lp\right)}{L} + \frac{U_{p,q+1}\left(K_r r - Lq\right)}{L} + \frac{U_{p+1,q+1}\left(K_e e - Lp\right)}{L}}{\frac{L(q+1) - K_r r}{L} + \frac{K_e e - Lp}{L} + \frac{K_r r - Lq}{L} + \frac{K_e e - Lp}{L}} \tag{G.8}$$

$$= \frac{\begin{array}{r}\left(U_{p+1,q} + U_{p+1,q+1}\right) K_e e + \left(-U_{p,q} + U_{p,q+1}\right) K_r r + qL\left(U_{p,q} - U_{p,q+1}\right) \\ + pL\left(U_{p+1,q} - U_{p+1,q+1}\right) + LU_{p,q}\end{array}}{2K_e e + L - 2Lp}$$

In case 7, the following inequalities can be obtained:

$$D = 2K_e e + L - 2Lp > L > 0 \ \ (\text{since } K_e e > Lp), \tag{G.9}$$

$$\left(G_e K_e + \frac{G_r K_r}{T}\right)e(k) - \frac{G_r K_r}{T}e(k-1) + C \le \left|G_e K_e + \frac{G_r K_r}{T}\right|\left|e_1(k)\right| + \left|-\frac{G_r K_r}{T}e(k-1) + C\right|$$

$$\le \frac{T\left|G_e K_e\right| + \left|G_r K_r\right|}{T}\left|e_1(k)\right| + \frac{T\left|C\right| + \left|G_r K_r\right|\left|e(k-1)\right|}{T} \tag{G.10}$$

As the output membership functions $U_{i,j}$ are bounded by $[-1,1]$, the following were used:

$$\begin{aligned} \left|U_{p+1,q} + U_{p+1,q+1}\right| &\le \left|U_{p+1,q}\right| + \left|U_{p+1,q+1}\right| \le 2 \\ \left|-U_{p,q} + U_{p,q+1}\right| &\le \left|-U_{p,q}\right| + \left|U_{p,q+1}\right| \le 2 \end{aligned} \tag{G.11}$$

From the definition of $S_1(e_1(k))$ in Eq. (2.32) and the above inequalities, the upper bound of $S_1(e_1(k))$ can be computed as follows:

$$\begin{aligned} S_1(e_1(k)) &= T\frac{\left(G_e K_e + \frac{G_r K_r}{T}\right)e(k) - \frac{G_r K_r}{T}e(k-1) + C}{2qL + 3L - 2K_r r} \\ &\le \frac{T\left|G_e K_e\right| + \left|G_r K_r\right|}{L}\left|e_1(k)\right| + \frac{T\left|C\right| + \left|G_r K_r\right|\left|e(k-1)\right|}{L} \\ &= \frac{TK_e\left|U_{p+1,q} + U_{p+1,q+1}\right| + K_r\left|-U_{p,q} + U_{p,q+1}\right|}{L}\left|e_1(k)\right| + \frac{T\left|C\right| + \left|G_r K_r\right|M_e}{L} \\ &\le \frac{2\left(K_e T + K_r\right)}{L}\left|e_1(k)\right| + \frac{T\left|C\right| + \left|G_r K_r\right|M_e}{L} = \gamma_1\left|e_1(k)\right| + \beta_1 \end{aligned} \tag{G.12}$$

where M_e is the maximum magnitude of the error signal $M_e = \sup_{k\ge 0}\left|e(k)\right|$, and

$$\gamma_1 = \frac{2\left(K_e T + K_r\right)}{L}, \qquad \beta_1 = \frac{T\left|C\right| + \left|G_r K_r\right|M_e}{L} \tag{G.13}$$

Hence, the gain of the operator S_1 in case 7 is $\left\|S_1\right\|_p = \gamma_1$.

APPENDIX H. GAIN CALCULATION OF THE MAMDANI PI FUZZY CONTROLLER IN CASE 8

The conditions of the error and the time rate of change of error relative to the activated membership functions for case 8 (Figure H-1) are given by:

$$Lp < \bar{e} < L\left(p+\frac{1}{2}\right) \text{ AND } Lq < \bar{r} < L\left(q+\frac{1}{2}\right) \text{ AND } \bar{e} - Lp > \bar{r} - Lq \quad \text{(H.1)}$$

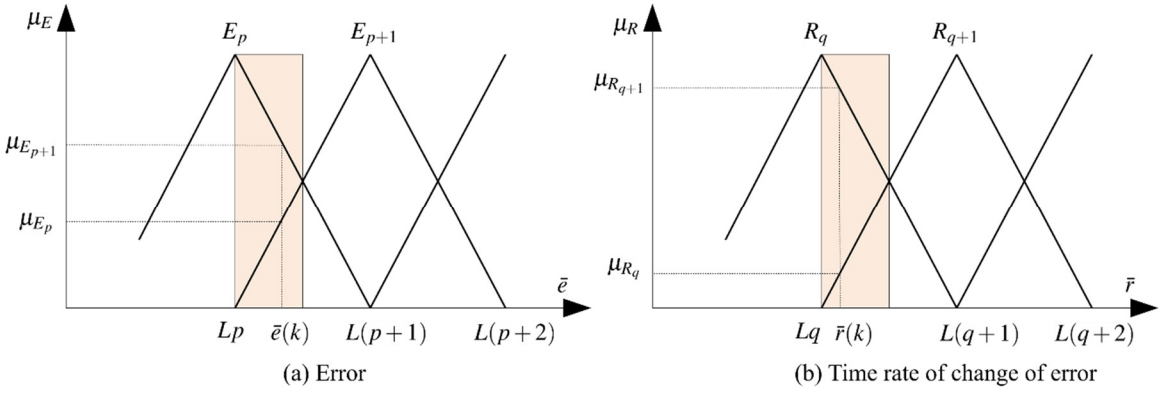

Figure H-1: Error and the time rate of change of the error in case 8.

By assuming that E_p, E_{p+1}, R_q, and R_{q+1} are four non-zero input membership functions of the error and the time rate of change of the error, the membership values can be found as follows:

$$\mu_{E_{\{p\}}} = \frac{L(p+1) - K_e e}{L}, \mu_{E_{\{p+1\}}} = \frac{K_e e - Lp}{L} \quad \text{(H.2)}$$

$$\mu_{R_{\{q\}}} = \frac{L(q+1) - K_r r}{L}, \mu_{R_{\{q+1\}}} = \frac{K_r r - Lq}{L} \quad \text{(H.3)}$$

The premises $H_{i,j}$ ($i = p, p+1$ and $j = q, q+1$) of the four activated rules for case 6 are calculated by using the minimum operations:

$$H_{p,q} = \min\left(\mu_{E_p}(e), \mu_{R_q}(r)\right) = \mu_{E_p}(e) = \frac{L(p+1) - K_e e}{L} \tag{H.4}$$

$$H_{p+1,q} = \min\left(\mu_{E_{p+1}}(e), \mu_{R_q}(r)\right) = \mu_{E_{p+1}}(e) = \frac{K_e e - Lp}{L} \tag{H.5}$$

$$H_{p,q+1} = \min\left(\mu_{E_p}(e), \mu_{R_{q+1}}(r)\right) = \mu_{R_{q+1}}(r) = \frac{K_r r - Lq}{L} \tag{H.6}$$

$$H_{p+1,q+1} = \min\left(\mu_{E_{p+1}}(e), \mu_{R_{q+1}}(r)\right) = \mu_{R_{q+1}}(r) = \frac{K_r r - Lq}{L} \tag{H.7}$$

The change in control output $\Delta u(k)$ can be calculated by using singleton fuzzification, minimum inference, and centroid defuzzification methods:

$$\Delta u(k) = \frac{\sum_{i,j} U_{i,j} \cdot \min\left[\mu_{E_i}(\bar{e}), \mu_{E_j}(\bar{r})\right]}{\sum_{i,j} \min\left[\mu_{E_i}(\bar{e}), \mu_{E_j}(\bar{r})\right]} = \frac{\sum_{i,j} U_{i,j} \cdot H_{i,j}}{\sum_{i,j} H_{i,j}}, \quad (i = p, p+1 \text{ and } j = q, q+1)$$

$$= \frac{\frac{U_{p,q}\left(L(p+1) - K_e e\right)}{L} + \frac{U_{p+1,q}\left(K_e e - Lp\right)}{L} + \frac{U_{p,q+1}\left(K_r r - Lq\right)}{L} + \frac{U_{p+1,q+1}\left(K_r r - Lq\right)}{L}}{\frac{L(p+1) - K_e e}{L} + \frac{K_e e - Lp}{L} + \frac{K_r r - Lq}{L} + \frac{K_r r - Lq}{L}} \tag{H.8}$$

$$= \frac{\begin{array}{r}\left(-U_{p,q} + U_{p+1,q}\right) K_e e + \left(U_{p,q+1} + U_{p+1,q+1}\right) K_r r + \\ qL\left(-U_{p,q+1} - U_{p+1,q+1}\right) + pL\left(U_{p,q} - U_{p+1,q}\right) + LU_{p,q}\end{array}}{2K_r r - 2qL + L}$$

In case 8, the following inequalities can be obtained:

$$D = 2K_r r - 2qL + L > L > 0 \ (\text{since } K_r r > Lq), \tag{H.9}$$

$$\left(G_e K_e + \frac{G_r K_r}{T}\right)e(k) - \frac{G_r K_r}{T}e(k-1) + C \le \left|G_e K_e + \frac{G_r K_r}{T}\right|\left|e_1(k)\right| + \left|-\frac{G_r K_r}{T}e(k-1) + C\right|$$

$$\le \frac{T\left|G_e K_e\right| + \left|G_r K_r\right|}{T}\left|e_1(k)\right| + \frac{T\left|C\right| + \left|G_r K_r\right|\left|e(k-1)\right|}{T} \tag{H.10}$$

As the output membership functions $U_{i,j}$ are bounded by $[-1,1]$, the following were used:

$$\begin{aligned} \left|-U_{p,q} + U_{p+1,q}\right| &\le \left|-U_{p,q}\right| + \left|U_{p+1,q}\right| \le 2 \\ \left|U_{p,q+1} + U_{p+1,q+1}\right| &\le \left|U_{p,q+1}\right| + \left|U_{p+1,q+1}\right| \le 2 \end{aligned} \tag{H.11}$$

From the definition of $S_1(e_1(k))$ in Eq. (2.32) and the above inequalities, the upper bound of $S_1(e_1(k))$ can be computed as follows:

$$\begin{aligned} S_1(e_1(k)) &= T\frac{\left(G_e K_e + \frac{G_r K_r}{T}\right)e(k) - \frac{G_r K_r}{T}e(k-1) + C}{2qL + 3L - 2K_r r} \\ &\le \frac{T\left|G_e K_e\right| + \left|G_r K_r\right|}{L}\left|e_1(k)\right| + \frac{T\left|C\right| + \left|G_r K_r\right|\left|e(k-1)\right|}{L} \\ &= \frac{TK_e\left|-U_{p,q} + U_{p+1,q}\right| + K_r\left|U_{p,q+1} + U_{p+1,q+1}\right|}{L}\left|e_1(k)\right| + \frac{T\left|C\right| + \left|G_r K_r\right|M_e}{L} \\ &\le \frac{2\left(K_e T + K_r\right)}{L}\left|e_1(k)\right| + \frac{T\left|C\right| + \left|G_r K_r\right|M_e}{L} = \gamma_1\left|e_1(k)\right| + \beta_1 \end{aligned} \tag{H.12}$$

where M_e is the maximum magnitude of the error signal $M_e = \sup_{k\ge 0}\left|e(k)\right|$, and

$$\gamma_1 = \frac{2\left(K_e T + K_r\right)}{L}, \qquad \beta_1 = \frac{T\left|C\right| + \left|G_r K_r\right|M_e}{L} \tag{H.13}$$

Hence, the gain of the operator S_1 in case 8 is $\left\|S_1\right\|_p = \gamma_1$.

APPENDIX I . COEFFICIENT MATRICES OF THE TYPE-2 T-S FUZZY MODEL REPRESENTING THE ETA

Rule R^1

$$\mathbf{A}_{1\min} = \begin{bmatrix} 1 & 0.001 & 0 \\ 0 & 1 & 0 \\ 0 & -78.366 & 1.0365 \end{bmatrix} \qquad \mathbf{A}_{1\max} = \begin{bmatrix} 1 & 0.001 & 0 \\ 0 & 1 & 0 \\ 0 & -72.107 & 1.0447 \end{bmatrix} \tag{I.1}$$

$$\mathbf{B}_{1\min} = \begin{bmatrix} 0 & 0 & 0.0245 \end{bmatrix} \qquad \mathbf{B}_{1\max} = \begin{bmatrix} 0 & 0 & 0.0249 \end{bmatrix} \tag{I.2}$$

Rule R^2

$$\mathbf{A}_{2\min} = \begin{bmatrix} 1 & 0.001 & 0 \\ 0 & 1 & 0 \\ 0 & -78.3412 & 1.0365 \end{bmatrix} \qquad \mathbf{A}_{1\max} = \begin{bmatrix} 1 & 0.001 & 0 \\ 0 & 1 & 0 \\ 0 & -72.0821 & 1.0447 \end{bmatrix} \tag{I.3}$$

$$\mathbf{B}_{2\min} = \begin{bmatrix} 0 & 0 & 0.0245 \end{bmatrix} \qquad \mathbf{B}_{2\max} = \begin{bmatrix} 0 & 0 & 0.0249 \end{bmatrix} \tag{I.4}$$

Rule R^3

$$\mathbf{A}_{3\min} = \begin{bmatrix} 1 & 0.001 & 0 \\ 0 & 1 & 0 \\ 0 & -89.0027 & 1.0329 \end{bmatrix} \qquad \mathbf{A}_{3\max} = \begin{bmatrix} 1 & 0.001 & 0 \\ 0 & 1 & 0 \\ 0 & -85.5089 & 1.0427 \end{bmatrix} \tag{I.5}$$

$$\mathbf{B}_{3\min} = \begin{bmatrix} 0 & 0 & 0.0265 \end{bmatrix} \qquad \mathbf{B}_{3\max} = \begin{bmatrix} 0 & 0 & 0.0269 \end{bmatrix} \tag{I.6}$$

Rule R^4

$$\mathbf{A}_{4\min} = \begin{bmatrix} 1 & 0.001 & 0 \\ 0 & 1 & 0 \\ 0 & -89.0252 & 1.0329 \end{bmatrix} \qquad \mathbf{A}_{4\max} = \begin{bmatrix} 1 & 0.001 & 0 \\ 0 & 1 & 0 \\ 0 & -83.5317 & 1.0427 \end{bmatrix} \tag{I.7}$$

$$\mathbf{B}_{4\min} = \begin{bmatrix} 0 & 0 & 0.0269 \end{bmatrix} \qquad \mathbf{B}_{4\max} = \begin{bmatrix} 0 & 0 & 0.0265 \end{bmatrix} \tag{I.8}$$

APPENDIX J . FEEDBACK GAINS OF THE RTSFC FOR CONTROLLING THE ETA

Table J-1: Feedback gains of the RTSFC for the EHA with $\alpha = 0.03$.

Rule R^j	$\mathbf{K}_j$	$\mathbf{k}_j$
1	$10^5 \cdot [-1.5068 \quad -0.0036 \quad -0.0001]$	$0.0187 \cdot 10^5$
2	$10^5 \cdot [-1.4550 \quad -0.0018 \quad -0.0001]$	$0.0180 \cdot 10^5$
3	$10^5 \cdot [-1.3753 \quad -0.0002 \quad -0.0001]$	$0.0169 \cdot 10^5$
4	$10^5 \cdot [-1.3486 \quad -0.0010 \quad -0.0001]$	$0.0166 \cdot 10^5$

Table J-2: Feedback gains of the RTSFC for the EHA with $\alpha = 0.05$.

Rule R^j	$\mathbf{K}_j$	$\mathbf{k}_j$
1	$10^5 \cdot [-2.8885 \quad -0.0092 \quad -0.0001]$	$0.0600 \cdot 10^5$
2	$10^5 \cdot [-2.7527 \quad -0.0068 \quad -0.0001]$	$0.0570 \cdot 10^5$
3	$10^5 \cdot [-2.6014 \quad -0.0049 \quad -0.0001]$	$0.0536 \cdot 10^5$
4	$10^5 \cdot [-2.5460 \quad -0.0035 \quad -0.0001]$	$0.0524 \cdot 10^5$

Table J-3: Feedback gains of the RTSFC for the EHA with $\alpha = 0.1$.

Rule R^j	$\mathbf{K}_j$	$\mathbf{k}_j$
1	$10^5 \cdot [-6.9056 \quad -0.0282 \quad -0.0002]$	$0.2632 \cdot 10^5$
2	$10^5 \cdot [-6.5493 \quad -0.0249 \quad -0.0002]$	$0.2487 \cdot 10^5$
3	$10^5 \cdot [-6.0553 \quad -0.0213 \quad -0.0002]$	$0.2275 \cdot 10^5$
4	$10^5 \cdot [-5.9091 \quad -0.0193 \quad -0.0002]$	$0.2220 \cdot 10^5$

Table J-4: Feedback gains of the RTSFC for the EHA with $\alpha = 0.2$.

Rule R^j	$\mathbf{K}_j$	$\mathbf{k}_j$
1	$10^6 \cdot [-2.3785 \quad -0.0103 \quad -0.0000]$	$0.1550 \cdot 10^6$
2	$10^6 \cdot [2.8299 \quad -0.0098 \quad -0.0000]$	$0.1487 \cdot 10^6$
3	$10^6 \cdot [-2.1143 \quad -0.0089 \quad -0.0000]$	$0.1359 \cdot 10^6$
4	$10^6 \cdot [-2.0772 \quad -0.0086 \quad -0.0000]$	$0.1335 \cdot 10^6$

APPENDIX K. COEFFICIENT MATRICES OF THE TYPE-2 T-S FUZZY MODEL REPRESENTING THE KEYHOLE DIAMETER

$\mathbf{A}_{i\min}$, $\mathbf{A}_{i\max}$, $\mathbf{B}_{i\min}$ and $\mathbf{B}_{i\max}$ are matrices that contain the lower and upper value of each element of matrices $\tilde{\mathbf{A}}_i$ and $\tilde{\mathbf{B}}_i$, respectively.

Rule R^1: $c_{X_1^1} = c_{X_2^1} = 1.112$ mm, $c_{U_1^1} = 800$ W

$$\mathbf{A}_{1\min} = \begin{bmatrix} 0 & 1 \\ -0.0229 & 0.3240 \end{bmatrix},\ \mathbf{A}_{1\max} = \begin{bmatrix} 0 & 1 \\ 0.3058 & 0.5777 \end{bmatrix},\ \Delta\mathbf{A}_{1m} = \begin{bmatrix} 0 & 1 \\ -0.0747 & 0.0681 \end{bmatrix}$$

$$\mathbf{B}_{1\min} = \begin{bmatrix} 0 & 4.2706\times10^{-4} \end{bmatrix}^{\mathrm{T}},\ \mathbf{B}_{1\max} = \begin{bmatrix} 0 & 6.3463\times10^{-4} \end{bmatrix}^{\mathrm{T}},\ \Delta\mathbf{B}_{1m} = \begin{bmatrix} 0 & -1.7428\times10^{-5} \end{bmatrix}^{\mathrm{T}}$$

$$\mathbf{C}_1 = \begin{bmatrix} 0 & 0.72788 \end{bmatrix}$$

Rule R^2: $c_{X_1^2} = c_{X_2^2} = 1.150$ mm, $c_{U_1^2} = 850$ W

$$\mathbf{A}_{2\min} = \begin{bmatrix} 0 & 1 \\ -0.1384 & 0.3051 \end{bmatrix},\ \mathbf{A}_{1\max} = \begin{bmatrix} 0 & 1 \\ 0.1834 & 0.5234 \end{bmatrix},\ \Delta\mathbf{A}_{2m} = \begin{bmatrix} 0 & 1 \\ -0.0704 & 0.0521 \end{bmatrix}$$

$$\mathbf{B}_{2\min} = \begin{bmatrix} 0 & 4.4947\times10^{-4} \end{bmatrix}^{\mathrm{T}},\ \mathbf{B}_{2\max} = \begin{bmatrix} 0 & 6.2645\times10^{-4} \end{bmatrix}^{\mathrm{T}},\ \Delta\mathbf{B}_{2m} = \begin{bmatrix} 0 & -1.6106\times10^{-5} \end{bmatrix}^{\mathrm{T}}$$

$$\mathbf{C}_2 = \begin{bmatrix} 0 & 0.65256 \end{bmatrix}$$

Rule R^3: $c_{X_1^3} = c_{X_2^3} = 1.204$ mm, $c_{U_1^3} = 900$ W

$$\mathbf{A}_{3\min} = \begin{bmatrix} 0 & 1 \\ -0.2319 & 0.2766 \end{bmatrix},\ \mathbf{A}_{3\max} = \begin{bmatrix} 0 & 1 \\ 0.0481 & 0.4434 \end{bmatrix},\ \Delta\mathbf{A}_{3m} = \begin{bmatrix} 0 & 1 \\ -0.0506 & 0.0285 \end{bmatrix}$$

$$\mathbf{B}_{3\min}=\begin{bmatrix}0 & 6.4584\times10^{-4}\end{bmatrix}^{\mathrm{T}},\ \mathbf{B}_{3\max}=\begin{bmatrix}0 & 7.9090\times10^{-4}\end{bmatrix}^{\mathrm{T}},\ \Delta\mathbf{B}_{3m}=\begin{bmatrix}0 & -1.4930\times10^{-5}\end{bmatrix}^{\mathrm{T}}$$

$$\mathbf{C}_3=\begin{bmatrix}0 & 0.52771\end{bmatrix}$$

Rule R^4 $\quad c_{X_1^4}=c_{X_2^4}=1.247\ \text{mm},\ c_{U_1^4}=950\ \text{W}$

$$\mathbf{A}_{4\min}=\begin{bmatrix}0 & 1\\ -0.1845 & 0.2474\end{bmatrix},\ \mathbf{A}_{4\max}=\begin{bmatrix}0 & 1\\ 0.0309 & 0.3713\end{bmatrix},\ \Delta\mathbf{A}_{4m}=\begin{bmatrix}0 & 1\\ -0.0212 & 0.0094\end{bmatrix}$$

$$\mathbf{B}_{4\min}=\begin{bmatrix}0 & 9.2720\times10^{-4}\end{bmatrix}^{\mathrm{T}},\ \mathbf{B}_{4\max}=\begin{bmatrix}0 & 0.0010\end{bmatrix}^{\mathrm{T}},\ \Delta\mathbf{B}_{4m}=\begin{bmatrix}0 & -1.3458\times10^{-5}\end{bmatrix}^{\mathrm{T}}$$

$$\mathbf{C}_4=\begin{bmatrix}0 & 0.35411\end{bmatrix}$$

Rule R^5 $\quad c_{X_1^5}=c_{X_2^5}=1.360\ \text{mm},\ c_{U_1^5}=1000\ \text{W}$

$$\mathbf{A}_{5\min}=\begin{bmatrix}0 & 1\\ 0.0296 & 0.2224\end{bmatrix},\ \mathbf{A}_{5\max}=\begin{bmatrix}0 & 1\\ 0.2043 & 0.3268\end{bmatrix},\ \Delta\mathbf{A}_{5m}=\begin{bmatrix}0 & 1\\ -0.0031 & 0.0022\end{bmatrix}$$

$$\mathbf{B}_{5\min}=\begin{bmatrix}0 & 9.0819\times10^{-4}\end{bmatrix}^{\mathrm{T}},\ \mathbf{B}_{5\max}=\begin{bmatrix}0 & 9.8927\times10^{-4}\end{bmatrix}^{\mathrm{T}},\ \Delta\mathbf{B}_{5m}=\begin{bmatrix}0 & -1.1022\times10^{-5}\end{bmatrix}^{\mathrm{T}}$$

$$\mathbf{C}_5=\begin{bmatrix}0 & 0.13531\end{bmatrix}$$

APPENDIX L . CROSS-SECTIONAL IMAGES OF THE WELDING SAMPLES

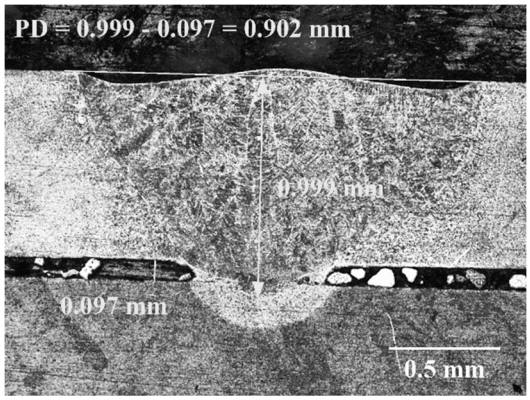

(a) Sample 1

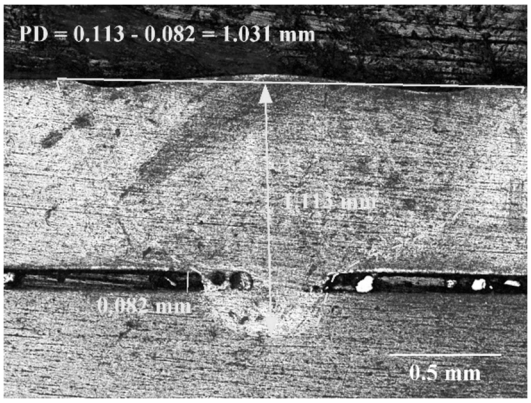

(b) Sample 2

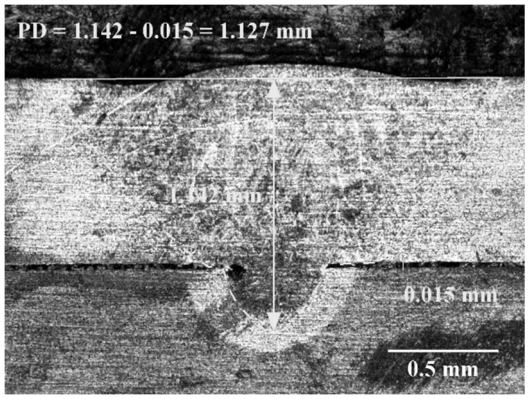

(c) Sample 3

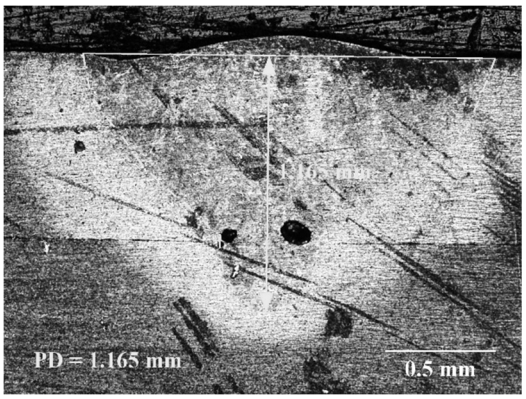

(b) Sample 4

Figure L-1: Microscopic images of the cross-sectional samples produced by the open loop system in case 1.

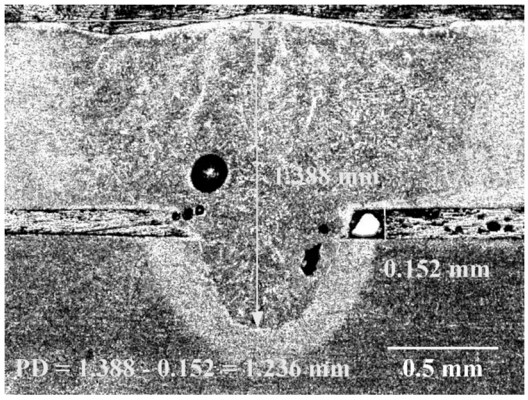

(a) Sample 1

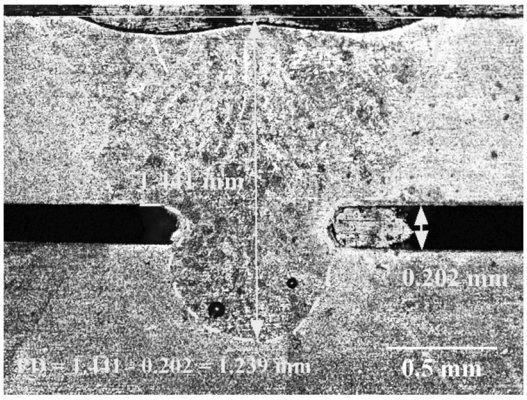

(b) Sample 2

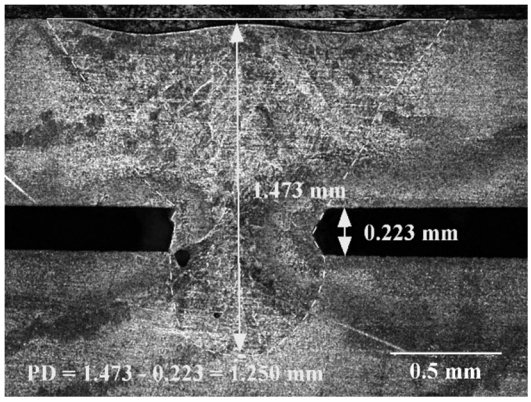

(c) Sample 3

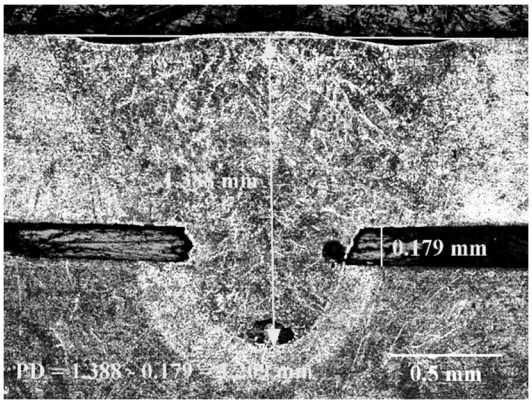

(b) Sample 4

Figure L-2: Microscopic images of the cross-sectional samples produced by the closed loop system in case 1.

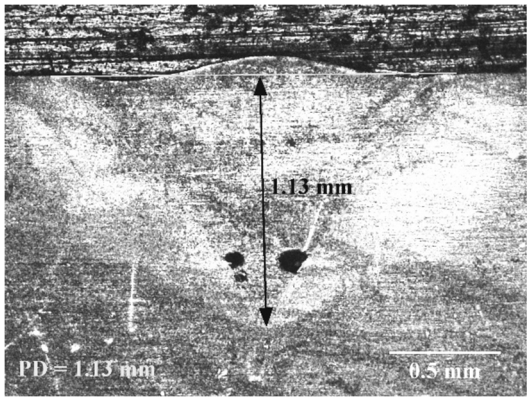

(a) Sample 1

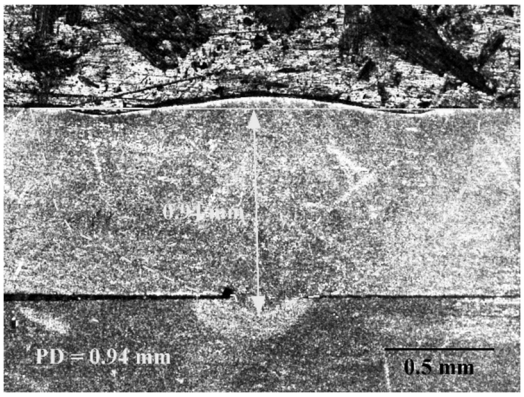

(b) Sample 2

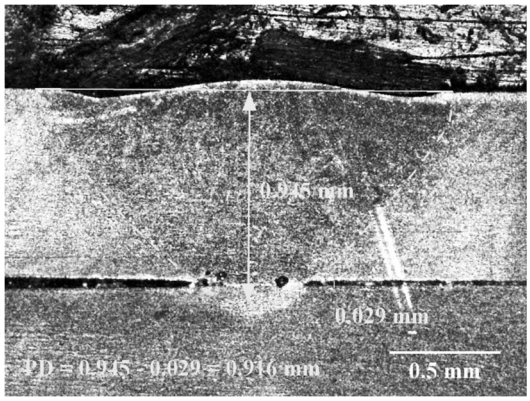

(c) Sample 3

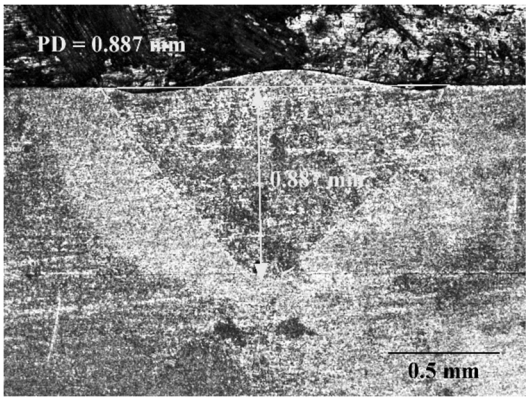

(b) Sample 4

Figure L-3: Microscopic images of the cross-sectional samples produced by the open loop system in case 2.

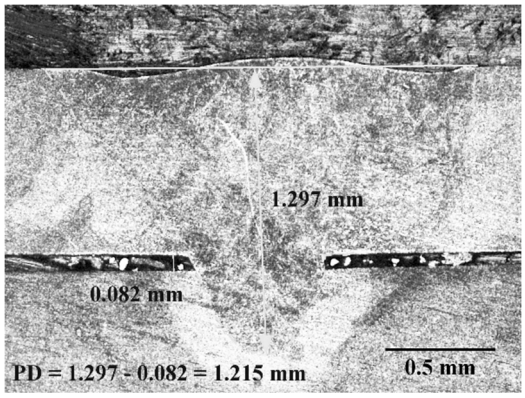

(a) Sample 1

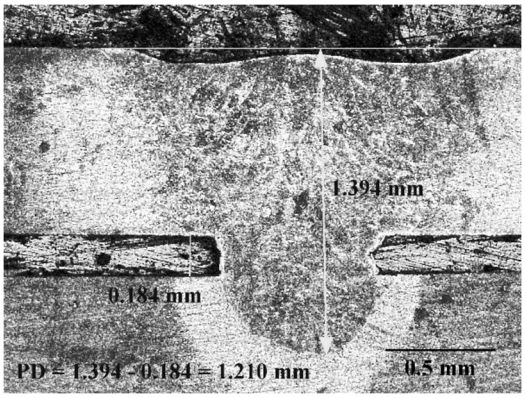

(b) Sample 2

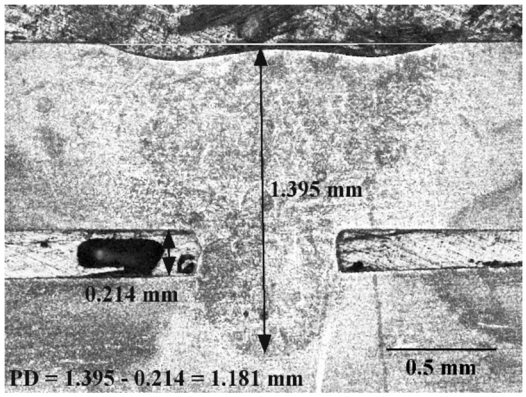

(c) Sample 3

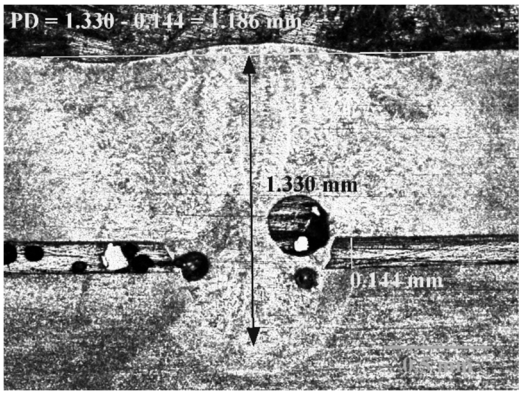

(b) Sample 4

Figure L-4: Microscopic images of the cross-sectional samples produced by the closed loop system in case 2.

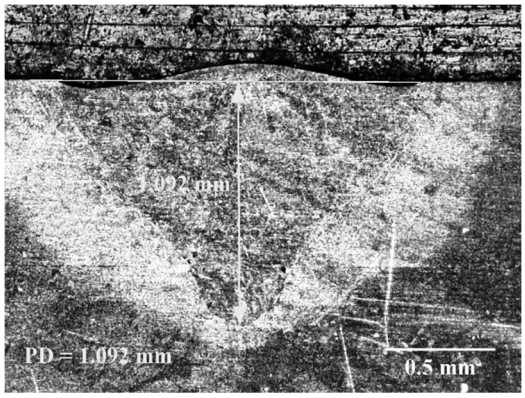

(a) Sample 1

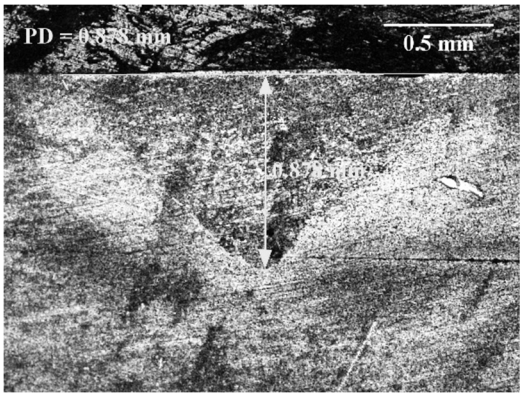

(b) Sample 2

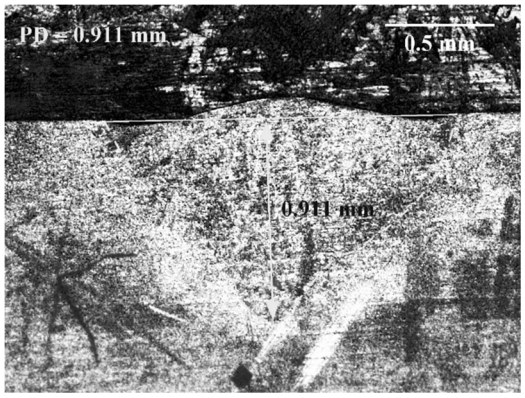

(c) Sample 3

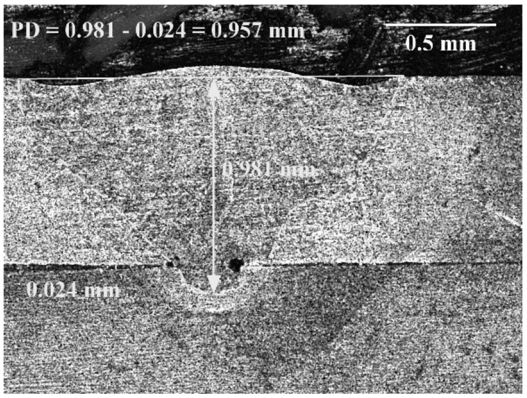

(b) Sample 4

Figure L-5: Microscopic images of the cross-sectional samples produced by the open loop system in case 3.

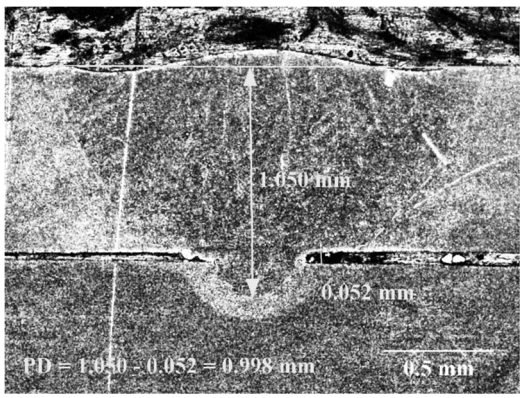

(a) Sample 1

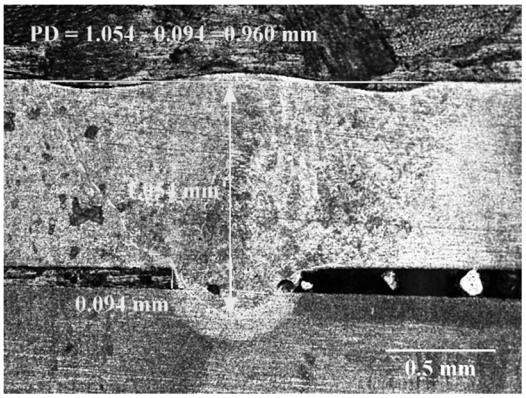

(b) Sample 2

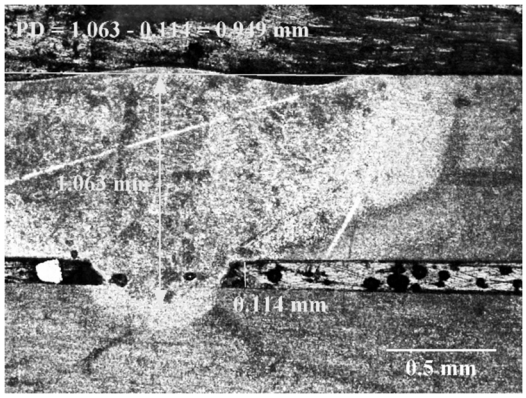

(c) Sample 3

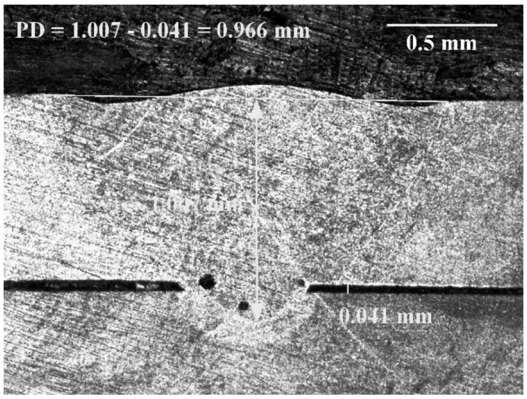

(b) Sample 4

Figure L-6: Microscopic images of the cross-sectional samples produced by the closed loop system in case 3.

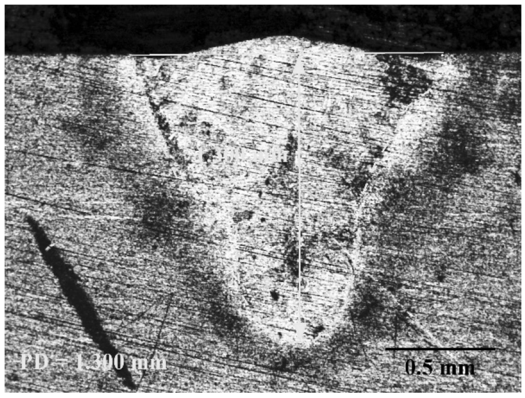

(a) Sample 1

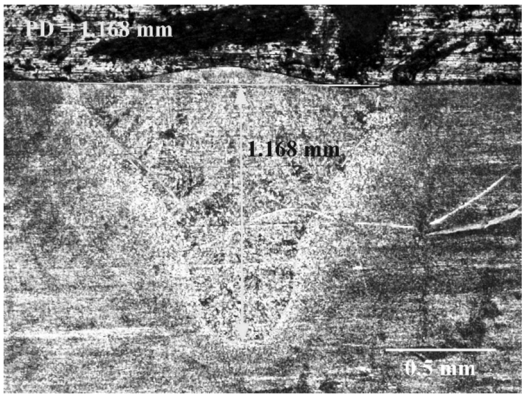

(b) Sample 2

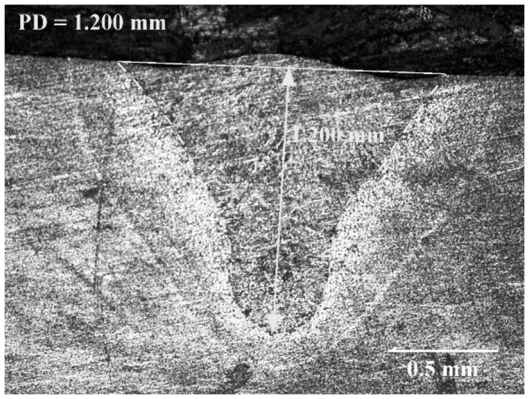

(c) Sample 3

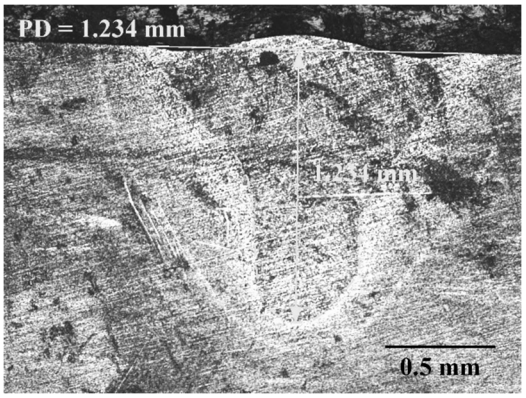

(b) Sample 4

Figure L-7: Microscopic images of the cross-sectional samples produced by the open loop system in case 4.

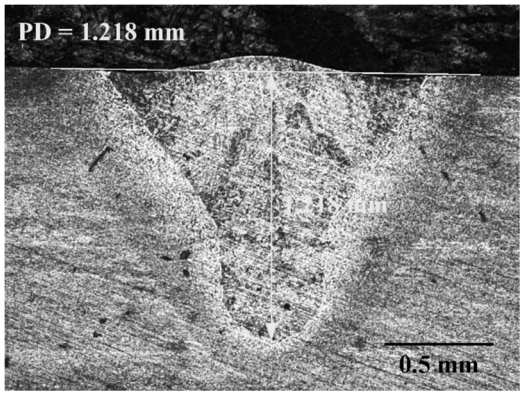

(a) Sample 1

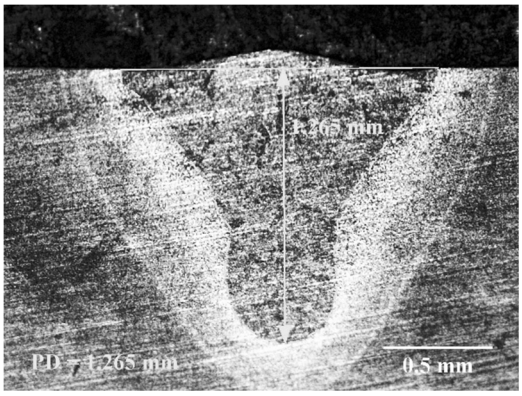

(b) Sample 2

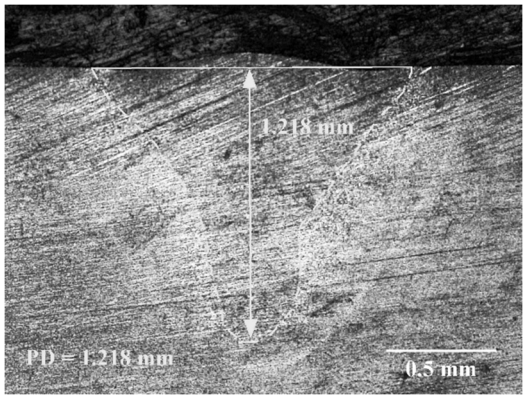

(c) Sample 3

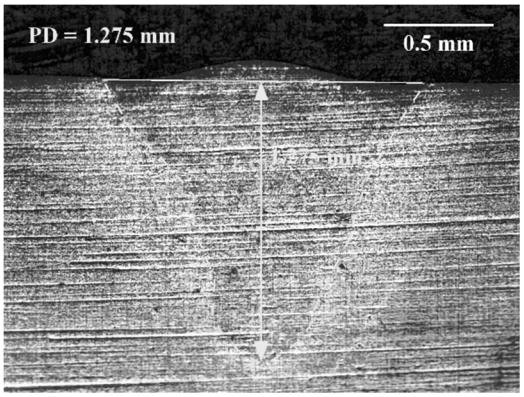

(b) Sample 4

Figure L-8: Microscopic images of the cross-sectional samples produced by the closed loop system in case 4.

VITA

VITA

Phuong Ngo received the Petronas scholarship for his bachelor study in Mechanical Engineering at the University of Technology Petronas, Malaysia and graduated in May 2008. He was then awarded the Vietnam Education Foundation fellowship for Ph.D. study. He is currently a candidate for the Ph.D. degree in Mechanical Engineering at Purdue University, Indiana, USA in August 2016. His research interests include intelligent systems, nonlinear control, mechatronics and manufacturing control.